UNIVERSITY OF CALIFORNIA, SAN DIEGO

Infrared and Ultraviolet Physics at Three Energy Scales

A dissertation submitted in partial satisfaction of the
requirements for the degree
Doctor of Philosophy

in

Physics

by

Brian Scott Shotwell

Committee in charge:

Professor Aneesh Manohar, Chair
Professor Benjamín Grinstein
Professor David Meyer
Professor Justin Roberts
Professor Frank Würthwein

2015

The dissertation of Brian Scott Shotwell is approved, and it is acceptable in quality and form for publication on microfilm and electronically:

_____

_____

_____

_____

_____

Chair

University of California, San Diego

2015

TABLE OF CONTENTS

LIST OF FIGURES

LIST OF TABLES

ACKNOWLEDGEMENTS

I have many professors to thank for introducing me to QFT: Thomas Appelquist, Witold Skiba, Benjamin Grinstein, and Kenneth Intriligator. I owe the biggest thanks though to my advisor, Aneesh Manohar, for teaching me the most about the subject. His vast knowledge of QFT, computational fortitude, and important and interesting contributions to the field have continually impressed me. His notes on EFTs are a big reason I came to UCSD, and I am glad I did.

The UCSD high-energy theory postdocs have also taught me a great deal. I have two postdocs in particular to thank: Wouter Waalewijn and Rodrigo Alonso. The former taught me almost everything I know about SCET, and Chapter 2 would not have been possible without him. Rodrigo Alonso, in addition to helping me with the project described in Chapter 4, has also been a good friend since his arrival. He and Jorge Camalich brought with them to UCSD a fun, gregarious Spanish quality that has enhanced the atmosphere of the high-energy theory group.

Finally, I am grateful for the high-energy theory graduate students, past and present. Grigor Aslanyan and Hsi-Ming Chang both put up with me as officemates over the past five years, and I enjoyed my 2-3 years with each of them. Several graduate students have left in the past few years: Casey Conger, David Stone, Chris Murphy, Andreas Stergiou, and Patipan Uttayarat — I am fortunate to have met all of them. Futhermore, I am confident Emily Nardoni, Miles Albert, Shauna Kravec, and Alex Kuczala will do great things in the years to come.

Portions of Chapter 2 are reprints of material as it appears in *Phys. Rev. D* **87**, 074013 (2012). A. Jain, M. Procura, B. Shotwell, and W. J. Waalewijn. The dissertation author was co-author of this paper.

Chapter 3 and Appendix C, in full, are reprints of material as it appears in *Phys. Lett. B* **740** 179 (2015). A. Manohar, B. Shotwell, C. Bauer, and S. Turczyk. The dissertation author and the Ph.D. committee chair were the principal investigators and co-authors of this paper.

Chapter 4 and Apprendix D, in full, are reprints of material as it appears in *Phys. Lett. B* **734** 302 (2014). R. Alonso, H.-M. Chang, E. Jenkins, A. Manohar, and B. Shotwell. The dissertation author was co-author of this paper.

VITA

2007	B.S. in Engineering Physics *with high honors*, University of California, Berkeley (United States)
2008	M.S. in Physics, Yale University (United States)
2007–2009	Teaching Fellow, Yale University
2010–2015	Teaching Assistant, University of California, San Diego (United States)
2013–2015	Instructor, University of California, San Diego
2015	Ph.D. in Physics, University of California, San Diego

PUBLICATIONS

A. Manohar, B. Shotwell, C. Bauer, and S. Turczyk, "Non-Cancellation of Electroweak Logarithms in High-Energy Scattering", *Phys. Lett. B* **740** 179 (2015). arXiv:1409.1918

R. Alonso, H.-M. Chang, E. Jenkins, A. Manohar, and B. Shotwell, "Renormalization group evolution of dimension-six baryon number violating operators", *Phys. Lett. B* **734** 302 (2014). arXiv:1405.0486

A. Jain, M. Procura, B. Shotwell, and W. J. Waalewijn, "Fragmentation with a Cut on Thrust: Predictions for B-Factories", *Phys. Rev. D* **87**, 074013 (2012). arXiv:1207.4788

ABSTRACT OF THE DISSERTATION

Infrared and Ultraviolet Physics at Three Energy Scales

by

Brian Scott Shotwell

Doctor of Philosophy in Physics

University of California, San Diego, 2015

Professor Aneesh Manohar, Chair

This dissertation covers three topics in particle physics phenomenology at three distinct energy scales: first, a discussion of thrust as an event shape variable and how it is useful in studying fragmentation at the GeV scale; second, an exploration into the (lack of) cancellation of electroweak large logarithms at the TeV scale; and third, a calculation of the renormalization group evolution of baryon number violating operators in the standard model effective field theory, relevant at energies well above the electroweak scale. The three topics are introduced as manifestations of infrared and ultraviolet physics in the context of effective field theories.

Chapter 1

Introduction

A thesis in particle physics phenomenology usually includes in its introduction a summary of the field content of the Standard Model and those fields' properties. I will not do that here. It is assumed that anyone reading this thesis, or even someone skimming the introduction to this thesis, has heard of the particles that comprise the underlying theory and knows as much about them as he/she sees fit. The purpose of this introduction is twofold: first, I would like to give an overview of Effective Field Theory (EFT) and stress its importance in physics; second, I would like to remind the reader of the two types of divergences encountered in perturbative quantum field theory (QFT): those of infrared (IR) origin and those of ultraviolet (UV) origin. It is with this general background that I can best unify the disparate topics that constitute this thesis.

1.1 Effective Field Theories

Effective field theory is a framework for understanding relevant physics at different energy scales. From Ref. [1],

> The basic premise of effective theories is that dynamics at low energies (or large distances) does not depend on the details of the dynamics at high energies (or short distances). As a result, low energy physics can be described using an effective Lagrangian that contains only a few degrees of freedom, ignoring additional degrees of freedom present at higher energies.

This idea is one that physicists have been using for several hundred years: Kepler could describe the motion of the planets without knowing the internal structure of the sun or planets, Newton could describe motion at low velocities without knowing special relativity, etc. The concept was made more quantitative by Lev Landau with his introduction of the order parameter, further developed in condensed matter systems by Leo Kadanoff and Michael Fisher through their use of effective actions, and formulated in its modern understanding by the late Ken Wilson (also giving our intuition behind the renormalization group).

Enrico Fermi and his four-point interaction, introduced in 1934 as a model to explain beta-decay, is arguably the most well-known particle physics EFT. In addition to the model's simplicity, it is especially instructive when studied in the context of Weinberg's $SU(2) \times U(1)$ electroweak interaction. We review qualitatively some important features of the four-fermion interaction and its history in the following subsection. Subsection 1.1.2 introduces Soft-Collinear Effective Theory (SCET), an EFT developed in the past 15 years to describe relevant degrees of freedom in collider physics events involving jets.

1.1.1 Fermi Interaction as an EFT

When Fermi first proposed his four-point interaction, the neutrino had already been proposed by Pauli to explain the conservation of energy in β-decay, and the positron had already been proposed by Paul Dirac as a consequence of the negative-energy solution of the Dirac Equation. Fermi combined these two concepts with his four-point interaction. He laid the groundwork for the later discoveries of beta-capture and of the $V - A$ tensor structure of the operator, and more generally proposed the idea that electron number is not conserved (in the strict sense, only counting electrons and not neutrinos).

As described above, Fermi's theory was formulated using a "bottom-up" approach to physics; it is a constructive theory (as opposed to a "principle" theory[1]) able to explain already-observed phenomena. Despite the theory's great

[1]This classification of theories is due to Einstein, who regarded his own theory of relativity as a "principle" theory.

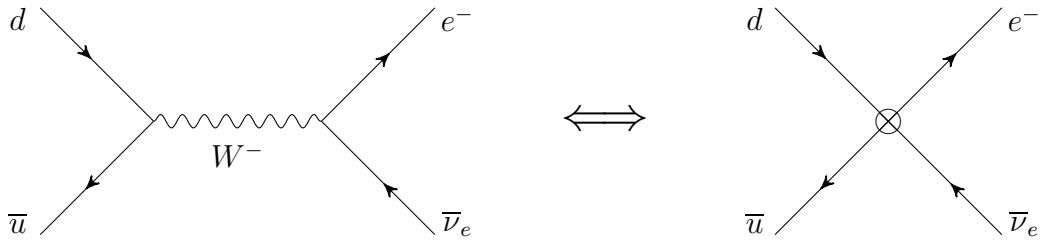

Figure 1.1: The interaction governing β-decay in the Standard Model (left), and in Fermi's Interaction (right). The latter emerges from the former at energy scales much less than the mass of the W boson.

success, it was known to be incomplete — cross-sections calculated using Fermi's interaction grow as the square of the CM energy, and therefore the theory violates unitarity. By a simple argument using dimensional analysis and Fermi's constant (the constant of proportionality multiplying the four-fermion operator, with units of $1/\text{energy}^2$), one can show that the theory breaks down at energy-scales of order 100 GeV. The fact that the W-boson (the mediator particle responsible for muon decay, with mass 80.4 GeV) was discovered 50 years after the four-fermion interaction was proposed shows the predictive power of EFTs to infer dynamics at short-distance scales despite not knowing the full theory.

The model of electroweak interactions developed by Glashow, Salam, and Weinberg explained that the 4-fermion interaction, upon closer examination, is actually comprised of two 3-point interactions among two fermions and one gauge boson, the latter of which is the emergent mass eigenstate of a $SU(2) \times U(1)$ gauge symmetry after spontaneous symmetry breaking. The details can be found in any QFT book. Knowing this, Fermi's model can be reinterpreted as an effective field theory using a "top-down" approach: the 4-point interaction emerges after integrating out the gauge bosons as dynamical degrees of freedom (i.e., in Figure 1.1, Fermi's interaction emerges when zooming out of the full-theory interaction diagram). This describes another way EFTs are useful: calculations using the full $SU(2) \times U(1)$ theory are often complicated and unnecessary, and Fermi's interaction is an excellent approximation to calculate any process at energies much less than the electroweak scale.

The $SU(2) \times U(1)$ theory is known as a "renormalizable" theory, whereas

Fermi's theory is "non-renormalizable." What is meant by this is that the former requires only a finite number of operators appearing in the Lagrangian to cancel UV-divergences appearing in the theory (so-called "counterterms"), whereas the latter requires an infinite number of counterterms. For a long time, particle physicists insisted that a theory be renormalizable. One argument for this is that a non-renormalizable theory has an infinite number of counterterms (requiring an infinite number of parameters) and therefore has no predictive power. Another argument is that the theory should be valid at very high energy scales Λ (if it is truly a fundamental theory), and the operators making the theory non-renormalizable are very heavily suppressed at energies much less than Λ. In fact, such operators are known as "irrelevant operators" — irrelevant at low energies. This demonstrates the inherent bias for a "top-down" approach to physics.

A "bottom-up" approach is not inferior to a "top-down" approach. Non-renormalizable theories can be valid descriptions of physics, and can help us infer high-energy new physics from a low-energy EFT. Effective field theory allows for this statement to be quantitative: the infinite number of counterterms arising from a non-renormalizabe theory are often suppressed by some small parameter (which depends on the problem at hand). Therefore, an EFT can be useful without being exact; the Standard Model, itself likely an effective field theory (assuming some new physics at energy scales much higher than the electroweak scale), has done very well and has predictive power despite not being valid at arbitrarily large energies.

1.1.2 Soft-Collinear Effective Theory (SCET)

Soft-Collinear Effective Theory (SCET) [2–5] was developed as an effective theory able to parameterize both collinear and soft degrees of freedom in processes involving energetic jets. The theory was an extension of Large Energy Effective Theory (LEET) [6] and Heavy Quark Effective Theory (HQET) [7–9]. The wide success of the theory has been due to its applicability to myriad processes, including inclusive and exclusive heavy meson decays, hard scattering processes, and jet-production. Originally used to describe QCD effects, it has also been extended

to incorporate electroweak effects, and a summary of those results is given in Appendix C.

The wide applicability of SCET is also what makes the theory relatively difficult for the uninitiated. The small power-counting parameter used in SCET, $\lambda \ll 1$, depends on the process studied, and is often defined in terms of the kinematics of some final state of interest. This is unusual: most EFTs use mass dimensions as their power-counting parameter(s), and therefore one can deduce the relative importance of an operator from dimensional analysis alone. SCET is not so nice in this regard. Nevertheless, SCET can systematically describe relevant degrees of freedom in a hierarchy of energy scales ($Q \ll \lambda Q \ll \lambda^2 Q$) while simultaneously resumming large logarithms for many different scenarios, and is consequently an essential tool for collider physics.

Another crowning achievement of SCET is its ability to provide a framework for factorization theorems. In processes described by SCET, there is a "hard" interaction at some scale Q, "collinear" degrees of freedom with virtuality $\sim \lambda Q$ (one for each jet), and "soft" degrees of freedom[2] with virtuality $\sim \lambda^2 Q$ (which could be $\mathcal{O}(\Lambda_{\rm QCD})$ or not, depending on the process). SCET provides a set of Feynman rules for these distinct sectors which propagate relatively freely from one another. The ability to consistently isolate the relevant physics at each scale is a great triumph of SCET.

Chapter 2 focuses on the computation of the "hard" coefficient for the process $e^+e^- \to q\bar{q}g$. The finite piece is extracted from the NLO computation, and the result is used to improve the SCET calculation with factorization structure given in Eq. 2.89. Chapter 3 focuses on the need for $\text{SCET}_{\rm EW}$ by looking at the importance of large logarithms in high-energy ($10 - 100\,\text{TeV}$) colliders.

[2]There is a actually a distinction between "soft" and "ultrasoft" modes ($\text{SCET}_{\rm II}$ vs. $\text{SCET}_{\rm I}$); for the purposes of this thesis, "soft" will be used to refer to "ultrasoft" modes with momentum scaling $p^\mu \sim Q(\lambda^2, \lambda^2, \lambda^2)$ in light cone coordinates. This is called $\text{SCET}_{\rm I}$.

1.2 Infrared and Ultraviolet Infinities

Ultraviolet infinities are discussed at length in standard second-quarter / second-semester quantum field theory classes in the context of the renormalization group and calculations involving loop diagrams. The fact that masses and coupling constants change with the energy scale at which they are evaluated is a consequence of these kinds of high-energy infinities, and the systematics of obtaining finite, physical (i.e., measurable) quantities from the theory were devised by Feynman, Schwinger, and Tomonaga. The decades after this formulation saw a generalization of these concepts in the construction of *effective field theories*, introduced in the previous section.

In addition to UV divergences, there are also low-energy infinities which appear in QFT calculations, so-called infrared divergences. These IR divergences are often not covered in detail in a standard one-year introductory sequence to quantum field theory. However, there are a variety of reasons why it is important to explore the nature of infrared divergences:

⋆ It is inconsistent to look at loop-corrections of internal gauge bosons without taking into account initial and final-state radiation associated with these mediator particles.

⋆ Their understanding is intimately related to the optical theorem through the appearance of on-shell virtual particles. Infrared divergences cancel in a unitary theory by the Kinoshita-Lee-Nauenberg (KLN) theorem, and the optical theorem is a consequence of unitarity.

⋆ Calculations using dimensional regularization, by far the dominant regulator in perturbative field theory calculations, are sometimes deceivingly simple and hide physical effects. For example, scaleless integrals vanish in dimensional regularization; upon further inspection, it becomes evident that the zero result is actually a cancellation between an ultraviolet infinity and an infrared infinity.

⋆ They emphasize the important role that kinematics and experimental observables play — not everything can be deduced from matrix elements alone. In

particular, infrared divergences only cancel at the cross-section level, and not at the amplitude level.

As noted in the last point, the infrared divergence at the *amplitude* level in a loop calculation involving virtual (internal) particles is cancelled by a corresponding infrared divergence in the real radiation at the *kinematic* level. The former occurs because of a divergent integral over arbitrarily small momenta of internal particles, whereas the latter occurs because of a divergent phase-space integral over the initial- or final-state kinematics. Because the two contributions appear at different stages of the computation, it is necessary to include an infrared regulator to handle these infinities.

For over 30 years, the regularization procedure of choice has been *dimensional regularization*, obtained by changing the dimension of spacetime from $d = 4$ dimensions to $d = 4 - 2\epsilon$ dimensions, with $d < 4$ to regulate UV infinities and $d > 4$ to regulate IR infinities. This regulation procedure is favored over most because (1) it is relatively easy computationally, (2) it is able to handle both IR and UV divergences, and (3) it respects gauge invariance in intermediate stages of the computation. This thesis will also look at two other kinds of (IR) regulators. First, in Chapter 2 we'll see that a cut on the event-shape variable thrust can serve as an IR regulator. Second, in Chapter 2 we'll also see that the real radiation cross section of (dijet + 1 hadron) events can be computed using a gluon mass as an infrared regulator (setting the unphysical mass to zero later in the computation). This calculation will be relevant for Chapter 3, where we'll look at a toy $SU(2)$ theory with a massive gauge boson (i.e., the mass of the $W^{\pm}$ or Z boson). Here the regulator is the physical gauge boson mass.

1.3 Thesis Outline

Chapter 2 will be the first of two chapters focusing primarily on infrared divergences. In it we review a very common and important calculation ($e^+ + e^- \to q\bar{q}g$), write the result in terms of the event-shape variable thrust, and extract a piece of this calculation to augment the SCET computation of the same process.

The purpose of the calculation is to improve accuracy in the determination of fragmentation functions from Belle data.

Chapter 3, the second chapter focusing on infrared divergences, looks at the real emission of electroweak gauge bosons in TeV-scale processes (specifically, top/bottom quark production). We show that electroweak large logarithms often do not cancel in final states probed at the LHC and therefore should be resummed using $\mathrm{SCET}_{\mathrm{EW}}$. The large logarithms appear because the experimental signatures of such events are inherently exclusive.

Chapter 4 shifts the focus over to ultraviolet divergences in the calculation of the Yukawa contribution to the anomalous dimension matrix of baryon number-violating (BNV) operators in the Standard Model effective field theory. In addition to presenting the result of the computation, we also discuss the flavor structure of the operators and discuss their importance under some simplifying hypotheses.

Chapter 2

Fragmentation with a Cut on Thrust

The Belle experiment at KEK in Japan uses the 10.52 GeV center-of-mass e^+e^- collider to probe flavor physics and CP violation. The data can also be used to study light-parton "fragmentation," which refers to the process by which a parton (a quark, antiquark, or gluon) hadronizes into the color-singlet hadron seen in the final state. Because the energy of the collider is such that many bottom-quarks are produced near resonance, the data is contaminated by large contributions from heavy quarks, and the study of light-parton fragmentation requires the removal of these events. To eliminate the large contamination, a cut on the event-shape variable thrust is used, and in doing so we can probe "dijet" events of the form $e^+ + e^- \to 2j + h$ (where h refers to the observed hadron). By focusing on these events and by using a factorization theorem in SCET applied to fragmentation, we can infer the non-perturbative fragmentation functions from the Belle data. Furthermore, the calculations demonstrate that there exist correlations between the thrust cut and the momentum fraction of the observed hadron, effects not previously taken into account by the Belle collaboration.

The organization of this chapter is as follows: first, thrust is introduced, and its relationship to Soft-Collinear Effective Theory (SCET) is explained. Next, the next-to-leading order (NLO) piece of the $e^+ + e^- \to q + \bar{q} + g$ cross-section is calculated, giving the singular and the non-singular pieces of the NLO result

and relating the result to thrust and fragmentation functions. Finally, I'll state how this is combined with the resummed SCET calculation to extract information about fragmentation functions.

This chapter is based on work in Ref. [10], of which I was co-author. The material presented here concentrates on my contribution to the work, which involved the calculation of the NLO pieces of the computation $e^+ + e^- \to q + \bar{q} + g$. The computation will be presented twice: first, using a gluon mass as an infrared regulator (and an intermediate result will be relevant for the next chapter of the dissertation); and second, using dimensional regularization to modify the infrared divergences. Most of the results are well-known, but details of the calculation are included here for completeness and to review fully the IR structure of the process. The result will be used to extract the nonsingular part of the NLO computation, which plays a role in the $\tau \gtrsim 0.2$ regime.

2.1 Thrust and SCET

Thrust is a global event-shape variable[1] originally defined as follows [11]:

$$T \equiv \max_{\hat{t}} \frac{\sum_i |\hat{t} \cdot \vec{p}_i|}{\sum_i |\vec{p}_i|}\,, \tag{2.1}$$

where the sum runs over all final-state particles and momenta are taken in the center-of-mass frame (actually, Ref. [11] defines thrust as half this quantity, but the physics community settled on T shortly afterwards and the above was the predominant definition of thrust in the 1980's). The axis $\hat{t}^*$ that maximizes the ratio above is called the *thrust axis*. The maximum value of T occurs for "pencil-like" / "jet-like" events where all final-state particles lie on the same axis, in which case $T = 1$. The minimum value of T depends on the number of final-state particles, but can be as low as $1/2$ for a large number of particles spherically distributed. Starting in the 1990's, the term "thrust" started to refer to the related variable τ, where

$$\tau \equiv 1 - T = 1 - \max_{\hat{t}} \frac{\sum_i |\hat{t} \cdot \vec{p}_i|}{\sum_i |\vec{p}_i|}\,. \tag{2.2}$$

[1] A variable related to the geometry of the final-state of the particle physics event.

We will use the term "thrust" throughout this chapter to refer to both T and τ; results of calculations will generally be written in terms of τ.

This chapter will often deal with how thrust relates to the final state $q\bar{q}g$. For this 3-body case, if a unique particle carries the maximum 3-momentum, this particle also defines the thrust axis. For the case where $\mathbf{p}_i = \mathbf{p}_j > \mathbf{p}_k$ $(i \neq j \neq k)$, the thrust axis is perpendicular to the particle with 3-momentum $\mathbf{p}_k$.

Thrust is defined for final-state particles, for which fragmentation / hadronization have already occurred. For events with center of mass energy $Q \gg \Lambda_{QCD}$, a differential cross section in thrust can be calculated at the partonic level with perturbative QCD. The wide separation of scales allows for SCET to be a useful tool, and the kinematic regimes for which SCET is useful correspond to the regions of final-state phase space where $\tau \to 0$. Intuitively, this is clear: for a three-body final state with $\tau \ll 1$, at least one of the following two statements must be true.

⋆ One particle has very small energy ("soft")

⋆ All particles lie roughly on the thrust axis ("collinear")

These are exactly the scenarios for which large logarithms appear in calculations, and SCET gives a good framework for resumming the large logarithms in these situations. $\sqrt{\tau}$ is used as the small parameter usually called λ in SCET, since a soft particle of energy $p_s^0 \ll Q$ gives thrust $\tau = \mathcal{O}(p_s^0/Q)$ (furthermore, we're using $\mathrm{SCET_I}$, where the momentum scaling of the soft particles is $p_s^\mu \sim \lambda^2 Q$).

We now pause the discussion of the effective theory, and concentrate on the leading order and NLO computations. We resume the discussion in Sec. 2.5 after the reader is throughly tired of the "basic" computation.

2.2 Leading Order Calculation; Notation

The leading order (LO) tree-level unpolarized cross section $e^+e^- \to q\bar{q}$ does not require an infrared regulator. The calculation arises from the single diagram of Figure 2.1, which gives the matrix element $T = g_{\mu\nu}\left[(4\pi i\alpha_{\mathrm{EM}})/s\right]\bar{v}_+\gamma^\mu u_-\bar{u}_1\gamma^\nu v_2$. We've adopted the notation $u_i \equiv u(p_i)$ (and similar with $u \to v$), $p_\pm$ is the momentum of the incoming $e^\pm$, p_1 is the momentum of the outgoing quark, and p_2 is the

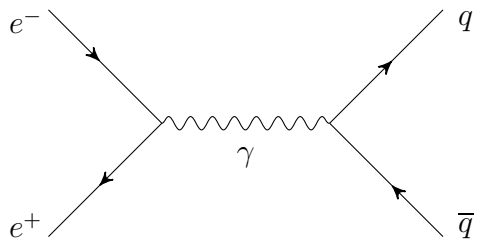

Figure 2.1: Tree-level contribution to $e^+e^- \to q\overline{q}$. Amplitude: T.

momentum of the outgoing antiquark. The coupling $\alpha_{\rm EM}$ is electromagnetic, as only the photon gives an appreciable contribution to the cross-section at the GeV scale. The Mandalstam variable s gives the square of the center-of-mass energy of the two electrons. The tree-level / "Born" cross section comes from the phase-space integral over the spin-summed amplitude-squared (averaged over initial spins):

$$\begin{aligned}\overline{|\mathcal{M}_0|^2} \equiv \frac{1}{4}\sum_{\substack{\text{spins}\\\text{colors}}} |T|^2 &= \frac{1}{4}\frac{16\pi^2\alpha_{\rm EM}^2 N_c}{s^2}\,\mathrm{Tr}\left\{\not{p}_+\gamma_\mu\not{p}_-\gamma_\nu\right\}\mathrm{Tr}\left\{\not{p}_1\gamma^\mu\not{p}_2\gamma^\nu\right\}\\ &= \frac{4\pi^2\alpha_{\rm EM}^2 N_c}{s^2}\Big[32\big[(p_+\cdot p_1)(p_-\cdot p_2)+(p_+\cdot p_2)(p_-\cdot p_1)\big]\Big]\end{aligned} \tag{2.3}$$

Notice $\overline{|\mathcal{M}_0|^2}$ does *not* factorize into the product of two traces, which is also true for the NLO calculation (there we will exploit the QED Ward identity to simplify the computation of traces). Also notice that we are ignoring the masses of all fermions. Overall, the tree-level / "Born" cross section $e^+e^- \to q\bar{q}$ can be computed in the CM frame by assigning momentum via $p_\mp^\mu = E(1,0,0,\pm 1)$, $p_1^\mu = E(1,\sin\theta,0,\cos\theta)$, and $p_2^\mu = E(1,-\sin\theta,0,-\cos\theta)$, where $E=\sqrt{s}/2$ is the energy of one particle in the CM frame. This gives:

$$\begin{aligned}\sigma_0 &= \frac{1}{2s}\int d\Pi_2\overline{|\mathcal{M}_0|^2} = \frac{1}{2s}\frac{1}{16\pi}\int \overline{|\mathcal{M}_0|^2} d\cos\theta\\ &= \frac{4\pi\alpha_{\rm EM}^2 N_c}{s^3}\int_{-1}^{1} E^4\left[(1+\cos\theta)^2+(1-\cos\theta)^2\right]d\cos\theta\\ &= \frac{4\pi\alpha_{\rm EM}^2 N_c}{3s}\,.\end{aligned} \tag{2.4}$$

N_c is the number of colors for the given final state dirac quark q.

The next two sections will each present the NLO calculation of $e^+ + e^- \to q + \bar{q} + g$. In both cases, q refers to the virtual photon momentum (and $q^\mu = (\sqrt{s}, 0, 0, 0)$ in the CM frame), p_3 refers to the momentum of the outgoing gluon, and k refers to the momentum of the virtual gluon. The relevant diagrams are shown in Figures 2.2–2.4.

2.3 NLO Calculation with a Gluon Mass

2.3.1 Virtual Diagram Amplitudes V and W

First we calculate the vertex amplitude V of Figure 2.2 in $d = 4 - 2\epsilon$ dimensions. Let C_F be the 2nd Casimir Invariant for $SU(3)$ (so that $T^A T^A = C_F \mathbb{1}$), let the overall momentum (and the momentum of the timelike virtual photon) be q (so that $q^2 = s$, the CM energy squared), and let the virtual gluon momentum be k going downwards in Figure 2.2. Integrals are expressed in Minkowski space, before Wick-rotating to a Euclidean measure; the relevant formulae are taken from Ref. [12] and summarized in Appendix A. Giving the gluon a mass M to control infrared divergences,

$$V = \bar{v}_+ \gamma_\mu u_- \frac{-i}{q^2} (-4\pi\alpha_{\mathrm{EM}}) \bar{u}_1 \mu^{2\epsilon} \int \bar{d}^d k (ig\gamma^\nu T^A) \frac{i(\not{k} + \not{p}_1)}{(k+p_1)^2 + i\epsilon} \gamma^\mu \frac{i(\not{k} - \not{p}_2)}{(k-p_2)^2 + i\epsilon} \times (ig\gamma_\nu T^A) \frac{-i}{k^2 - M^2} v_2 \quad (2.5)$$

$$V = C_F (4\pi\alpha_{\mathrm{EM}}) \frac{g^2}{s} \bar{v}_+ \gamma_\mu u_- \bar{u}_1 \mu^{2\epsilon} \int \bar{d}^d k \gamma^\nu \frac{\not{k} + \not{p}_1}{(k+p_1)^2 + i\epsilon} \gamma^\mu \frac{\not{k} - \not{p}_2}{(k-p_2)^2 + i\epsilon} \times \gamma_\nu \frac{1}{k^2 - M^2} v_2 \quad (2.6)$$

Define I such that $V = C_F (4\pi\alpha_{\mathrm{EM}})(g^2/s) \bar{v}_+ \gamma_\mu u_- \bar{u}_1 I v_2$:

$$\begin{aligned} I &= \mu^{2\epsilon} \int \bar{d}^d k \frac{\gamma^\nu (\not{k} + \not{p}_1) \gamma^\mu (\not{k} - \not{p}_2) \gamma_\nu}{(k^2 - M^2)(k+p_1)^2 (k-p_2)^2} \\ &= 2! \int dx dy dz \; \delta(1 - x - y - z) \; \mu^{2\epsilon} \int \bar{d}^d k \frac{N}{D^3} \end{aligned} \quad (2.7)$$

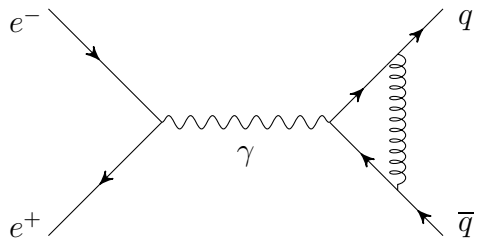

Figure 2.2: Vertex contribution to $e^+e^- \to q\overline{q}(g)$. Amplitude: V.

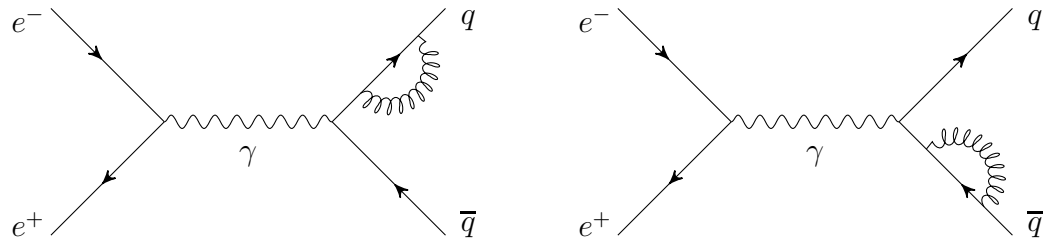

Figure 2.3: Wavefunction renomalization diagrams for $e^+e^- \to q\overline{q}(g)$. Amplitude: $W = W_q + W_{\bar{q}}$ (W_q and $W_{\bar{q}}$ for the left and right diagrams, respectively).

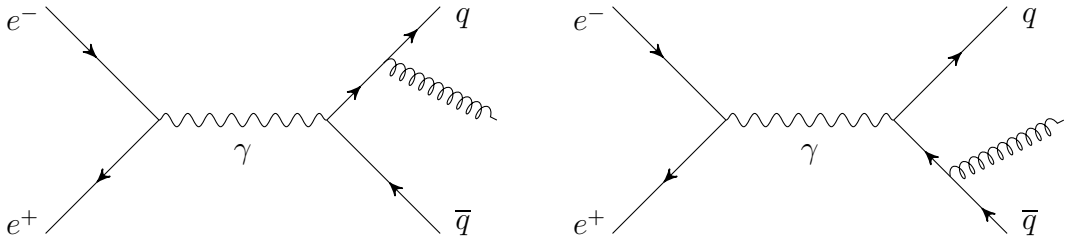

Figure 2.4: Real radiation diagrams for $e^+e^- \to q\overline{q}g$. Amplitude: $R = R_q + R_{\bar{q}}$ (R_q and $R_{\bar{q}}$ for the left and right diagrams, respectively).

Eq. (2.7) comes from the Feynman parameterization in Appendix Eq. (A.1). N and D as defined at the end of Eq. (2.7) (which are intended to stand for "numerator" and "denominator," respectively) are given by:

$$\begin{aligned} N &= -2(\not{k} - \not{p}_2)\gamma^\mu(\not{k} + \not{p}_1) + 2\epsilon(\not{k} + \not{p}_1)\gamma^\mu(\not{k} - \not{p}_2) \\ &= \left[-2(1-\epsilon)\gamma^\mu \frac{2-d}{d}\right]\ell^2 - 2s\gamma^\mu\Big[1 - (z+y) + zy(1-\epsilon)\Big] \\ D &= x(k^2 - M^2) + y(k+p_1)^2 + z(k-p_2)^2 + i\epsilon \\ &= k^2 + 2yk\cdot p_1 - 2zk\cdot p_2 - xM^2 + i\epsilon = \ell^2 - \Delta + i\epsilon \end{aligned} \tag{2.8}$$

where

$$\ell \equiv k + yp_1 - zp_2 \quad \text{and} \quad \Delta \equiv -2yzp_1\cdot p_2 + xM^2 = -syz + (1-y-z)M^2 \tag{2.9}$$

(note $s = (p_1+p_2)^2$ is the Mandelstam variable). Using Eq. (A.2), we can evaluate the integral. Implicit in the formula is that fact that when Δ is negative, we evaluate the logarithm according to the prescription $\Delta - i\epsilon$.

$$\begin{aligned} I &= \gamma^\mu\Gamma(\epsilon)\frac{i}{(4\pi)^{d/2}}\int_{y+z<1} dydz\ \left(\frac{\mu^2}{\Delta}\right)^\epsilon\left[-2(1-\epsilon)\frac{2-d}{2}\right. \\ &\qquad\left. + \epsilon\frac{2s}{\Delta}\Big(1-(z+y)+zy(1-\epsilon)\Big)\right] \\ I &= \gamma^\mu\left[\frac{1}{\epsilon} + \mathcal{O}(\epsilon)\right]\frac{i}{(4\pi)^2}\int_{y+z<1} dydz\ \left(\frac{\tilde{\mu}^2}{\Delta}\right)^\epsilon\left[-2(1-\epsilon)(-1+\epsilon)\right. \\ &\qquad\left. - \epsilon\frac{2}{yz-(1-y-z)\beta}\left(1-(z+y)+zy(1-\epsilon)\right)\right] \\ I &= \gamma^\mu\left[\frac{1}{\epsilon} + \mathcal{O}(\epsilon)\right]\frac{2i}{(4\pi)^2}\int_{y+z<1} dydz\ \left[1 - \epsilon\ln(s/\tilde{\mu}^2) + \mathcal{O}(\epsilon^2)\right] \\ &\quad\times\left[\Big(1 - \epsilon\ln\left(-yz + (1-y-z)\beta\right) - 2\epsilon + \mathcal{O}(\epsilon^2)\Big) - \epsilon\frac{1-(z+y)+yz(1-\epsilon)}{yz-(1-y-z)\beta}\right] \end{aligned} \tag{2.10}$$

We have defined $\beta \equiv M^2/s > 0$, and $\tilde{\mu} \equiv 4\pi e^{-\gamma}\mu^2$ (and $\gamma \approx 0.5772$ is the Euler-Mascheroni constant). The following integrals over the Feynman parameters use branch cuts consistent with the prescription above:

$$\int_{y+z<1} dydz\ \frac{1-(z+y)+yz(1-\epsilon)}{yz-(1-y-z)\beta} = \frac{5}{2} + 2i\pi - \frac{\pi^2}{6} + 2\ln\beta + i\pi\ln\beta + \frac{1}{2}\ln^2\beta + \mathcal{O}(\epsilon,\beta) \tag{2.11}$$

$$\int_{y+z<1} dydz\ \Big[\ln\left(-yz+(1-y-z)\beta\right)\Big] = -\frac{3}{2} - \frac{1}{2}i\pi + \mathcal{O}(\beta)$$

Thus,

$$I = \gamma^\mu \frac{1}{\epsilon}\frac{i}{(4\pi)^2} + \gamma^\mu \frac{2i}{(4\pi)^2}\int_{y+z<1} dydz\ \left[-\ln\Big((-yz+(1-y-z)\beta\Big) - \ln(s/\tilde{\mu}^2) - 2 - \frac{1-(z+y)+yz(1-\epsilon)}{(yz-(1-y-z)\beta)^{1+\epsilon}}\right]$$

$$I = \gamma^\mu \frac{i}{(4\pi)^2}\left[\frac{1}{\epsilon} + \frac{\pi^2}{3} - 4 - \ln(s/\tilde{\mu}^2) - 4\ln\beta - \ln^2\beta - 3i\pi - 2i\pi\ln\beta\right] \tag{2.12}$$

$$V = C_F(4\pi\alpha_{\rm EM})\frac{g^2}{s}\bar{v}_+\gamma_\mu u_- \bar{u}_1 I v_2$$

$$V = iC_F\frac{\alpha_s\alpha_{\rm EM}}{s}\bar{v}_+\gamma_\mu u_-\bar{u}_1\gamma^\mu v_2\left[\frac{1}{\epsilon} + \frac{\pi^2}{3} - 4 - \ln\left(\frac{s}{\tilde{\mu}^2}\right) - 4\ln\beta - \ln^2\beta - 3i\pi - 2i\pi\ln\beta\right] \tag{2.13}$$

The wavefunction renormalization diagrams of Figure 2.3 are also required. Note the following integral, which is evaluated similar to the above:

$$(-ig)^2 C_F\int\frac{d^dk}{(2\pi)^d}\frac{-i}{k^2-M^2}\frac{\gamma_\mu i(\not{p}+\not{k})\gamma^\mu}{(p+k)^2} = iC_F\not{p}\frac{\alpha_s}{4\pi}\left[\frac{1}{\epsilon} + \ln\left(\frac{\tilde{\mu}^2}{M^2}\right) - \frac{1}{2}\right] \tag{2.14}$$

(p is the momentum of the fermion which contains the virtual gluon). The wavefunction renormalization contribution is therefore

$$W = -iC_F\frac{\alpha_s\alpha_{\rm EM}}{s}\bar{v}_+\gamma_\mu u_-\bar{u}_1\gamma^\mu v_2\left[\frac{1}{\epsilon} + \ln\left(\frac{\tilde{\mu}^2}{M^2}\right) - \frac{1}{2}\right] \tag{2.15}$$

Adding this to the virtual gluon amplitude V, we see that the $1/\epsilon$ and $\tilde{\mu}$ dependence cancels and

$$V + W = iC_F \frac{\alpha_s \alpha_{\rm EM}}{s} \bar{v}_+ \gamma_\mu u_- \bar{u}_1 \gamma^\mu v_2 \left[\frac{\pi^2}{3} - \frac{7}{2} - 3\ln\beta - \ln^2\beta - 3i\pi - 2i\pi\ln\beta \right] \tag{2.16}$$

More generally, the cancellation of the ultraviolet regulator ϵ and mass scale $\tilde{\mu}$ is a consequence of the conservation of the QED vector current; the QED vector current is not renormalized.[2]

2.3.2 Real Radiation Diagram Amplitude R

$$R = \frac{-4\pi\alpha_{\rm EM}}{s} (\bar{v}_+ \gamma_\mu u_-)(-ig) \Bigg[\bar{u}_1 \epsilon^*_\nu(p_3) \gamma^\nu \frac{i(\not{p}_1 + \not{p}_3)}{(p_1+p_3)^2} \gamma^\mu T^A v_2 + \bar{u}_1 \gamma^\mu \frac{-i(\not{p}_2 + \not{p}_3)}{(p_2+p_3)^2} \epsilon^*_\nu(p_3) \gamma^\nu T^A v_2 \Bigg] \tag{2.17}$$

Note $s = (p_1+p_2+p_3)^2 = 2(p_1\cdot p_2 + p_1\cdot p_3 + p_2\cdot p_3) + M^2$. Simplifying the above, and using the abbreviations $a = 2p_1\cdot p_2$, $b = 2p_1\cdot p_3$, and $c = 2p_2\cdot p_3$,

$$R = \frac{-4g\pi\alpha_{\rm EM}}{s(b+M^2)(c+M^2)} (\bar{v}_+ \gamma_\mu u_-) \epsilon^*_\nu(p_3) \bar{u}_1 \Big[(c+M^2)(2p_1^\nu + \gamma^\nu \not{p}_3)\gamma^\mu - (b+M^2)\gamma^\mu (2p_2^\nu + \not{p}_3 \gamma^\nu) \Big] T^A v_2 \tag{2.18}$$

2.3.3 Spin-Summed Amplitudes Squared

We now need to sum over final spins and average over initial spins of the amplitudes squared and do the analog of Eq. (2.3) separately for the virtual (2-body final state) and real (3-body final state) amplitudes.

[2]There are some subtleties to this point, as explained in Ref. [13]

At NLO, the virtual diagram interferes with the tree level diagram when taking the square of the $q\bar{q}$ amplitude. Thus, we need to compute

$$\begin{aligned}\overline{|\mathcal{M}|^2_{q\bar{q}}} &\equiv \frac{1}{4}\sum_{\substack{\text{spins}\\ \text{colors}}} |T+(V+W)|^2 = \frac{1}{4}\sum_{\{\text{spins}\}}\sum_{\{\text{colors}\}}\Big\{T^*T + 2\text{Re}\Big[T^*(V+W)\Big]\Big\} \\ &\equiv \overline{|\mathcal{M}_0|^2} + \overline{|\mathcal{M}_{V+W}|^2}\end{aligned} \tag{2.19}$$

Note the $(V+W)^*(V+W)$ term can be ignored at the order we're interested in. We've already computed $\overline{|\mathcal{M}_0|^2}$ in Eq. (2.3). The interference sum from the virtual gluon is

$$\overline{|\mathcal{M}_{V+W}|^2} = \overline{|\mathcal{M}_0|^2}\ \frac{\alpha_s C_F}{2\pi}\left[\frac{\pi^2}{3} - \frac{7}{2} - 3\ln\beta - \ln^2\beta\right] \tag{2.20}$$

We also need to compute

$$\begin{aligned}\overline{|\mathcal{M}|^2_{q\bar{q}g}} &\equiv \frac{1}{4}\sum_{\{\text{spins}\}}\sum_{\{\text{colors}\}}\sum_{\{\text{polarizations}\}}|R|^2 = \sum_{\{\text{all}\}} RR^* \\ &= \frac{1}{4}\sum_{\{\text{all}\}}\frac{16g^2\pi^2\alpha^2_{\text{EM}}C_F}{s^2(b+M^2)^2(c+M^2)^2}\epsilon^*_\nu(p_3)\epsilon_\beta(p_3)(\bar{v}_+\gamma_\mu u_-\bar{u}_-\gamma_\alpha v_+)\bar{u}_1 \\ &\qquad\qquad \times\Big[(c+M^2)(2p_1^\nu + \gamma^\nu \not{p}_3)\gamma^\mu - (b+M^2)\gamma^\mu(2p_2^\nu + \not{p}_3\gamma^\nu)\Big]v_2\bar{v}_2 \\ &\qquad\qquad \times\Big[(c+M^2)\gamma^\alpha(2p_1^\beta + \not{p}_3\gamma^\beta) - (b+M^2)(2p_2^\beta + \gamma^\beta\not{p}_3)\gamma^\alpha\Big]u_3 \\ &= \frac{-16\pi^3\alpha_s\alpha^2_{\text{EM}}C_F N_c}{s^2(b+M^2)^2(c+M^2)^2}L_{\mu\alpha}H^{\mu\alpha}\end{aligned} \tag{2.21}$$

where

$$\begin{aligned}L_{\mu\alpha} &= \text{Tr}\left[\not{p}_+\gamma_\mu\not{p}_-\gamma_\alpha\right] = 4\left[p_{+\mu}p_{-\alpha} + p_{+\alpha}p_{-\mu} - \frac{s}{2}g_{\mu\alpha}\right] \\ H^{\mu\alpha} &= (c+M^2)^2\,\text{Tr}\left[\not{p}_1(2p_1^\nu + \gamma^\nu\not{p}_3)\gamma^\mu\not{p}_2\gamma^\alpha(2p_{1\nu} + \not{p}_3\gamma_\nu)\right] \\ &\quad + (b+M^2)^2\,\text{Tr}\left[\not{p}_1\gamma^\mu(2p_2^\nu + \not{p}_3\gamma^\nu)\not{p}_2(2p_{2\nu} + \gamma_\nu\not{p}_3)\gamma^\alpha\right] \\ &\quad - (b+M^2)(c+M^2)\,\text{Tr}\left[\not{p}_1\gamma^\mu(2p_2^\nu + \not{p}_3\gamma^\nu)\not{p}_2\gamma^\alpha(2p_{1\nu} + \not{p}_3\gamma_\nu)\right] \\ &\quad - (b+M^2)(c+M^2)\,\text{Tr}\left[\not{p}_1(2p_1^\nu + \gamma^\nu\not{p}_3)\gamma^\mu\not{p}_2(2p_{2\nu} + \gamma_\nu\not{p}_3)\gamma^\alpha\right]\end{aligned} \tag{2.22}$$

The Ward identity for the virtual photon gives $q^\mu L_{\mu\alpha} = q^\mu H_{\mu\alpha} = 0$. This fact, combined with the fact that the 3-body phase space integral over $H_{\mu\alpha}$ gives a function only of q^2 (defined to be $H = H(q^2)$), allows us to write

$$H^{\mu\alpha} = \left(g^{\mu\alpha} - \frac{q^\mu q^\alpha}{q^2} \right) H \tag{2.23}$$

$$L_{\mu\alpha} H^{\mu\alpha} = 4 \left[2p_+ \cdot p_- - \frac{d}{2} s - \frac{2(q \cdot p_+)(q \cdot p_-)}{q^2} + \frac{1}{2} s \right] H = (4 - 2d)\, s\, H \tag{2.24}$$

$$g^{\mu\alpha} L_{\mu\alpha} = 4s(1 - d/2) \tag{2.25}$$

$$g^{\mu\alpha} H_{\mu\alpha} = (d - 1) H \tag{2.26}$$

Looking at Eqs. (2.24) – (2.26), we can make the replacement

$$L_{\mu\alpha} H^{\mu\alpha} \to \frac{1}{d-1} \Big[g^{\mu\alpha} L_{\mu\alpha} \Big] \cdot \Big[g_{\rho\sigma} H^{\rho\sigma} \Big] \tag{2.27}$$

Using this replacement, the traces in $H^{\mu\alpha}$ are easier to evaluate:

$$\begin{aligned} g_{\mu\alpha} H^{\mu\alpha} &= (c + M^2)^2 [-8aM^2 + 8bc] + (b + M^2)^2 [-8aM^2 + 8bc] \\ &\quad - (b + M^2)(c + M^2)[-16a^2 - 32aM^2 - 16a(b + c)] \\ \frac{1}{s^4} g_{\mu\alpha} H^{\mu\alpha} &= 8(1 - x_1)(1 - x_2)(x_1^2 + x_2^2) \\ &\quad + 8\beta \Big[-2 + 4(x_1 + x_2) - 3(x_1^2 + x_2^2) - 4x_1 x_2 + 2(x_1^2 x_2 + x_2^2 x_1) \Big] \end{aligned}$$

x_i is the momentum fraction of particle i (e.g. $x_1 = 2p_1 \cdot q/s$) and $\sum_i x_i = 2$. Note that by exploiting the dot product (i.e. $(q - x_3)^2 = (p_1 + p_2)^2$, etc.),

$$\begin{aligned} a &= s(1 - x_3 + \beta) = s(x_1 + x_2 - 1 + \beta) \\ b &= s(1 - x_2 - \beta) \\ c &= s(1 - x_1 - \beta) \end{aligned} \tag{2.28}$$

Overall then, to $\mathcal{O}(\beta)$,

$$\begin{aligned}\overline{|\mathcal{M}|^2_{q\bar{q}g}} &= \frac{1}{4}\sum_{\{\text{all}\}}|R|^2 \\ &= \frac{512\pi^3\alpha_s\alpha_{\text{EM}}^2 C_F N_c}{3s}\Bigg[\frac{x_1^2+x_2^2}{(1-x_1)(1-x_2)} \\ &\qquad + \beta\frac{-2+4(x_1+x_2)-3(x_1^2+x_2^2)-4x_1x_2+2(x_1^2x_2+x_2^2x_1)}{(1-x_1)^2(1-x_2)^2}\Bigg]\end{aligned} \tag{2.29}$$

2.3.4 Phase-Space Integrals, Total Cross-Section

By combining Eqs. (2.4) and (2.20), the total virtual NLO cross section (in the CM frame) is straighforward:

$$\sigma_{V+W} = \sigma_0\frac{\alpha_s C_F}{2\pi}\left[\frac{\pi^2}{3}-\frac{7}{2}-3\ln\beta-\ln^2\beta\right] \tag{2.30}$$

The $q\bar{q}g$ cross section requires an integral over three-particle phase space:

$$\begin{aligned}\sigma_R = \frac{1}{2s}\int\left(\frac{d^3p_1}{(2\pi)^3}\frac{1}{2E_1}\right)\left(\frac{d^3p_2}{(2\pi)^3}\frac{1}{2E_2}\right)\left(\frac{d^3p_3}{(2\pi)^3}\frac{1}{2E_3}\right)\overline{|\mathcal{M}|^2_{q\bar{q}g}} \\ \times(2\pi)^4\delta^4\big(q-(p_1+p_2+p_3)\big)\end{aligned} \tag{2.31}$$

We can write $d^3p_3/(2E_3) = d^4p_3\,\delta^+(p_3^2-M^2)$ and perform the d^4p_3 integral by using the energy-momentum delta function, leaving us with

$$\sigma_R = \frac{1}{2s}\frac{1}{(2\pi)^5}\int\left(\frac{d^3p_1}{2E_1}\right)\left(\frac{d^3p_2}{2E_2}\right)\overline{|\mathcal{M}|^2_{q\bar{q}g}}\;\delta^+\left((q-p_1-p_2)^2-M^2\right) \tag{2.32}$$

By using $p_1\cdot p_2 = E_1E_2 - \mathbf{p_1}\cdot\mathbf{p_2} = x_1x_2(s/4)(1-\cos\theta_{12})$ (where θ_{12} is the angle between $\mathbf{p_1}$ and $\mathbf{p_2}$), we may write

$$\begin{aligned}\sigma_R = \frac{1}{2s}\frac{1}{(2\pi)^5}\int\left(\frac{d^3p_1}{2E_1}\right)\left(\frac{d^3p_2}{2E_2}\right)\overline{|\mathcal{M}|^2_{q\bar{q}g}} \\ \times\delta^+\left\{s\left(1-\beta-x_1-x_2+\frac{x_1x_2}{2}(1-\cos\theta_{12})\right)\right\}\end{aligned} \tag{2.33}$$

There are six integrals left to do, but we can perform four of the integrals by exploiting the delta function and the isotropy of the problem (reflected in the fact that the amplitude is a function only of x_1 and x_2). We can change the d^3p_1 and d^3p_2 measures to spherical coordinates, and perform the integral over the solid angle of particle 1 (giving a factor of 4π). Next, we can perform one integral over the azimuthal angle of particle 2, giving a factor of 2π. This gives

$$\begin{aligned}\sigma_R &= \frac{1}{s}\frac{1}{(2\pi)^3}\int \frac{dE_1 dE_2 E_1^2 E_2^2\, d\cos\theta_{12}}{4E_1E_2}\overline{|\mathcal{M}|^2_{q\bar{q}g}}\,\delta^+\left\{s\left(\cdots+\frac{x_1x_2}{2}(1-\cos\theta_{12})\right)\right\} \\ &= \frac{1}{s}\frac{1}{(2\pi)^3}\int \frac{dE_1 dE_2 E_1 E_2}{4}\overline{|\mathcal{M}|^2_{q\bar{q}g}}\frac{2}{sx_1x_2} \qquad \left(\text{note } E_i = x_i\frac{\sqrt{s}}{2}\right) \\ &= \frac{1}{256\pi^3}\int dx_1 dx_2 \overline{|\mathcal{M}|^2_{q\bar{q}g}}\end{aligned} \tag{2.34}$$

The kinematics of the three-body final state are such that $2\sqrt{\beta} \le x_3 \le 1+\beta$, $x_1 \le 1-\beta$, and $x_2 \le 1-\beta$. This leads to the real-radiation cross section

$$\begin{aligned}\sigma_R &= \frac{2\alpha_a\alpha_{\rm EM}^2 C_F N_c}{3s}\int_0^{1-\beta} dx_1 \int_{1-\beta-x_1}^{1-\frac{\beta}{1-x_1}} dx_2 \left[\frac{x_1^2+x_2^2}{(1-x_1)(1-x_2)}\right. \\ &\qquad \left. + \beta\frac{-2+4(x_1+x_2)-3(x_1^2+x_2^2)-4x_1x_2+2(x_1^2x_2+x_2^2x_1)}{(1-x_1)^2(1-x_2)^2}\right] \\ &= \sigma_0\frac{\alpha_s C_F}{2\pi}\left[5-\frac{\pi^2}{3}+3\ln\beta+\ln^2\beta\right]\end{aligned} \tag{2.35}$$

Putting everything together, the total cross section up to NLO is

$$\sigma_0+\sigma_1 = \sigma_0+\sigma_{V+W}+\sigma_R = \sigma_0\left(1+\frac{3\alpha_s C_F}{4\pi}\right) \tag{2.36}$$

2.3.5 Cross-Section and Thrust

Here we will restrict final-states to those that have thrust $T \le T^c$, where T^c is a thrust cut that regulates the infrared divergence. To find $\sigma_R(T^c)$, we may take the expression for σ_R in the previous section and change the limits of integration to functions of T^c; we can set $\beta = 0$ as it is no longer needed. The cross section becomes (changing to the other thrust variable $\tau^c \equiv 1-T^c$):

$$\begin{aligned}
\sigma_R(T^c) &= \frac{4\pi\alpha_{\rm EM}^2 N_c}{3s}\frac{\alpha_s C_F}{2\pi}\int_{2-2T^c}^{T^c} dx_3 \int_{2-T^c-x_3}^{T^c} dx_4 \left[\frac{x_3^2+x_4^2}{(1-x_3)(1-x_4)}\right] \\
&= \sigma_0\frac{\alpha_s C_F}{2\pi}\Bigg[-8 - \frac{\pi^2}{3} + 15T^c - \frac{9}{2}(T^c)^2 + 6(1-2T^c)\mathrm{Tanh}^{-1}\left(3-\frac{2}{T^c}\right) \\
&\qquad + 2\ln^2\left(-1+\frac{1}{T^c}\right) + 4\,\mathrm{Li}_2\left(-1+\frac{1}{T^c}\right)\Bigg] \\
\sigma_R(\tau^c) &= \sigma_0\frac{\alpha_s C_F}{2\pi}\left[\frac{5}{2} - \frac{\pi^2}{3} + 3\ln(\tau^c) + 2\ln^2(\tau^c) + \mathcal{O}(\tau^c)\right] \\
\frac{d\sigma_R(\tau^c)}{d\tau^c} &= \sigma_0\frac{\alpha_s C_F}{2\pi}\frac{1}{\tau^c(1-\tau^c)}\Bigg[3 - 9\tau^c - 3(\tau^c)^2 + 9(\tau^c)^3 \\
&\qquad - \left(4 - 6\tau^c + 6(\tau^c)^2\right)\ln\left(\frac{1-2\tau^c}{\tau^c}\right)\Bigg]
\end{aligned} \tag{2.37}$$

2.3.6 Fragmentation and Quark Momentum Fraction

The differential cross section over the momentum fraction z of the quark is determined by taking Eq. (2.35) with the replacement $x_1 \to z$. The superscript q on σ refers to the fact that we're looking at the cross-section of the quark — the variable z is the momentum fraction of the quark. The next subsection will look at $d\sigma_R^q/dz$.

$$\begin{aligned}
\frac{d\sigma_R^q}{dz} &= \sigma_0\frac{\alpha_s C_F}{2\pi}\theta(1-(z+\beta))\int_{1-\beta-z}^{1-\frac{\beta}{1-z}} dx_2 \Bigg[\frac{z^2+x_2^2}{(1-z)(1-x_2)} \\
&\qquad + \beta\frac{-2+4(z+x_2)-3(z^2+x_2^2)-4zx_2+2(z^2x_2+x_2^2z)}{(1-z)^2(1-x_2)^2}\Bigg] \\
&= \sigma_0\frac{\alpha_s C_F}{2\pi}\frac{\theta(1-(z+\beta))}{2(1-z)}\Bigg[-2-z^2+2(1+z^2)\ln\left(z(1-z)\right) \\
&\qquad - 2(1+z^2)\ln\beta + \frac{5}{4}\delta(1-(z+\beta))\Bigg]
\end{aligned} \tag{2.38}$$

The above was obtained by doing the integral in Mathematica then series expanding in β. When keeping only terms up to and including $\mathcal{O}(\beta^0)$, the delta function piece $\delta(1-(z+\beta))$ needs to be put in by hand in order to reproduce the correct overall cross section for σ_R^q. Note that the step-function θ will be used in this and future subsections to emphasize the physical bounds of parameters.

In order for the plus distributions to be well-defined at $z \approx 1$ (that is, in order to include the appropriate delta functions $\delta(1-z)$ to cancel the β-dependence in the virtual diagrams), we will replace $z \to z-\beta$:

$$\frac{d\sigma_R^q}{dz} = \sigma_0 \frac{\alpha_s C_F}{2\pi} \frac{\theta(1-z)}{2(1-z+\beta))} \Big[-2 - z^2 + 2(1+z^2)\ln\big(z(1-z+\beta)\big) - 2(1+z^2)\ln\beta \Big] \tag{2.39}$$

Note the following identities to replace the $z \to 1$ divergences with plus distributions and delta functions:

$$\begin{aligned}
\frac{-1-z^2/2-(1+z^2)\ln\beta}{(1-z+\beta)} &= \left(\frac{-1-z^2/2-(1+z^2)\ln\beta}{(1-z+\beta)}\right)_+ \\
&\qquad + \left(\frac{3}{4} + 3\ln\beta + 2\ln^2\beta\right)\delta(1-z) \\
&= \frac{-1-z^2/2-(1+z^2)\ln\beta}{(1-z)_+} \\
&\qquad + \left(\frac{3}{2}\ln\beta + 2\ln^2\beta\right)\delta(1-z) \\
\frac{(1+z^2)\ln(1-z+\beta)}{(1-z+\beta)} &= \left(\frac{(1+z^2)\ln(1-z+\beta)}{1-z+\beta}\right)_+ + \left(\frac{7}{4} - \ln^2\beta\right)\delta(1-z) \\
&= (1+z^2)\left(\frac{\ln(1-z)}{1-z}\right)_+ - (\ln^2\beta)\delta(1-z)
\end{aligned} \tag{2.40}$$

Most of the β-dependent pieces (all but those that explicitly multiply the splitting function) explicitly cancel with those of the virtual+wavefunction diagram contribution:

$$\frac{d\sigma_{V+W}^q}{dz} = \sigma_{V+W}\delta(1-z) = \sigma_0 \frac{\alpha_s C_F}{2\pi}\left[\frac{\pi^2}{3} - \frac{7}{2} - 3\ln\beta - \ln^2\beta\right]\delta(1-z) \tag{2.41}$$

Note

$$\frac{-1-z^2/2}{(1-z)_+} = -\frac{3}{2}\frac{1}{(1-z)_+} + \frac{1}{2} + \frac{z}{2} \tag{2.42}$$

$$P_{qq}(z) = \left(\frac{1+z^2}{1-z}\right)_+ = \frac{1+z^2}{(1-z)_+} + \frac{3}{2}\delta(1-z) \tag{2.43}$$

Putting everything together, we have

$$\frac{d\sigma_1^q}{dz} = \sigma_0 \frac{\alpha_s C_F}{2\pi}\Bigg\{ - P_{qq}(z)\ln\beta + (1+z^2)\left[\left(\frac{\ln(1-z)}{1-z}\right)_+ + \frac{\ln z}{1-z}\right] - \frac{3}{2}\frac{1}{(1-z)_+} + \frac{1}{2} + \frac{z}{2} + \left(\frac{\pi^2}{3} - \frac{7}{2} + \frac{5}{4}\right)\delta(1-z)\Bigg\} \tag{2.44}$$

We must subtract the fragmentation function from this to obtain the partonic $d\hat{\sigma}_1^q/dz$. The reason for this will be explained in Eq. (2.78). From Eq. (3.29) of Ref. [14], the fragmentation function with a gluon mass is given by

$$D_{q,1}^q(z,\beta) = \frac{\alpha_s C_F}{2\pi}\theta(z)\Bigg[P_{qq}(z)\left(\ln\frac{\tilde{\mu}^2}{M^2} - \ln z\right) - \left(\frac{\pi^2}{3} - \frac{9}{4}\right)\delta(1-z) - 2(1-z)\theta(1-z)\Bigg] \tag{2.45}$$

This leaves us with the result

$$\frac{d\hat{\sigma}_1^q}{dz} = \sigma_0 \frac{\alpha_s C_F}{2\pi}\Bigg\{ P_{qq}(z)\ln\frac{s}{\tilde{\mu}^2} + (1+z^2)\left[\left(\frac{\ln(1-z)}{1-z}\right)_+ + 2\frac{\ln z}{1-z}\right] - \frac{3}{2}\frac{1}{(1-z)_+} + \frac{5}{2} - \frac{3z}{2} + \left(\frac{2\pi^2}{3} - \frac{9}{2}\right)\delta(1-z)\Bigg\} \tag{2.46}$$

2.3.7 Fragmentation and Gluon Momentum Fraction

The computation of $d\hat{\sigma}_1^g/dz$ is similar to previous subsection, except we need only look at the real emission diagram, as this is the only one that contributes to

first order in α_s. Note that the phase space integrand must have the replacement $x_1 \to 2 - x_2 - x_3$ and the limits of integration change accordingly.

$$\begin{aligned}\frac{d\sigma_R^g}{dz} &= \sigma_0 \frac{\alpha_s C_F}{2\pi}\theta(1-(z-\beta)) \int_{\frac{1}{2}\left(2-z-\sqrt{z^2-4\beta}\right)}^{\frac{1}{2}\left(2-z+\sqrt{z^2-4\beta}\right)} dx_2 \left[\begin{array}{c}\text{same integrand as Eq. (2.38)} \\ \text{with } z \to 2-x_2-z\end{array}\right] \\ &= \sigma_0 \frac{\alpha_s C_F}{2\pi}\frac{\theta(1-(z-\beta))}{z}\Big[-4z^2 + (2-2z+z^2)(4\ln z - 2\ln\beta)\Big] \\ &= \sigma_0 \frac{\alpha_s C_F}{2\pi}\Big[\theta(1-z)(-4z) + P_{gq}(z)(4\ln z - 2\ln\beta)\Big]\end{aligned} \tag{2.47}$$

where we've used the fact that the splitting function is $P_{gq}(z) = \theta(1-z)\frac{1+(1-z)^2}{z} = \theta(1-z)\frac{2-2z+z^2}{z}$. We must subtract twice the fragmentation function (for a quark and antiquark) from this to obtain $d\hat{\sigma}_1^g$. From Eq. (3.29) of Ref. [14], the fragmentation function with a gluon mass is given by:

$$D_{q,1}^g(z,\mu) = \frac{\alpha_s C_F}{2\pi}\theta(z)\left\{\left[\ln\frac{\tilde{\mu}^2}{M^2} - \ln(1-z)\right]P_{gq}(z) - 2\theta(1-z)z\right\} \tag{2.48}$$

Combining terms, we get

$$\frac{d\hat{\sigma}_1^g}{dz} = \sigma_0 \frac{\alpha_s C_F}{2\pi} P_{gq}(z)\left[2\ln\frac{s}{\tilde{\mu}^2} + 2\ln(1-z) + 4\ln z\right] \tag{2.49}$$

2.3.8 Fragmentation with a Thrust Cut

We can also look at the differential cross sections over momentum fractions z given a thrust cut τ^c on the final state. Again, the thrust cut regulates the IR-divergence, and so we can set $\beta = 0$. For the quark,

$$\begin{aligned}\frac{d\hat{\sigma}_1^q(T \le T^{\text{cut}})}{dz} &= \sigma_0 \frac{\alpha_s C_F}{2\pi}\theta(T^{\text{cut}} - z)\theta(z + 2T^{\text{cut}} - 2)\int_{2-T^c-z}^{T^c} dx_2 \left[\frac{z^2+x_2^2}{(1-z)(1-x_2)}\right] \\ \frac{d\hat{\sigma}_1^q(\tau \ge \tau^c)}{dz} &= \sigma_0 \frac{\alpha_s C_F}{2\pi}\theta(1-z-\tau^c)\theta(z-2\tau^c)\left[\frac{z^2-4z+8\tau^c-2z\tau^c}{2(1-z)}\right. \\ &\qquad \left. + P_{qq}(z)\ln\frac{z-\tau^c}{\tau^c}\right]\end{aligned} \tag{2.50}$$

For the gluon,

$$\frac{d\hat{\sigma}_1^g(T \leq T^{\rm cut})}{dz} = \sigma_0 \frac{\alpha_s C_F}{2\pi} \theta(T^{\rm cut} - z)\theta(z + 2T^{\rm cut} - 2) \int_{2-T^c-z}^{T^c} dx_2 \big[\cdots\big]$$
$$\frac{d\hat{\sigma}_1^g(\tau \geq \tau^c)}{dz} = \sigma_0 \frac{\alpha_s C_F}{2\pi} \theta(1 - z - \tau^c)\theta(z - 2\tau^c) \left[4\tau^c - 2z + P_{gq}(z) \ln \frac{z - \tau^c}{\tau^c}\right] \tag{2.51}$$

where the $[\cdots]$ in Eq. (2.51) is the same integrand as in Eq. (2.50), but with the replacement $x_2 \to 2 - x_2 - z$. Eqs. (2.50) and (2.51) agree with the calculations performed in Refs. [15–17].

2.4 NLO Calculation with Dimensional Regularization

This section will redo the computations done in the previous section, now using dimensional regularization (in $d = 4-2\epsilon$ dimensions) to regulate the infrared divergences. Many of the equations in the previous section which were β-dependent (divergent in the $\beta \to 0$ limit) will be replaced with their analogous ϵ-dependent counterparts (divergent in the $\epsilon \to 0$ limit). The splitting functions and physical differential cross sections will remain the same, but the fragmentation functions and other intermediate results are regulator-dependent and will be different here than in the previous section.

2.4.1 Virtual Diagram Amplitudes V and W

Following the same conventions as in the previous section, the virtual diagram is given by Eqs. (2.7)-(2.8) but with $\beta = 0$ (no gluon mass). At this point in the computation, ϵ is regulating both UV and IR-divergences, where $\epsilon > 0$ is required to regulate the UV divergences (i.e., $d < 4$) and $\epsilon < 0$ is required to regulate the IR divergences (i.e., $d > 4$). In what follows, however, ϵ is understood to be positive; a discussion of the UV and IR pieces of the computation will follow shortly.

Write $I = I_1 + I_2$, where I_1 is the part of I resulting from N_1 and I_2 is the part of I resulting from N_2. The analogous computation leading up to Eq. (2.12) here gives

$$\begin{aligned} I_1 &= \gamma^\mu \frac{i}{(4\pi)^2}\left[\frac{1}{\epsilon} + 1 + L_s\right] \\ I_2 &= \gamma^\mu \frac{i}{(4\pi)^2}\left[-\frac{2}{\epsilon^2} + \frac{2L_s - 4}{\epsilon} - 9 + \frac{\pi^2}{6} + 4L_s - L_s^2\right] \end{aligned} \tag{2.52}$$

where $L_s \equiv \ln(-s/\tilde{\mu}^2 - i0^+)$. We can omit the imaginary pieces with the foresight that they will not contribute to the overall cross section (as in the previous section), with the caveat that the L_s^2 piece has real part $\ln^2(s/\tilde{\mu}^2) - \pi^2$. Note the integral I_2 necessarily only contains IR-divergences, as this was the piece that involved an integral over $(d^d\ell)/\ell^6$, which converges as $|\ell^2| \to \infty$ for $d = 4$. Therefore, even though the ϵ pieces of I_2 above are positive, we can think ϵ as being a negative regulator for the integral and then redefining the regulator after the integration to a positive quantity. The integral I_1 is an integral over $(d^d\ell)\ell^2/\ell^6$ and ostensibly contains both ultraviolet and infrared divergences; it turns out that the only divergence is ultraviolet. This can be seen by knowing that the ultraviolet divergence must match the UV divergence in Eq. (2.12). Adding the two together, and giving subscripts to keep track of the origin of the two infinities, gives

$$I = \gamma^\mu \frac{i}{(4\pi)^2}\left[\frac{1}{\epsilon_{\rm UV}} - \frac{2}{\epsilon_{\rm IR}^2} + \frac{2L_s - 4}{\epsilon_{\rm IR}} - 8 + \frac{\pi^2}{6} + 3L_s - L_s^2\right] \tag{2.53}$$

in agreement with Eq. (17) of Ref. [18].

The contribution from the wavefunction renormalization diagrams in dimensional regularization, analogous to Eq. (2.14) in the previous section, gives $\not{p}$ times a scaleless integral and is therefore zero in dimensional regularization. However, the integral (over $(d^d\ell)/\ell^4$) includes UV and IR diverges which cancel: the UV divergence is the same as before, and from that we can infer the IR divergence is equal and opposite to this. Thus, the total wavefunction renormalization contributes a piece

$$W = -iC_F \frac{\alpha_s \alpha_{\rm EM}}{s} \bar{v}_+ \gamma_\mu u_- \bar{u}_1 \gamma^\mu v_2 \left[\frac{1}{\epsilon_{\rm UV}} - \frac{1}{\epsilon_{\rm IR}}\right] \tag{2.54}$$

Adding this to the virtual amplitude, the $1/\epsilon_{\rm UV}$ pieces cancel, and

$$V+W = iC_F\frac{\alpha_s\alpha_{\rm EM}}{s}\bar{v}_+\gamma_\mu u_-\bar{u}_1\gamma^\mu v_2\left[-\frac{2}{\epsilon_{\rm IR}^2}+\frac{2L_s-3}{\epsilon_{\rm IR}}-8+\frac{\pi^2}{6}+3L_s-L_s^2\right] \tag{2.55}$$

$$V+W = iC_F\frac{\alpha_s\alpha_{\rm EM}}{s}\bar{v}_+\gamma_\mu u_-\bar{u}_1\gamma^\mu v_2\Bigg[-\frac{2}{\epsilon_{\rm IR}^2}+\frac{2\ln(s/\tilde{\mu}^2)-3}{\epsilon_{\rm IR}}-8+\frac{7\pi^2}{6} + 3\ln(s/\tilde{\mu}^2)-\ln^2(s/\tilde{\mu}^2)\Bigg] \tag{2.56}$$

where Eq. (2.56) omits the imaginary pieces, which do not contribute to the physical cross section.

2.4.2 Real Radiation Diagram Amplitude R

The amplitude R for the real radiation diagrams is given by Eq. (2.18) under the limit $M^2 \to 0$:

$$R = \frac{-4g\pi\alpha_{\rm EM}}{s}(\bar{v}_+\gamma_\mu u_-)\epsilon_\nu^*(p_3)\bar{u}_1\left[\frac{2p_1^\nu+\gamma^\nu\not{p}_3}{2p_1\cdot p_3}\gamma^\mu-\gamma^\mu\frac{2p_2^\nu+\not{p}_3\gamma^\nu}{2p_2\cdot p_3}\right]T^A v_2 \tag{2.57}$$

2.4.3 Spin-Summed Amplitudes Squared

We now need to sum over final spins and average over initial spins of the amplitudes squared.

The discussion above and leading to Eq. (2.20) applies here, and the analogous quantity here is

$$\overline{|\mathcal{M}_{V+W}|^2} = \overline{|\mathcal{M}_0|^2}\,\frac{\alpha_s C_F}{2\pi}\left[\frac{-2}{\epsilon_{\rm IR}^2}+\frac{2\ln(s/\tilde{\mu}^2)-3}{\epsilon_{\rm IR}}-8+\frac{7\pi^2}{6}+3\ln(s/\tilde{\mu}^2)-\ln^2(s/\tilde{\mu}^2)\right] \tag{2.58}$$

We also need to compute

$$\begin{aligned}\overline{|\mathcal{M}|^2_{q\bar{q}g}} &\equiv \frac{1}{4}\sum_{\{\rm spins\}}\sum_{\{\rm colors\}}\sum_{\{\rm polarizations\}}|R|^2 = \frac{1}{4}\sum_{\{\rm all\}}RR^* \\ &= \frac{-16\pi^3\alpha_s\alpha_{\rm EM}^2 C_F N_c}{s^2b^2c^2}L_{\mu\alpha}H^{\mu\alpha}\end{aligned} \tag{2.59}$$

where $L_{\mu\alpha}$ and $H^{\mu\alpha}$ are defined as in Eq. (2.22) with $M^2 \to 0$. The calculation is nearly identical to Eqs. (2.23) to (2.28), but care must be taken in trace identities in $d = 4 - 2\epsilon$. The result is not just Eq. (2.29) with the replacement $\beta \to 0$, but modified to

$$\overline{|\mathcal{M}|^2_{q\bar{q}g}} = \frac{1}{4}\sum_{\{\text{all}\}} |R|^2 = \frac{512\pi^3\alpha_s\alpha^2_{\text{EM}}C_F N_c}{(3-2\epsilon)s}\left[\frac{x_1^2 + x_2^2 - \epsilon x_3^2}{(1-x_1)(1-x_2)}\right](1-\epsilon)^2 \tag{2.60}$$

It is still the case that $x_1 + x_2 + x_3 = 2$, and so the above is a function of x_1 and x_2 alone.

2.4.4 Phase-Space Integrals, Total Cross-Section

$\overline{|\mathcal{M}_{V+W}|^2}$ has no dependence on the particular kinematics of the final state, and the integral over the d-dimensional, two-body phase space (with flux factor) simply gives

$$\sigma_{V+W} = \sigma_0^d \frac{\alpha_s C_F}{2\pi}\left[-\frac{2}{\epsilon^2_{\text{IR}}} + \frac{2\ln(s/\tilde{\mu}^2) - 3}{\epsilon_{\text{IR}}} - 8 + \frac{7\pi^2}{6} + 3\ln(s/\tilde{\mu}^2) - \ln^2(s/\tilde{\mu}^2)\right] \tag{2.61}$$

where σ_0^d is the tree-level cross section in d-dimensions (this is given explicitly in Eq. (2.71))

In d-dimensions, the three-body phase space integrals are modified. Here we generalize the derivation in subsection 2.3.4:

$$\sigma_R = \frac{1}{2s}\int\left(\frac{d^{d-1}p_1}{(2\pi)^{d-1}}\frac{1}{2E_1}\right)\left(\frac{d^{d-1}p_2}{(2\pi)^{d-1}}\frac{1}{2E_2}\right)\left(\frac{d^{d-1}p_3}{(2\pi)^{d-1}}\frac{1}{2E_3}\right)\overline{|\mathcal{M}|^2_{q\bar{q}g}} \times (2\pi)^d\delta^d\big(q - (p_1+p_2+p_3)\big) \tag{2.62}$$

We can write $d^{d-1}p_3/(2E_3) = d^dp_3\,\delta\,(p_3^2)$ and perform the d^dp_3 integral by using the energy-momentum delta function, leaving us with

$$\sigma_R = \frac{1}{2s}\frac{1}{(2\pi)^{2d-3}}\int\left(\frac{d^{d-1}p_1}{(2\pi)^{d-1}}\frac{1}{2E_1}\right)\left(\frac{d^{d-1}p_2}{(2\pi)^{d-1}}\frac{1}{2E_2}\right)\overline{|\mathcal{M}|^2_{q\bar{q}g}}\;\delta\left((q-p_1-p_2)^2\right) \tag{2.63}$$

By using $p_1 \cdot p_2 = E_1 E_2 - \mathbf{p_1} \cdot \mathbf{p_2} = x_1 x_2 (s/4)(1 - \cos\theta_{12})$ (where θ_{12} is the angle between $\mathbf{p_1}$ and $\mathbf{p_2}$), we may write

$$\sigma_R = \frac{1}{2s} \frac{1}{(2\pi)^{2d-3}} \int \left(\frac{d^{d-1}p_1}{(2\pi)^{d-1}} \frac{1}{2E_1} \right) \left(\frac{d^{d-1}p_2}{(2\pi)^{d-1}} \frac{1}{2E_2} \right) \overline{|\mathcal{M}|^2_{q\bar{q}g}} \times \delta\left\{ s \left(1 - x_1 - x_2 + \frac{x_1 x_2}{2}(1 - \cos\theta_{12}) \right) \right\} \tag{2.64}$$

There are $2d-2$ integrals left to do, but we can perform $2d-4$ of the integrals by exploiting the delta function and the isotropy of the problem (reflected in the fact that the amplitude is a function only of x_1 and x_2). We can change the $d^{d-1}p_1$ and $d^{d-1}p_2$ measures to spherical coordinates, and perform $d-2$ integrals over the solid angle of particle 1. When $d = 4$ ($n = 3$), this is simply 4π, but in general this must be derived from the volume / surface area of an $(n-1)$-sphere:

$$V_n(R) = \frac{\pi^{n/2}}{\Gamma(n/2+1)} R^n \qquad S_{n-1}(R) = \frac{n\pi^{n/2}}{\Gamma(n/2+1)} R^{n-1} = \frac{2\pi^{n/2}}{\Gamma(n/2)} R^{n-1} \tag{2.65}$$

This gives a "solid-angle" of $2\pi^{d/2-1/2} / \Gamma(d/2 - 1/2)$. Next, we can perform $d-3$ integrals over all angles of particle 2 other than a polar angle θ_1 (describing the angle between particles 1 and 2). For this we need the volume element of the $(n-2)$-sphere in terms of the angles of the generalized spherical coordinate system:

$$\begin{aligned} d_{S_{n-2}} V &= r^{n-2} \sin^{n-3}\theta_1 \sin^{n-4}\theta_2 \cdots \sin\theta_{n-3}\, dr d\theta_1 \cdots d\theta_{n-2} \\ &= \sin^{n-3}\theta_1\, d\theta_1 r d_{S_{n-3}} V \end{aligned} \tag{2.66}$$

(where $\theta_i \in [0, \pi]$ for $i = 1, \ldots, n-3$ and $\theta_{n-2} \in [0, 2\pi)$). The integral over the $d-3$ remaining angles of particle 2 gives a factor $2\pi^{d/2-1} / \Gamma(d/2-1)$, and we can combine the two gamma functions with the identity $\Gamma(d/2 - 1/2)\,\Gamma(d/2-1) = 2^{3-d}\sqrt{\pi}\,\Gamma(d-2)$. So far, this gives

$$\sigma_R = \frac{1}{2s} \frac{4\pi^{d-3/2}}{(2\pi)^{2d-3} 2^{3-d}\sqrt{\pi}\Gamma(d-2)} \int \frac{dE_1 dE_2 E_1^{d-2} E_2^{d-2}\, d\cos\theta_1}{4E_1 E_2} \overline{|\mathcal{M}|^2_{q\bar{q}g}} \sin^{d-4}\theta_1 \times \delta\left\{ s \left(1 - x_1 - x_2 + \frac{x_1 x_2}{2}(1 - \cos\theta_1) \right) \right\} \tag{2.67}$$

The delta function gives

$$\cos\theta_1 = 1 - \frac{2}{x_1 x_2}(x_1 + x_2 - 1) \implies \sin^2\theta_1 = \frac{4(1-x_1)(1-x_2)(1-x_3)}{x_1^2 x_2^2} \tag{2.68}$$

$$\sigma_R = \frac{1}{2s}\frac{4\pi^{d-3/2}}{(2\pi)^{2d-3}2^{3-d}\sqrt{\pi}\Gamma(d-2)}\int \frac{dE_1 dE_2 E_1^{d-2}E_2^{d-2}}{4E_1E_2}\overline{|\mathcal{M}|^2_{q\bar{q}g}} \times \left[\frac{4(1-x_1)(1-x_2)(1-x_3)}{x_1^2x_2^2}\right]^{(d-4)/2} \tag{2.69}$$
$$= \left(\frac{4\pi\mu^4}{s}\right)^{2\epsilon}\frac{1}{\Gamma(2-2\epsilon)}\frac{1}{256\pi^3}\int dx_1dx_2\overline{|\mathcal{M}|^2_{q\bar{q}g}}\prod_{i=1}^{3}\frac{1}{(1-x_i)^\epsilon}$$

where, again, $x_3 = 2 - x_1 - x_2$, and $x_i \equiv 2E_i/\sqrt{s}$.

Plugging Eq. (2.60) into the above,

$$\sigma_R = \frac{512\pi^3\alpha_s\alpha_{\rm EM}^2 C_F N_c}{(3-2\epsilon)s}\left(\frac{4\pi}{s}\right)^{2\epsilon}\frac{1}{\Gamma(2-2\epsilon)}\frac{1}{256\pi^3}(1-\epsilon)^2 \times \int dx_1dx_2\prod_{i=1}^{3}\frac{1}{(1-x_i)^\epsilon}\left[\frac{x_1^2+x_2^2-\epsilon x_3^2}{(1-x_1)(1-x_2)}\right]$$
$$= \sigma_0^d\frac{\alpha_s C_F}{2^{1-2\epsilon}\pi^{1-\epsilon}\Gamma(1-\epsilon)}\left(\frac{\mu^2}{s}\right)^\epsilon\int dx_1dx_2\prod_{i=1}^{3}\frac{1}{(1-x_i)^\epsilon}\left[\frac{x_1^2+x_2^2-\epsilon x_3^2}{(1-x_1)(1-x_2)}\right] \tag{2.70}$$

Eq. (2.70) used the fact that the tree-level cross section is modified in dimensional regularization to (Eq. (20.A.86) of Ref. [19])

$$\sigma_0^d = \sigma_0\,\mu^{2(4-d)}\left(\frac{4\pi}{s}\right)^{(4-d)/2}\frac{3\sqrt{\pi}(d-2)^2}{2^d\Gamma(d/2+1/2)} \tag{2.71}$$

This can be obtained by deriving the 2-body phase space in d-dimensions and combining with the hadronic and leptonic components of the spin-summed amplitude squared. The appropriate factors of μ have been inserted, (1) to make σ_0^d have dimensions of $1/(\text{energy})^{2-\epsilon}$ (the dimensions of cross-section in $d = 4-2\epsilon$ dimensions), and (2) for the rest of the expression to be dimensionless. With

$$\int_0^1 dx_1\int_{1-x_1}^1 dx_2\left[\frac{x_1^2+x_2^2-\epsilon(2-x_1-x_2)^2}{(1-x_1)^{1+\epsilon}(1-x_2)^{1+\epsilon}(x_1+x_2-1)^\epsilon}\right] = \frac{6(1-2\epsilon)(2-(2-\epsilon)\epsilon)\Gamma(2-\epsilon)\Gamma(-\epsilon)^2}{\Gamma(4-3\epsilon)} \tag{2.72}$$

and replacing $\mu^2 \to e^\gamma\tilde{\mu}^2/(4\pi)$ for $\overline{\rm MS}$, we obtain

$$\sigma_R = \sigma_0^d\frac{\alpha_s C_F}{2\pi}\left[\frac{2}{\epsilon_{\rm IR}^2}+\frac{3-2\ln(s/\tilde{\mu}^2)}{\epsilon_{\rm IR}}+\frac{19}{2}-\frac{7\pi^2}{6}-3\ln(s/\tilde{\mu}^2)+\ln^2(s/\tilde{\mu}^2)\right] \tag{2.73}$$

This gives the well-known, previously-obtained result $\sigma_0^d + \sigma_1^d = \sigma_0^d \left(1 + \frac{3\alpha_s C_F}{4\pi}\right)$.

2.4.5 Cross-Section and Thrust

The following relations hold between the angles:[3]

$$\cos\theta_{ij} = \cos(\theta_i - \theta_j) = \frac{x_i x_j - 2x_i - 2x_j + 2}{x_i x_j}$$

$$\cos(\theta_i - \theta) = \cos(\theta_i - \theta_j + \theta_j - \theta) = \cos\theta_{ij}\cos(\theta_j - \theta) + \sin\theta_{ij}\sin(\theta_j - \theta)$$

One can use $\sin\theta_{ij} = \pm\sqrt{\cos^2\theta_{ij}}$. The sign is arbitrary, but $\sin\theta_{12}$ and $\sin\theta_{13}$ should have opposite signs. In addition, the thrust axis is always along the direction with the largest x_i; assuming $x_1 > x_2, x_3$:

$$T = \frac{1}{2}\left(x_1 - x_2\cos\theta_{12} - x_3\cos\theta_{13}\right) = x_1 \tag{2.74}$$

The phase-space for $T \le T^{\rm cut}$ corresponds to the requirement that $x_i \le T^{\rm cut}$:

$$2 - 2T \le x_1 \le T, \qquad 2 - T - x_1 \le x_2 \le T. \tag{2.75}$$

$T^{\rm cut}$ regulates all IR divergences, and so we can simply set $\epsilon = 0$ in the phase-space integral

$$\begin{aligned}
\sigma_R(T \le T^{\rm cut}) &= \sigma_0^d \frac{\alpha_s C_F}{2\pi}\int_{2-2T}^{T} dx_1 \int_{2-T-x_1}^{T} dx_2 \left[\frac{x_1^2 + x_2^2}{(1-x_1)(1-x_2)}\right] \\
&= \sigma_0^d \frac{\alpha_s C_F}{2\pi}\left[4{\rm Li}_2\left(\frac{1-T^{\rm cut}}{T^{\rm cut}}\right) + 2\ln^2\frac{1-T^{\rm cut}}{T^{\rm cut}}\right. \\
&\qquad + (6T^{\rm cut} - 3)\left(\ln\frac{1-T^{\rm cut}}{T^{\rm cut}} - \ln\frac{2-T^{\rm cut}}{T^{\rm cut}}\right) \\
&\qquad \left. - \frac{9}{2}(T^{\rm cut})^2 + 15T^{\rm cut} - 8 - \frac{\pi^2}{3}\right] \\
\sigma_R(\tau \ge \tau^{\rm c}) &= \sigma_0^d \frac{\alpha_s C_F}{2\pi}\left[2\ln^2\tau^{\rm c} + 3\ln\tau^{\rm c} + \frac{5}{2} - \frac{\pi^2}{3} + \mathcal{O}(\tau^{\rm c})\right]
\end{aligned} \tag{2.76}$$

[3]Some of the following results on fragmentation using dimensional regularization are taken from Wouter Waalewjin's notes, unpublished.

where $\tau = 1 - T$ and $\tau^{\rm c} \equiv 1 - T^{\rm cut}$. This reproduces Eq. (2.37), which was previously obtained with a gluon mass IR regulator. The differential cross section in τ^c is the same as before, also in Eq. (2.37). At this point, we will drop the superscript d on the tree-level cross section in d-dimensions.

2.4.6 Fragmentation and Parton Momentum Fractions

The factorization theorem for the production of a hadron h with momentum fraction z, up to $\Lambda_{\rm QCD}/Q$ power corrections, is

$$\frac{d\sigma^h}{dz} = \sum_{i=\{q,\bar{q},g\}} \int \frac{dx}{x} \frac{d\hat{\sigma}^i}{dx} D_i^h\left(\frac{z}{x}\right) \tag{2.77}$$

Replacing h by a quark or a gluon, we find at one-loop order that

$$\begin{aligned}
\frac{d\sigma_1^q}{dz} &= \int \frac{dx}{x}\left[\frac{d\hat{\sigma}_0^q}{dx} D_{q,1}^q\left(\frac{z}{x}\right) + \frac{d\hat{\sigma}_1^q}{dx} D_{q,0}^q\left(\frac{z}{x}\right)\right] \\
&= \int \frac{dx}{x}\left[\sigma_0 \delta(1-x) \times \left(-\frac{1}{\epsilon_{\rm IR}}\right) \frac{\alpha_s C_F}{2\pi} P_{qq}\left(\frac{z}{x}\right) + \frac{d\hat{\sigma}_1^q}{dx}\delta\left(1-\frac{z}{x}\right)\right] \\
&= -\sigma_0 \frac{1}{\epsilon_{\rm IR}} \frac{\alpha_s C_F}{2\pi} P_{qq}(z) + \frac{d\hat{\sigma}_1^q}{dz} \\
\frac{d\sigma_1^g}{dz} &= \int \frac{dx}{x}\left[2\frac{d\hat{\sigma}_0^q}{dx} D_{q,1}^g\left(\frac{z}{x}\right) + \frac{d\hat{\sigma}_1^g}{dx} D_{g,0}^g\left(\frac{z}{x}\right)\right] \\
&= -\sigma_0 \frac{1}{\epsilon_{\rm IR}} \frac{\alpha_s C_F}{\pi} P_{gq}(z) + \frac{d\hat{\sigma}_1^g}{dz}
\end{aligned} \tag{2.78}$$

The factor of 2 in front of the D_q^g term arises because there is a quark and anti-quark contribution (working with a single quark flavor). Subscripts 0 and 1 refer to the order of α_s. We used the fact that in pure dimensional regularization

$$\begin{aligned}
D_q^q(z) &= \delta(1-z) + \frac{\alpha_s C_F}{2\pi} P_{qq}(z)\left(\frac{1}{\epsilon_{\rm UV}} - \frac{1}{\epsilon_{\rm IR}}\right) \\
D_q^g(z) &= \frac{\alpha_s C_F}{2\pi} P_{gq}(z)\left(\frac{1}{\epsilon_{\rm UV}} - \frac{1}{\epsilon_{\rm IR}}\right) \\
D_g^g(z) &= \delta(1-z) + \mathcal{O}(\alpha_s)
\end{aligned} \tag{2.79}$$

$P_{ji} \equiv P_{j\leftarrow i}$ is the splitting function from parton i to parton j [20]:

$$\begin{aligned}
P_{qq}(z) &= \left(\frac{1+z^2}{1-z}\right)_+ = \frac{1+z^2}{(1-z)_+} + \frac{3}{2}\delta(1-z) \\
P_{gq}(z) &= \theta(1-z)\frac{1+(1-z)^2}{z}
\end{aligned} \tag{2.80}$$

When we calculate $d\sigma_1^q/dz$, we should reproduce these IR divergences, such that we are left with a finite $d\hat{\sigma}_1^q/dz$:

$$\begin{aligned}
\frac{d\sigma_R^q}{dz} &= \frac{\sigma_0\,\alpha_s C_F}{2^{1-2\epsilon}\pi^{1-\epsilon}\Gamma(1-\epsilon)}\left(\frac{\mu^2}{s}\right)^{\epsilon}\int_{1-z}^{1}dx_2\left[\frac{z^2+x_2^2-\epsilon(2-z-x_2)^2}{(1-z)^{1+\epsilon}(1-x_2)^{1+\epsilon}(z+x_2-1)^{\epsilon}}\right] \\
&= \frac{\sigma_0\,\alpha_s C_F}{2^{1-2\epsilon}\pi^{1-\epsilon}\Gamma(1-\epsilon)}\left(\frac{\mu^2}{s}\right)^{\epsilon}\left[\frac{\sqrt{\pi}\,\Gamma(-\epsilon)}{2^{2(1-\epsilon)}\Gamma(3/2-\epsilon)}\frac{2(1+z^2)+\epsilon(-5z^2+4z-4)}{(1-z)^{1+\epsilon}z^{2\epsilon}}\right. \\
&\qquad\qquad\left. + \frac{2(1-z)^2+\epsilon(2z-3)+\epsilon^2)}{(1-\epsilon)(2-\epsilon)(1-z)^{1+\epsilon}z^{\epsilon}}\right] \\
&= \frac{\sigma_0\,\alpha_s C_F}{2\pi\Gamma(1-\epsilon)}\left(\frac{e^{\gamma}\tilde{\mu}^2}{s}\right)^{\epsilon}\frac{1}{(1-z)^{1+\epsilon}}\left[\frac{-1}{\epsilon}(1+z^2)+2(1+z^2)\ln z+\frac{3}{2}z^2-4z+1\right. \\
&\qquad\left. +\epsilon\left(-2(1+z^2)\ln^2 z+(-2z^2+6z-1)\ln z+\left(\frac{5}{2}+\frac{\pi^2}{6}\right)z^2-6z+\frac{\pi^2}{6}\right)\right] \\
&= \frac{\sigma_0\,\alpha_s C_F}{2\pi\Gamma(1-\epsilon)}\left(\frac{e^{\gamma}\tilde{\mu}^2}{s}\right)^{\epsilon}\left\{\frac{2}{\epsilon^2}\delta(1-z)+\frac{1}{\epsilon}\left[3\,\delta(1-z)-\left(\frac{1+z^2}{1-z}\right)_+\right]\right. \\
&\qquad\qquad +(1+z^2)\left[\left(\frac{\ln(1-z)}{1-z}\right)_+ + \frac{2\ln z}{1-z}\right] \\
&\qquad\qquad \left. +\frac{1}{(1-z)_+}\left[\frac{3}{2}z^2-4z+1\right]+\delta(1-z)\left(\frac{7}{2}-\frac{\pi^2}{3}\right)\right\} \\
&= \sigma_0\frac{\alpha_s C_F}{2\pi}\left\{\frac{2}{\epsilon^2}\delta(1-z)+\frac{1}{\epsilon}\left[\left(3-2\ln(s/\tilde{\mu}^2)\right)\delta(1-z)-\left(\frac{1+z^2}{1-z}\right)_+\right]\right. \\
&\qquad +\left(\ln^2(s/\tilde{\mu}^2)-\frac{\pi^2}{6}\right)\delta(1-z)-3\ln(s/\tilde{\mu}^2)\delta(1-z) \\
&\qquad +\left(\frac{1+z^2}{1-z}\right)_+\ln(s/\tilde{\mu}^2)+(1+z^2)\left[\left(\frac{\ln(1-z)}{1-z}\right)_+ + \frac{2\ln z}{1-z}\right] \\
&\qquad \left. +\frac{1}{(1-z)_+}\left[\frac{3}{2}z^2-4z+1\right]+\delta(1-z)\left(\frac{7}{2}-\frac{\pi^2}{3}\right)\right\}
\end{aligned} \tag{2.81}$$

where we used the plus distribution identity in Eq. (B.2).

We must also add the virtual contribution:

$$\frac{d\sigma^q_{V+W}}{dz} = \sigma_0 \frac{\alpha_s C_F}{2\pi}\left[-\frac{2}{\epsilon^2} + \frac{2\ln(s/\tilde{\mu}^2) - 3}{\epsilon} - 8 + \frac{7\pi^2}{6} + 3\ln(s/\tilde{\mu}^2) - \ln^2(s/\tilde{\mu}^2)\right] \times \delta(1-z) \tag{2.82}$$

Adding the virtual and real contributions, most of the $\epsilon \to 0$ divergences cancel, except for a $1/\epsilon$ pole multiplying the Altarelli-Parisi splitting function:

$$\begin{aligned}\frac{d\sigma^q_1}{dz} &= \sigma_0 \frac{\alpha_s C_F}{2\pi}\left\{ \left(-\frac{1}{\epsilon} + \ln\frac{s}{\tilde{\mu}^2}\right) P_{qq}(z) + (1+z^2)\left[\left(\frac{\ln(1-z)}{1-z}\right)_+ + 2\frac{\ln z}{1-z}\right] \right. \\ &\qquad \left. - \frac{3}{2}\frac{1}{(1-z)_+} + \frac{5}{2} - \frac{3z}{2} + \left(\frac{2\pi^2}{3} - \frac{9}{2}\right)\delta(1-z)\right\} \\ \frac{d\hat{\sigma}^q_1}{dz} &= \sigma_0 \frac{\alpha_s C_F}{2\pi}\left\{ P_{qq}(z)\ln\frac{s}{\tilde{\mu}^2} + (1+z^2)\left[\left(\frac{\ln(1-z)}{1-z}\right)_+ + 2\frac{\ln z}{1-z}\right] \right. \\ &\qquad \left. - \frac{3}{2}\frac{1}{(1-z)_+} + \frac{5}{2} - \frac{3z}{2} + \left(\frac{2\pi^2}{3} - \frac{9}{2}\right)\delta(1-z)\right\}\end{aligned} \tag{2.83}$$

This reproduces the same result found using a gluon mass as the IR-regulator.

Doing the same calculation for the gluon (with only a real radiation contribution, so that $d\sigma^g_1/dz = d\sigma^g_R/dz$) gives:

$$\begin{aligned}\frac{d\sigma^q_1}{dz} &= \frac{\sigma_0\,\alpha_s C_F}{2^{1-2\epsilon}\pi^{1-\epsilon}\Gamma(1-\epsilon)}\left(\frac{\mu^2}{s}\right)^\epsilon \int_{1-z}^1 dx_2 \left[\frac{(2-z-x_2)^2 + x_2^2 - \epsilon z^2}{(z+x_2-1)^{1+\epsilon}(1-x_2)^{1+\epsilon}(1-z)^\epsilon}\right] \\ &= \frac{\sigma_0\,\alpha_s C_F}{2\pi\Gamma(1-\epsilon)}\left(\frac{e^\gamma\tilde{\mu}^2}{s}\right)^\epsilon \frac{1+(1-z)^2}{z}\left[-\frac{2}{\epsilon} + 2\ln(1-z) + 4\ln z\right] \\ &= \sigma_0\frac{\alpha_s C_F}{2\pi}\frac{1+(1-z)^2}{z}\left[-\frac{2}{\epsilon} + 2\ln(s/\tilde{\mu}^2) + 2\ln(1-z) + 4\ln z\right]\end{aligned} \tag{2.84}$$

Subtracting off the divergent piece as per Eq. (2.78), we again obtain

$$\frac{d\hat{\sigma}^g_1}{dz} = \sigma_0\frac{\alpha_s C_F}{2\pi}P_{gq}(z)\left[2\ln\frac{s}{\tilde{\mu}^2} + 2\ln(1-z) + 4\ln z\right] \tag{2.85}$$

2.4.7 Fragmentation with a Thrust Cut

The differential cross section describing the production of a hadron h with momentum fraction z with a cut on thrust is given by a factorization theorem very similar to Eq. (2.77):

$$\frac{d\sigma^h(\tau \geq \tau^c)}{dz} = \sum_{i=\{q,\bar{q},g\}} \int \frac{dx}{x} \frac{d\hat{\sigma}^i(\tau \geq \tau^c)}{dx} D_i^h\left(\frac{z}{x}\right) \tag{2.86}$$

Recall from the analogous computation using a gluon mass that the IR regulator is not required anymore at this stage of the computation: the thrust cut regulates the divergence. Thus the computations for $d\hat{\sigma}_1^q(\tau \geq \tau^c)/dz$ and $d\hat{\sigma}_1^g(\tau \geq \tau^c)/dz$ are exactly the same as in Eqs. (2.50) and (2.51).

All of the above cross sections with thrust cuts give cross sections for $\tau \geq \tau^c$, so that τ^c regulates the infrared divergence and we are left with finite cross sections. However, to remove the b-quark contamination from on-resonance Belle data we actually want to keep events with $\tau \leq \tau^c$! The easiest way to calculate the fragmentation cross section with this thrust cut at NLO is

$$\frac{d\sigma^h(\tau \leq \tau^c)}{dz} = \frac{d\sigma^h}{dz} - \frac{d\sigma^h(\tau \geq \tau^c)}{dz} \tag{2.87}$$

The first term on the right hand side of Eq. (2.87) is calculated via Eq. (2.77) (with the partonic $d\sigma^i/dz$ calculated in that subsection), and the second term is given by Eq. (2.86).

2.5 Factorization Structure of Fragmentation

We return to the discussion of SCET and its relationship to $e^+ + e^- \to q + \bar{q} + g$. The factorization formula we need is similar to Eq. (2.86), focusing on $\tau \leq \tau^c$ events as required to remove the b-quark contamination [14, 21]:

$$\frac{d\sigma^h(\tau \leq \tau^c)}{dz} = \int_0^{\tau^c} d\tau \frac{d^2\sigma^h}{d\tau^c dz} = \sum_{j=g,\,u,\,\bar{u},\,d\ldots} \int_z^1 \frac{dx}{x}\, D_j^h(x,\tilde{\mu})\; C_j\Big(\tau^c, \frac{z}{x}, Q^2, \tilde{\mu}\Big) \tag{2.88}$$

$Q = \sqrt{s}$ is the center-of-mass energy, $D_j^h(x,\tilde{\mu})$ is the unpolarized fragmentation function for parton j hadronizing into h (with h carrying a fraction x of the energy

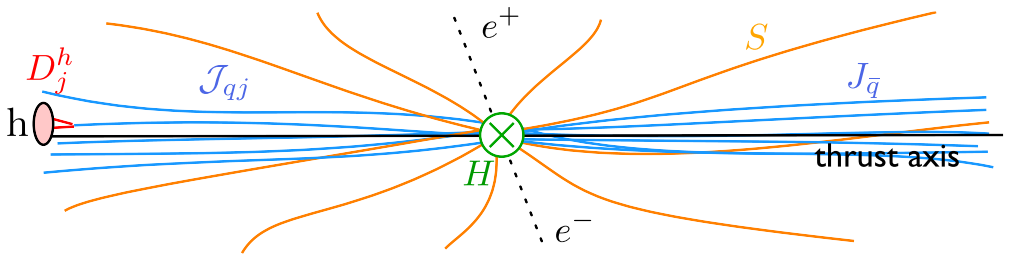

Figure 2.5: A schematic of the various subprocesses in $e^+e^- \to \text{dijet} + h$: The (green) vertex denotes the hard interaction H, the (blue) jets are described by J and $\mathcal{J}_{ij}$ (the latter for the jet in which the hadron is observed), the fragmentation $j \to h$ is described by the fragmentation function D_j^h and the effects of the (orange) soft radiation are contained in S.

of the parent parton j), and C_j is a coefficient describing the partonic event. The fragmentation functions D_j^h are non-perturbative and describe the long-distance hadronization event, whereas the C_j coefficients describing the short-distance partonic event are calculable in SCET and contain large logarithms of τ^c and $(1-z)$.

The coefficients C_j are calculable in SCET. Schematically,

$$C_j\Big(\tau^c, Q^2, \frac{x}{z}, \tilde{\mu}\Big) = \sum_{q\bar{q}=u\bar{u},\, d\bar{d}\ldots} \sigma_0^q\, H(Q^2) \otimes \Big[\mathcal{J}_{qj}(\tau^c Q^2, x/z) \otimes J_{\bar{q}}(\tau^c Q^2) + J_q(\tau^c Q^2) \otimes \mathcal{J}_{\bar{q}j}(\tau^c Q^2, x/z)\Big] \otimes S_\tau^c\Big((\tau^c)^2 Q^2\Big) \Big\{1 + \mathcal{O}\Big[\frac{\Lambda_{\rm QCD}^2}{(1-z)\tau^c Q^2}, \Big(\frac{\Lambda_{\rm QCD}}{\tau^c Q}\Big)^2\Big]\Big\} + C_j^{\rm ns}\Big(\tau^c, Q^2, \frac{x}{z}, \tilde{\mu}\Big) \tag{2.89}$$

C_j is factored into a "hard" coefficient H, "collinear" jet functions[4] $\mathcal{J}$ and J, and a "soft" function S. These pieces describe physics at the various energy scales in the problem: the hard coefficient describes the $e^+e^- \to q\bar{q}$ event, the collinear jet functions describe the showering of the jet, and the soft function describes interactions between the jets; the process is depicted in Figure 2.5. These occur at scales Q, $\sqrt{\tau^c}Q$, and $\tau^c Q$, respectively. $\mathcal{J}_{qj}$ also depends on the fractional energy carried off by parton j (which later hadronizes to h) relative to the energy of its parent quark or antiquark. Quark and hadron masses are treated as negligible;

[4] J is the jet function usually encountered in SCET, while $\mathcal{J}$ is a perturbatively-calculable coefficient which, when convoluted with a fragmentation function, gives a "fragmenting jet function" $\mathcal{G}$. For more information, see Ref. [21], which introduced the fragmenting jet function.

these lead to corrections $\mathcal{O}(m_i^2/(\tau^c Q^2))$ and $\mathcal{O}(m_h^2/(z^2 Q^2))$, respectively.

The hard, collinear, and soft pieces of Eq. (2.89) are given to NNLL in Ref. [14] and references within. Taken together, the pieces resum (singular) large logarithms, but they do not accurately give $C_j^{\rm ns}$, the nonsingular (as $\tau \to 0$) contribution to C_j in Eq. (2.88). A thrust cut τ^c cannot be too low, as (1) we want to have as many events as possible, and (2) we require that $\tau^c Q \gg \Lambda_{\rm QCD}$ so that the soft scale in SCET is still much larger than the hadronization scale $\Lambda_{\rm QCD}$. In fact, a thrust-cut of $\tau^c = 0.2$ will get rid of $\approx$98% of the b-quark contamination [22], allowing us to probe light-quark fragmentation. It is for this reason we need to extract the non-singular contribution $C_j^{\rm ns}$.

2.5.1 Nonsingular Contribution at NLO

The nonsingular contribution to Eq. (2.89) may be obtained from taking the NLO computation and subtracting the singular portion of C_j in Eq. (2.89). To obtain the NLO differential cross section in z and τ^c for a given hadron h (i.e., $d^2\sigma^h/(d\tau^c dz)$ in Eq. (2.88)), take Eqs. (2.50) and (2.51), differentiate with respect to τ^c, convolute with the fragmentation function D_i^h, and sum over patrons i.

Figure 2.6 plots the total differential cross section for $h = \pi^+$ as a function of τ^c for $z = 0.2$ and $z = 0.8$. We use the HKNS Fragmentation Functions [23], and have set $\tilde{\mu} = Q$. The total NLO cross section is given by

$$\begin{aligned}\frac{d^2\sigma^{\pi^+}}{dz d\tau} = \sum_{i=g,\,u,\,\bar{u},\,d\ldots} \int_{\mathrm{Max}\{2\tau^c,\,z\}}^{1-\tau^c} \frac{dx}{x} \frac{d^2\sigma^i(\tau^c)}{dx d\tau} D_i^{\pi^+}\left(\frac{z}{x},\tilde{\mu}\right) \\ + \theta(2\tau^c - z)\frac{1}{x}\frac{d\sigma^i(\tau^c)}{dx} D_i^{\pi^+}\left(\frac{z}{x},\tilde{\mu}\right)\Bigg|_{x\to 2\tau^c} - \frac{1}{x}\frac{d\sigma^i(\tau^c)}{dx} D_i^{\pi^+}\left(\frac{z}{x},\tilde{\mu}\right)\Bigg|_{x\to 1-\tau^c}\end{aligned} \tag{2.90}$$

The terms on the second line of Eq. (2.90) appear because the theta-functions in Eqs. (2.50) and (2.51) give delta-functions when differentiating with respect to τ^c.

Figure 2.6 also gives the nonsingular contribution to the full NLO differential cross section. The nonsingular portion is finite as $\tau \to 0$, providing a check on our result. Note there is a kinematic threshold at NLO for $(\tau^c)^* = \mathrm{Min}\{1/3, 1-z\}$;

for $\tau \geq (\tau^c)^*$, the singular and nonsingular portions cancel in this region because the total differential cross section vanishes.

2.5.2 Correlations Between τ and z

As noted at the beginning of this section, the ingredients to Eq. (2.89) were largely calculated in Ref. [14] and references within. When also taking into account the NLO non-singular contribution, the resummation of threshold logarithms of $(1 - z)$ as in Ref. [24], and the leading nonperturbative correction to the soft function S given in Ref. [25], we find the correlations between τ^c and z as shown in Figure 2.7. These correlations are in agreement with those found in PYTHIA, and they are much more pronounced than at NLO. These correlations must be taken into account when extracting the fragmentation functions from Belle data; a framework for how to do so working in moment space is outlined in Section IV of Ref. [10].

2.6 Conclusions

We have gone through the NLO computation of the (differential) cross-section for $e^+e^- \to q\bar{q}g$, focusing separately on virtual and real radiation diagrams to explore the IR behavior of such a process. It was seen that we could do this computation with various regulators to control IR divergences, and we showed how the IR regulator could be replaced with a cut on the event-shape variable thrust. Even with such a replacement, particular IR divergenes remained, but they could be described in terms of "splitting functions" (described via plus distributions) which are well-behaved in the calculation of any physical process.

Next, we took our NLO result (at the partonic level) and applied it to observables actually seen in the final state (after hadronization occurs). The hadronization process is well-described using Soft-Collinear Effective Theory (SCET), and we used our NLO result to extract the non-singular contribution to the differential cross-section in the dijet limit ($\tau \to 0$). When taking into account other corrections to the SCET calculation, correlations could be seen between the thrust

cut and the momentum fraction of the observed hadron. These correlations need to be taken into account when using Belle data to extract the fragmentation functions from the observed dijet + hadron final-state data.

Portions of Chapter 2 are reprints of material as it appears in *Phys. Rev. D* **87**, 074013 (2012). A. Jain, M. Procura, B. Shotwell, and W. J. Waalewijn. The dissertation author was co-author of this paper.

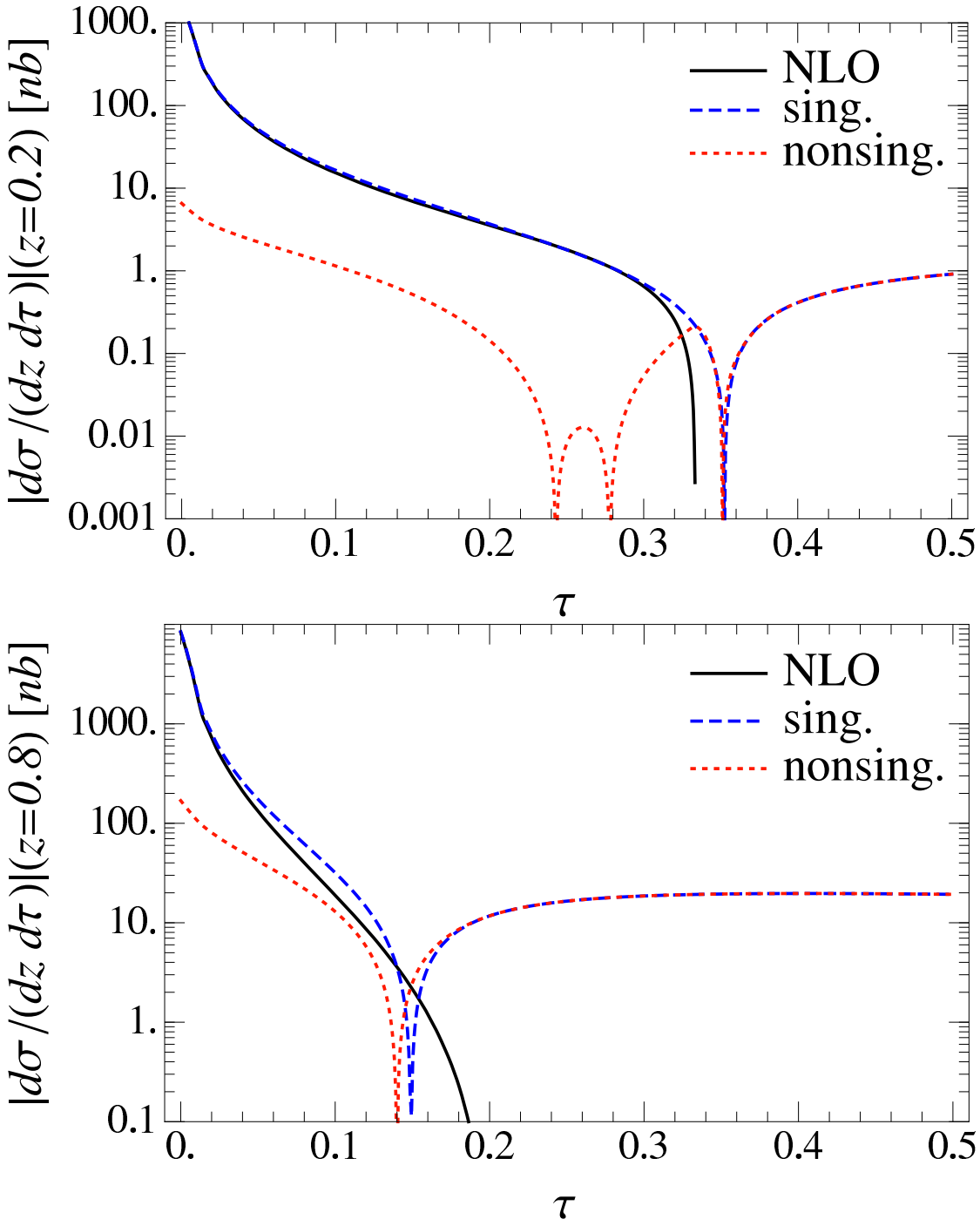

Figure 2.6: The cross section for $e^+e^- \to \text{dijet}+\pi^+$ at $Q = 10.52$ GeV, differential in the momentum fraction z and thrust τ, and separated into its singular and nonsingular contribution. Since these separate pieces can be negative, absolute values are plotted.

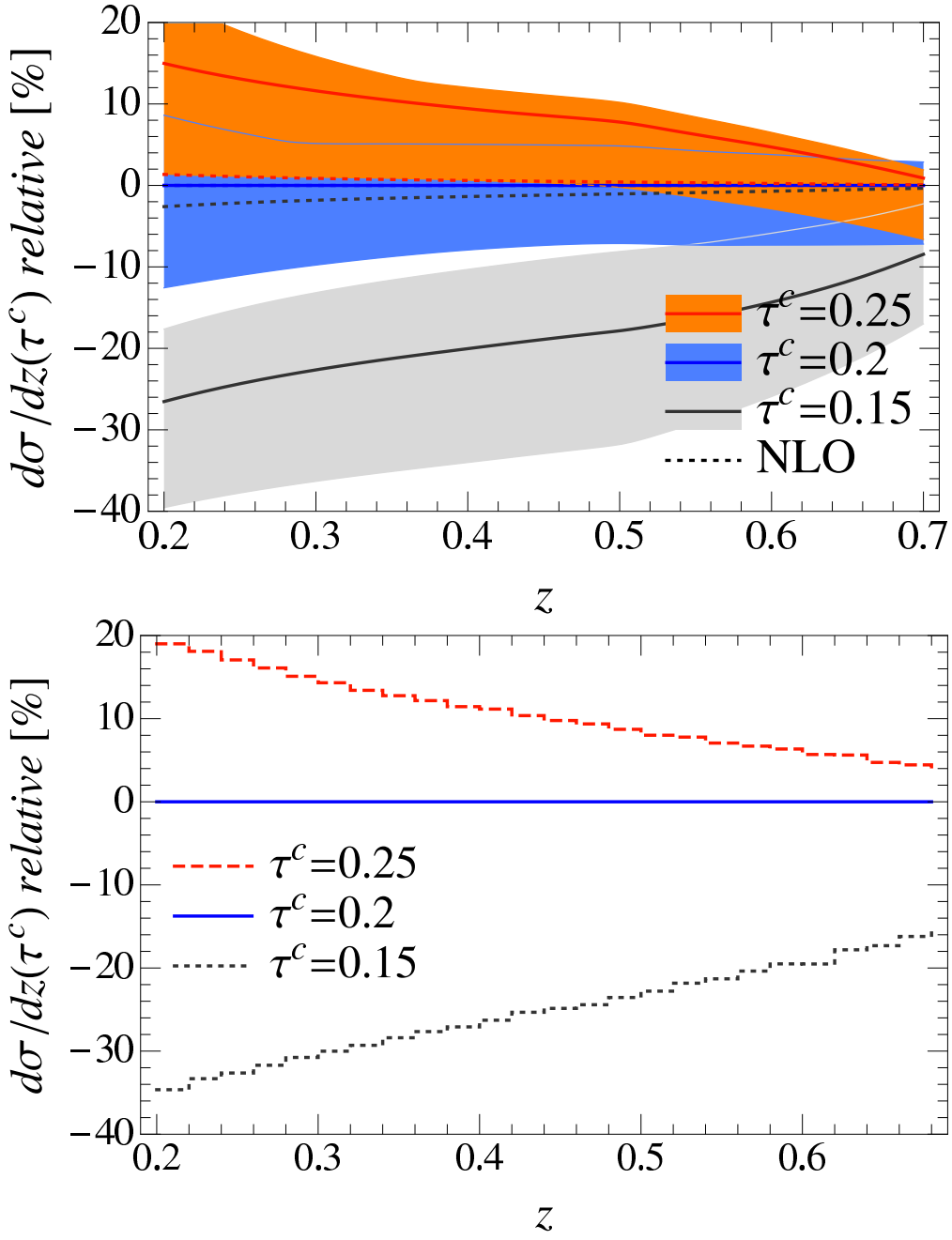

Figure 2.7: Correlations between the thrust cut $\tau \leq \tau^c$ and the observed momentum fraction z in the cross section of $e^+e^- \to$ dijet $+ \pi^+$ for $Q = 10.52$ GeV. Curves and bands are plotted relative to the case $\tau^c = 0.2$. A cut on thrust changes the shape in z. Top panel: our NNLL+NLO results with perturbative uncertainty bands. The result at NLO (dotted lines) contains negligible correlations. As input we use the HKNS fragmentation functions $D_i^{\pi^+}$ [23] at NLO. Bottom panel: the same observable using PYTHIA.

Chapter 3

Electroweak Large Logarithms

We study electroweak Sudakov corrections in high energy scattering, and the cancellation between real and virtual Sudakov corrections. Numerical results are given for the case of heavy quark production by gluon collisions involving the rates $gg \to t\bar{t}, b\bar{b}, t\bar{b}W, t\bar{t}Z, b\bar{b}Z, t\bar{t}H, b\bar{b}H$. Gauge boson virtual corrections are related to real transverse gauge boson emission, and Higgs virtual corrections to Higgs and longitudinal gauge boson emission. At the LHC, electroweak corrections become important in the TeV regime. At the proposed 100 TeV collider, electroweak interactions enter a new regime, where the corrections are very large and need to be resummed.

3.1 Introduction

Electroweak corrections grow with energy due to the presence of Sudakov double logarithms $\alpha_W \ln^2 s/M_W^2$, and are already relevant for LHC analyses with invariant masses in the TeV region. The corrections arise because of soft and collinear infrared divergences from the emission of electroweak bosons. The infrared singularities are cutoff by the gauge boson mass, and lead to finite $\alpha_W \ln^2 s/M_W^2$ corrections. Unlike in QCD, the electroweak logarithms do not cancel even for totally inclusive processes, because the initial states are not electroweak singlets [26–28].

In this paper, we discuss the cancellation (or lack thereof) between real and virtual corrections. We will use $gg \to t\bar{t}, b\bar{b}$ as an explicit numerical example. In

this process, the initial state *is* an electroweak singlet, so the total cross section does not contain $\alpha_W \ln^2 s/M_W^2$ corrections. This allows us to compare the electroweak corrections in this process to the more familiar case of α_s corrections to the R ratio for $e^+e^- \to$ hadrons. Even though electroweak Sudakov corrections cancel for the total cross section, they do not cancel for interesting experimentally measured rates, and are around 10% for invariant masses of $\sim 2\,\text{TeV}$. Some earlier work related to our paper can be found in Refs. [29–32]. Electroweak corrections to processes involving electroweak-charged initial states, such as Drell-Yan production, $q\overline{q} \to WW$, or $q\overline{q} \to t\overline{t}$, are larger than for $gg \to t\overline{t}$.

At present, omitted electroweak corrections are the largest error in many LHC cross section calculations, and are more important than higher order QCD corrections. Furthermore, the resummed electroweak corrections to *all* hard scattering processes at NLL order are known explicitly [33–35], and have a very simple form, so they can be incorporated into LHC cross section calculations. Recently, there has been interest in building a hadron collider with an energy of around 100 TeV. For such a machine, electroweak corrections are no longer small, and resummed corrections must be included to get reliable cross sections. The numerical plots in this paper go out to $\sqrt{\hat{s}} = 30\,\text{TeV}$ to emphasize the importance of electroweak corrections at future machines.

We will make one simplification in this paper, by computing electroweak corrections in a pure $SU(2)_W$ gauge theory, neglecting the $U(1)$ part. The reason is that in the Standard Model (SM), after spontaneous symmetry breaking, there is a massless photon. Electromagnetic corrections produce infrared divergences which are not regularized by a gauge boson mass. Instead they have to be treated by defining infrared safe observables, as done for QCD. Initial state infrared corrections can be absorbed into the parton distribution functions (PDFs). To implement this consistently requires electromagnetic corrections to be included in the parton evolution equations. These additional complications are separate from the main point of the paper, and can be avoided by using the $SU(2)_W$ theory.

The numerical results will be given for an $SU(2)_W$ gauge theory with α_W equal to the Standard Model value $\alpha/\sin^2\theta_W$. We will treat $W^{1,2}$ as the SM W

bosons, and W^3 as the SM Z^0, and use the notation $\mathsf{L} \equiv \ln s/M_W^2$.

The structure of electroweak corrections is discussed in Sec. 3.2, and a summary of the $\mathrm{SCET}_{\mathrm{EW}}$ results for computing these is given in Appendix C. The cancellation of real and virtual electroweak corrections is discussed in Sec. 3.3 for an example where one can do the full computation analytically, and Sec. 3.4 discusses the cancellation for heavy quark production, where the rates have to be computed numerically. Some subtleties for an unstable t-quark are discussed in Sec. 3.4.3. The implications of electroweak corrections for experimental measurements is given in Sec. 3.5.

3.2 Electroweak Logarithms

Electroweak radiative corrections have a typical size of order $\alpha_W/\pi \sim 0.01$. However, in some cases, the radiative corrections have a Sudakov double logarithm, $(\alpha_W/\pi)\mathsf{L}^2$, and become important. The regime where this happens is high energy, $s \gg M_W^2$, where one can apply soft-collinear effective theory (SCET) [2–5]. The electroweak version of SCET ($\mathrm{SCET}_{\mathrm{EW}}$) was developed in a series of papers Refs. [33–41], and has important differences from the QCD case, namely the presence of a broken gauge symmetry, massive gauge bosons, and multiple mass scales M_Z, M_W, M_H and m_t. The effective theory is a systematic expansion in M_W^2/s, and at leading order, all $(M_W^2/s)^n$ power corrections are omitted. The neglect of these power corrections greatly simplifies the computation, and the electroweak corrections have an elegant universal form. We are in the lucky situation where the theory simplifies in the regime where the electroweak corrections are important. Electroweak corrections have been computed by many groups by other methods [26–28, 42–60].

It is instructive to compare the SCET result with the vastly more difficult conventional fixed order approach to computing electroweak corrections. At fixed order one gets an expansion $\sum_{n,r} c_{n,r} \alpha_W^n \mathsf{L}^r$ with $r \leq 2n$, which breaks down at high energies. Furthermore, one has to do a very difficult multi-scale computation (with scales s, M_Z, M_H, m_t) for each new process being considered. The fixed

order results are available only for a few cases, and often with the approximation that $M_W = M_Z = M_H$. In contrast, the SCET result, Eq. (C.2) has a simple form where all the pieces are known, so each new process can be computed by multiplying the appropriate factors, which are all known in closed form. The reason the fixed order calculation is much harder, of course, is that it includes the M_Z^2/s power corrections, which then have to be expanded out. The M_Z^2/s power corrections are negligible in the region where electroweak corrections are large and experimentally important. We summarize the $\mathrm{SCET}_{\mathrm{EW}}$ results in Appendix C. More details can be found in Refs. [33–40].

An explicit numerical analysis comparing fixed order and $\mathrm{SCET}_{\mathrm{EW}}$ results is given in Sec. 3.3.

3.3 Cancellation of Real and Virtual Corrections

Recall the familiar example of the total cross section for $e^+e^- \to$ hadrons, which has an expansion in $\alpha_s(Q^2)$, with no large logarithms. At one-loop, the virtual correction to $e^+e^- \to q\overline{q}$ is infrared divergent, as is the $e^+e^- \to q\overline{q}g$ real radiation rate, but the sum of the two is infrared finite, and gives the correction to the ratio of the e^+e^- total cross section to its tree-level value, $R = 1 + \alpha_s/\pi$.

The electroweak corrections to $gg \to q\overline{q}$ have a similar cancellation. Rather than study this process, we first start with the simpler case of $J \to q\overline{q}$, where $J^\mu = \overline{q}\gamma^\mu P_L q$ is an external gauge invariant current that produces the doublet $q_L = (t, b)_L$, where we treat t and b as massless quarks. The main reason for doing this is to avoid complicated phase space integrals for real radiation, and fermion mass effects, and because it is closely related to the familiar QCD case of R. The $gg \to q\overline{q}$ case with $q_L = (t, b)_L$will be studied numerically in Sec. 3.4.

The total cross section for $J \to q\overline{q}$ can be written as the imaginary part of the vacuum bubbles $\Pi(Q^2)$ in Fig. 3.1. $\Pi(Q^2)$ at Euclidean Q^2 is infrared finite. Thus the analytic continuation to Minkowski space is also infrared finite, and the sum of the real and virtual rates, which is equal to the imaginary part of $\Pi(Q^2)$, is infrared finite.

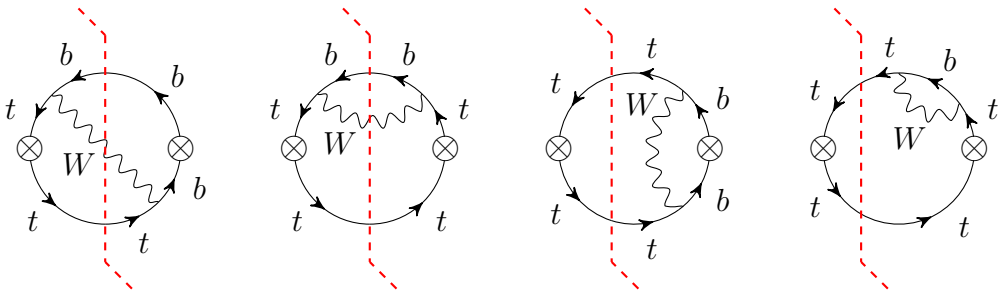

Figure 3.1: Graphs contributing to the α_W correction to the $J \to q\bar{q}$ rate.

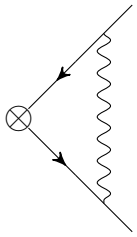

Figure 3.2: Virtual correction to $J \to q\overline{q}$.

The virtual correction to $J \to q\overline{q}$ is given by the graph in Fig. 3.2 and wave-function graphs, which gives the vertex form-factor

$$F_V = 1 + \frac{C_F \alpha_W}{4\pi}\Big\{-\frac{7}{2} + 2\widetilde{r} - (3-2\widetilde{r})\ln\widetilde{r} + (1-\widetilde{r})^2\left[2\mathrm{Li}_2(\widetilde{r}) - \ln^2\widetilde{r} + 2\ln\widetilde{r}\ln(1-\widetilde{r}) - \frac{2\pi^2}{3}\right]\Big\} \tag{3.1}$$

at Euclidean momentum transfer $q^2 = -Q^2 < 0$, with

$$\widetilde{r} = \frac{M_W^2}{Q^2}, \tag{3.2}$$

where M_W is the gauge boson mass.[1] Analytically continuing to time-like $q^2 = s > 0$,

$$r = \frac{M^2}{s} = -\widetilde{r}, \qquad\qquad \ln\widetilde{r} = \ln r - i\pi, \tag{3.3}$$

[1]Eq. (12) of Ref. [33] is incorrect near threshold.

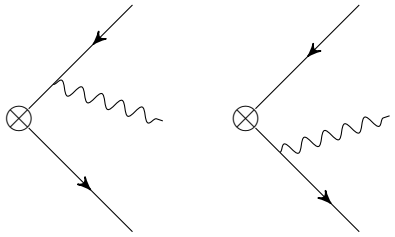

Figure 3.3: Real radiation from $J \to q\overline{q}W$.

gives

$$\begin{aligned} F_V = 1 + \frac{C_F \alpha_W}{4\pi}\Big\{ & -\frac{7}{2} - 2r - (3+2r)\ln r \\ & + (1+r)^2\left[2\mathrm{Li}_2(-r) - \ln^2 r + 2\ln r \ln(1+r) + \frac{\pi^2}{3}\right] \\ & + i\pi\big[(3+2r) + 2\,(1+r)^2\,(\ln r - \ln(1+r))\big]\Big\} \end{aligned} \tag{3.4}$$

which for $s \to \infty$ is

$$F_V = 1 + \frac{C_F \alpha_W}{4\pi}\Big\{ -\ln^2 r - 3\ln r + \frac{\pi^2}{3} - \frac{7}{2} + i\pi\,(2\ln r + 3)\Big\} \tag{3.5}$$

The $\mathrm{SCET}_{\mathrm{EW}}$ computation gives radiative corrections to the $Jq\overline{q}$ operator neglecting M^2/s power corrections, and gives precisely Eq. (3.5), when expanded out to order α_W [36].

The one-loop virtual correction to the $Jq\overline{q}$ cross section is (neglecting power corrections)

$$\begin{aligned} \sigma_V &= \sigma_0\left[|F_V|^2 - 1\right] \\ &= \sigma_0 \frac{C_F \alpha_W}{2\pi}\Big\{ -\ln^2 r - 3\ln r + \frac{\pi^2}{3} - \frac{7}{2}\Big\} \end{aligned} \tag{3.6}$$

where σ_0 is the tree-level cross section. The $-\ln^2 r$ and $-3\ln r$ terms lead to large corrections at high energy.

The real radiation $J \to q\overline{q}W$ arises from the graphs in Fig. 3.3, and is

$$\begin{aligned} \sigma_R = \frac{C_F \alpha_W}{2\pi}\sigma_0\Big\{ & 5(1-r^2) + (3+4r+3r^2)\ln r \\ & + (1+r)^2\Big[\ln^2 r - 4\ln r \ln(1+r) - 4\,\mathrm{Li}_2\,(-r) - \frac{\pi^2}{3}\Big]\Big\}. \end{aligned} \tag{3.7}$$

Expanding in r gives

$$\sigma_R = \frac{C_F \alpha_W}{2\pi} \sigma_0 \left\{ \ln^2 r + 3 \ln r - \frac{\pi^2}{3} + 5 + \ldots \right\}. \tag{3.8}$$

The total radiative correction is

$$\begin{aligned} \sigma_T &= \sigma_R + \sigma_V \\ &= \frac{C_F \alpha_W}{2\pi} \sigma_0 \left\{ \frac{3}{2} - 2r - 5r^2 + (2+3r) r \ln r \right. \\ &\qquad \left. - 2(1+r)^2 \left[\ln r \ln(1+r) + \mathrm{Li}_2(-r) \right] \right\} \end{aligned} \tag{3.9}$$

and as $r \to 0$ gives

$$\sigma_T = \frac{3 C_F \alpha_W}{4\pi} \sigma_0 \,. \tag{3.10}$$

The $\ln^2 r$ and $\ln r$ terms cancel between $\sigma_{R,V}$. The correction to R in QCD is given by Eq. (3.10) with the replacement $\alpha_W \to \alpha_s$ and $C_F \to 4/3$.

The real and virtual corrections are shown in Fig. 3.4. Also shown is the virtual correction computed using the $\mathrm{SCET}_{\mathrm{EW}}$ result of Eq. (C.2). The $\mathrm{SCET}_{\mathrm{EW}}$ and exact calculations for the virtual correction have only very small differences, which are below 1% for $E > 2M_W \sim 160$ GeV, and $< 0.5\%$ by 400 GeV, whereas the real and virtual corrections each exceed 5% by the time $E > 15 M_W \sim 1.2$ TeV. This shows that in the regime where the electroweak corrections are relevant at the LHC, the $\mathrm{SCET}_{\mathrm{EW}}$ computation is sufficiently accurate. The figure also shows that the large real and virtual electroweak corrections cancel in the total cross section.

The above calculation demonstrates the usual cancellation of the L^2 and L terms between real and virtual graphs for the total cross section summed over all final states. This cancellation is not guaranteed to hold if the cross section is modified by restrictions on the final state. One can impose phase space restrictions on the kinematics of the emitted gauge boson. Consequences of doing so were studied in detail in Ref. [31], and lead to incomplete cancellation of the logarithms if the phase space cuts restrict the soft or collinear radiation. One can also investigate the possibility that, because electroweak charge is an experimental observable, one

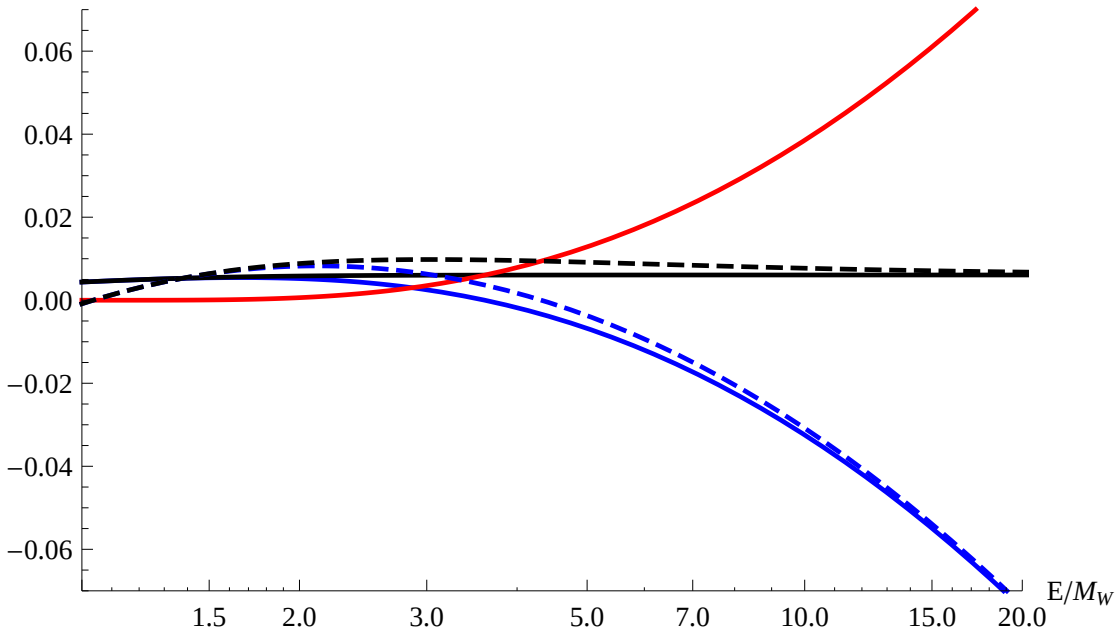

Figure 3.4: Plot of the real and virtual corrections to $J \to q\bar{q}$. Plotted are the exact virtual correction (solid blue), the virtual corrections using SCET_{EW} (dashed blue), real radiation (red), exact total rate (black) and the total rate using the SCET_{EW} virtual correction (dashed black).

can separate the total cross section ($J \to t\bar{t}$, $b\bar{b}$, $t\bar{t}Z$, $b\bar{b}Z$, $t\bar{b}W^-$, $b\bar{t}W^+$) into subprocesses tagged by the final state particles, without restricting phase space. This is useful because the different channels have different experimental signatures, and are often measured separately [61]. The second possibility is studied below, and is complementary to the non-cancellation of logarithmic terms due to phase space restrictions, and due to electroweak non-singlet initial states [26–28].

The real and virtual cross sections are modified if one does not sum over all final states. In the simple example we are considering with degenerate fermions and bosons, the only change is that Eqs. (3.6,3.8) are modified by the replacement of the group theory factor NC_F ($N = 2$) by G_V and G_R, which need not be equal, so that the total cross section

$$\sigma_T = \frac{\alpha_W}{2\pi} (G_R - G_V) \widehat{\sigma}_0 \Big\{ \ln^2 r + 3 \ln r + \ldots \Big\} \tag{3.11}$$

can have large corrections at high energy. The dependence of the cross section on $\ln^2 r + 3 \ln r$ is characteristic of the IR structure of a vector current [18].

To study this non-cancellation, we tabulate the group theory factors $G_{V,R}$ in Table 3.1 for some possible choices of final state, for an $SU(N)$ gauge theory. In Eq. (3.11), $\sigma_0 = N\widehat{\sigma}_0$ is the total tree-level rate, so that $\hat{\sigma}_0$ is N-independent. The different cases are:

1. Any fermion with or without any gauge bosons, i.e. the full inclusive rate.
2. Any fermion but no gauge boson, e.g. $t\bar{t}$, $b\bar{b}$, but not $t\bar{t}Z$, $b\bar{b}Z$, $t\bar{b}W^-$, $b\bar{t}W^+$.
3. Specify one fermion with or without any gauge bosons, e.g. $t+X$, with $X = \bar{t}$, $\bar{t}Z$, $\bar{b}W^-$.
4. Specify one fermion and no gauge bosons, e.g. $t + X$, with $X = \bar{t}$.
5. Specify both fermions (labeled by i, j) with or without any gauge bosons, e.g. $i = j = 1$ is $t\bar{t}X$, $i = 1, j = 2$ is $t\bar{b}X$, etc.
6. Specify both fermions and require no gauge bosons. Same as the previous case but X cannot contain gauge bosons.

One can see that for cases 1 and 3, the logarithmic terms are absent, while for all other cases, the logarithms survive and give rise to large corrections at high energies.

3.4 Heavy Quark Production

In this section, we study the real and virtual corrections to heavy quark production via gluon fusion, $gg \to q\bar{q}$. The tree-level graphs are given in Fig. 3.5. The real radiation is computed by numerical integration using the parton-level event generator MadGraph5_aMC@NLO [62]. The virtual corrections use the SCET results of Ref. [34]. Since the real emission rate is a fixed order result, the virtual correction is expanded out to order α_W to study the real-virtual cancellation.

The $gg \to q\bar{q}$ total cross-section has a t-channel singularity for forward scattering, and a u-channel singularity for backward scattering, from the graphs in Fig. 3.5. To avoid these singularities, we impose rapidity cuts. We require the

Table 3.1: Group theory factors for real and virtual emission for an $SU(N)$ gauge theory. $C_F = (N^2-1)/(2N)$. The different cases are described in the text.

Case	G_R	G_V	$G_R - G_V$
1	NC_F	NC_F	0
2	0	NC_F	$-NC_F$
3	C_F	C_F	0
4	0	C_F	$-C_F$
5	$\frac{1}{2} - \frac{1}{2N}\delta_{ij}$	$C_F\delta_{ij}$	$\frac{1}{2} - \frac{N}{2}\delta_{ij}$
6	0	$C_F\delta_{ij}$	$-C_F\delta_{ij}$

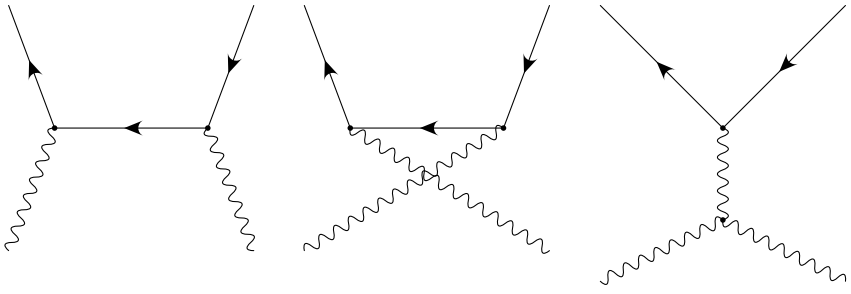

Figure 3.5: Tree-level graphs for $gg \to q\bar{q}$. The first and second graphs have singularities for forward and backward scattering, respectively.

particle with highest transverse momentum to have $|\eta| < 1$ or $|\eta| < 3$. We will refer to these as $|\eta| < 1, 3$ cuts, respectively. We also require that the particle with second highest p_T satisfy $|\eta| < 5$. These cuts allow for collinear and soft W emission from energetic quarks, but avoid the forward and backward singularities. They are applied to both the $gg \to q\bar{q}$ and $gg \to q\bar{q}W$ rates.

The scattering cross section can depend on the collision energy $s = E_{\rm CM}^2$, the rapidity cut η, and the particle masses $\{M\}$. If the cross section is infrared finite as $\{M\} \to 0$, then it cannot contain $\ln s/M^2$ terms. The Sudakov logarithms are a sign that the cross section is divergent in the massless limit. In the $gg \to q\bar{q}$ case, the real and virtual corrections have Sudakov logarithms which cancel in the total rate.

We study the $gg \to q\bar{q}, q\bar{q}W$ rates for three cases:

1. $q = u, d$
2. $q = t, b$ with m_b=100 GeV and $m_t = 173\,\text{GeV}$
3. $q = t, b$ with m_b=4.7 GeV and $m_t = 173\,\text{GeV}$.

Case (1) allows us to explain the structure of the gauge corrections without worrying about mass effects and Higgs corrections. Case (2) also involves Higgs radiative corrections, but has a stable t quark since $m_t < m_b + m_W$. Finally case (3) is the physical case with an unstable t, which can decay via $t \to bW$ decay.

The virtual corrections can be computed from the results in Ref. [34] (including also the y_b terms), and are obtained by averaging the electroweak corrections for left- and right-handed quarks. The virtual corrections to the cross sections are

$$\begin{aligned} \sigma_V(gg \to t\bar{t}) &= \sigma_{0,t}\,\{v_W + 3v_t + v_b\} \\ \sigma_V(gg \to b\bar{b}) &= \sigma_{0,b}\,\{v_W + v_t + 3v_b\} \end{aligned} \tag{3.12}$$

where

$$
\begin{aligned}
v_W &= \frac{C_F \alpha_W}{4\pi} \left[-\mathsf{L}^2 + 3\mathsf{L} \right], \\
v_t &= -\frac{y_t^2}{32\pi^2} \mathsf{L}, \\
v_b &= -\frac{y_b^2}{32\pi^2} \mathsf{L}
\end{aligned}
\tag{3.13}
$$

$\sigma_{0,t} = \sigma(gg \to t\bar{t})$, and $\sigma_{0,b} = \sigma(gg \to b\bar{b})$ are the corresponding tree-level rates, $C_F = 3/4$ for $SU(2)$, and $y_{t,b}$ are the quark Yukawa couplings. The corrections for u, d quarks are given by $y_{t,b} \to 0$. The tree-level cross section σ_0 depends on the η cut. The virtual rates depend on the η cut in the same way as the tree-level rates. The reason is that the virtual electroweak corrections for $gg \to q\bar{q}$ do not depend on the kinematic variables (such as the scattering angle) in this case, so the radiative correction is an overall multiplicative factor. In other cases, such as $q\overline{q} \to q\bar{q}$, the virtual electroweak corrections depend on kinematic variables, and have to be integrated over phase space. The gauge radiative corrections have both L^2 and L terms, whereas the Higgs radiative corrections are linear in L.

3.4.1 u, d Quark Production

The tree-level processes are $gg \to u\bar{u}$ and $gg \to d\bar{d}$, and the real radiation processes are $gg \to u\bar{u}Z$, $gg \to d\bar{d}Z$, $gg \to u\bar{d}W^-$ and $gg \to d\bar{u}W^+$. Since we are working in an $SU(2)_W$ theory (with $Z = W^3$), custodial $SU(2)$ implies that the $\sigma(u\bar{u}) = \sigma(d\bar{d})$, and $\sigma(u\bar{d}W^-) = \sigma(d\bar{u}W^+) = 2\sigma(u\bar{u}Z) = 2\sigma(d\bar{d}Z)$.

Figure 3.6 shows the real and virtual corrections to the $u\bar{u}, d\bar{d}$ production rate, as a function of E_{CM}, for $|\eta| < 1, 3$ cuts. All rates have been normalized by dividing by the tree-level $gg \to u\bar{u}$ rate for the corresponding η cut. This removes the overall $1/s$ dependence of the cross sections. The graph clearly shows that the virtual and real cross sections become large at high energy, and the L^2 dependence is reflected in the quadratic shape of the curves. The virtual correction is independent of the η cut, and as is typical of Sudakov effects, is negative. The real correction depends on the η cut. The L^2, L corrections arise from soft and collinear radiation; the real radiation kinematics for the final state quarks in $gg \to q\bar{q}W$ is

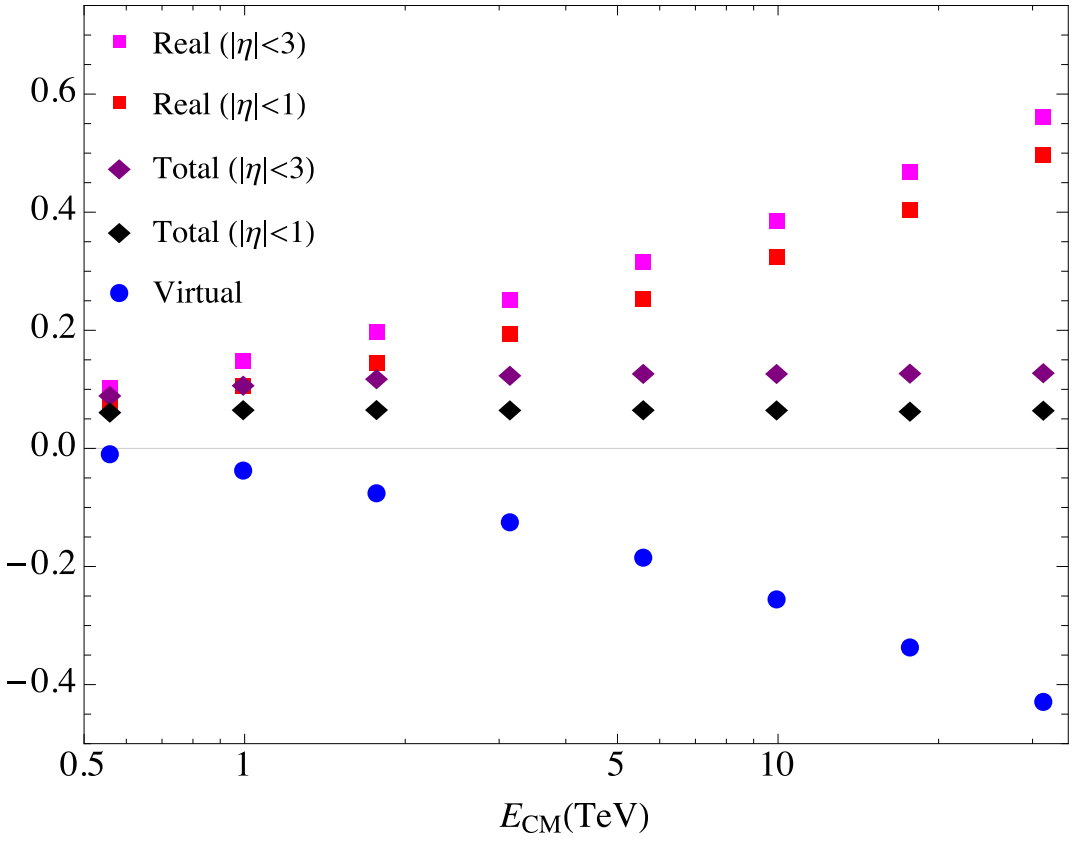

Figure 3.6: Plot of real and virtual corrections to $gg \to q\bar{q}$ for $q = u, d$. All rates have been normalized to the tree-level $gg \to u\bar{u}$ rate. The virtual correction to $gg \to q\bar{q}$ is shown as blue dots. The $gg \to q\bar{q}W$ real emission rate as a function of $E_{\rm CM}$ for $|\eta| < 1, 3$ cuts are shown as red and purple squares, respectively. The α_W correction to the total rate with $|\eta| < 1$ and $|\eta| < 3$ cuts are shown as red and purple diamonds, respectively.

similar to that for the tree-level $gg \to q\bar{q}$ process. As a result, the L^2, L terms do not depend on the η cut, and only the constant L^0 term does. This is reflected in the figure by the fact that the difference in cross sections between the two values of the η cut remains constant as $E_{\rm CM}$ is changed.

The L^2, L terms cancel in the total cross section, as is evident by the curves for the total rate becoming horizontal for large energy, and only the constant terms survive. The electroweak corrections to the total cross section are at the 10% level. At partonic center-of-mass energies of about one TeV, the individual corrections from the real and virtual corrections are also at the 10% level, but they rise quickly as $E_{\rm CM}$ is increased.

For a 100 TeV machine, partonic center-of-mass energies can exceed 10 TeV, and the corrections become large (factors of 2). For most experimentally relevant processes there is never a complete cancellation of the logarithms (since one is typically not measuring a totally inclusive rate, and furthermore the initial state is not an $SU(2)$ singlet), the resummed expressions are needed.

The cancellation between real and virtual corrections is

$$3\sigma(u\bar{d}W) + 2v_W\sigma(u\bar{u}) \to 0 \tag{3.14}$$

using the isospin relations mentioned earlier and Eqs. (3.12,3.13), where $\to 0$ means that the L^2, L dependence cancels, but there can be constant terms left over.

It is important to note that for initial states that are not electroweak singlets, such as for $q\bar{q} \to q\bar{q}$, the real and virtual corrections have *different* L^2, L dependence, and the large corrections persist in the total cross section. This non-cancellation persists even at the hadron level. The $pp \to t\bar{t}$ rate has large corrections from the $q\bar{q} \to q\bar{q}$ channel, since the u and d quark distributions in the proton are not the same.

3.4.2 t, b Quark Production with $m_b = 100\,\mathrm{GeV}$

We now consider the case of $gg \to t\bar{t}, b\bar{b}$ for $m_t = 173\,\mathrm{GeV}$ and $m_b = 100$ GeV. An unphysical b mass has been chosen, so that the $t \to bW$ decay is forbidden. The case of unstable top is discussed in Sec. 3.4.3. The virtual corrections for $t\bar{t}$

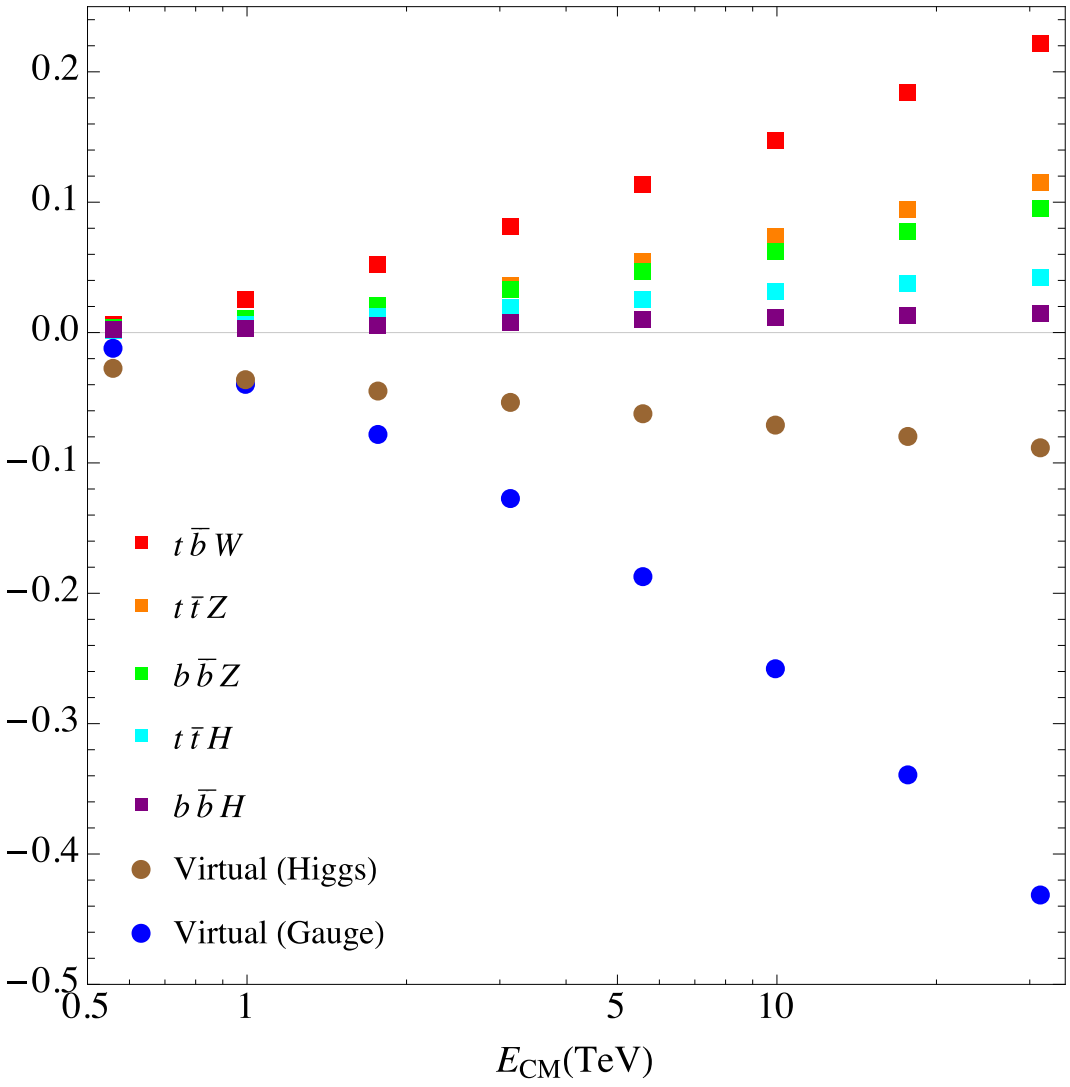

Figure 3.7: Plot of real and virtual corrections to $gg \to q\bar{q}$ for $q = t, b$ for $m_b = 100\,\text{GeV}$ with an $|\eta| < 1$ cut. All rates have been normalized to the tree-level $gg \to u\bar{u}$ rate. The points are: virtual correction gauge corrections (blue dots), virtual Higgs corrections (brown dots), $t\bar{b}W^-$ (red squares), $t\bar{t}Z$ (orange squares), $b\bar{b}Z$ (green squares), $t\bar{t}H$ (cyan squares) and $b\bar{b}H$ (purple squares).

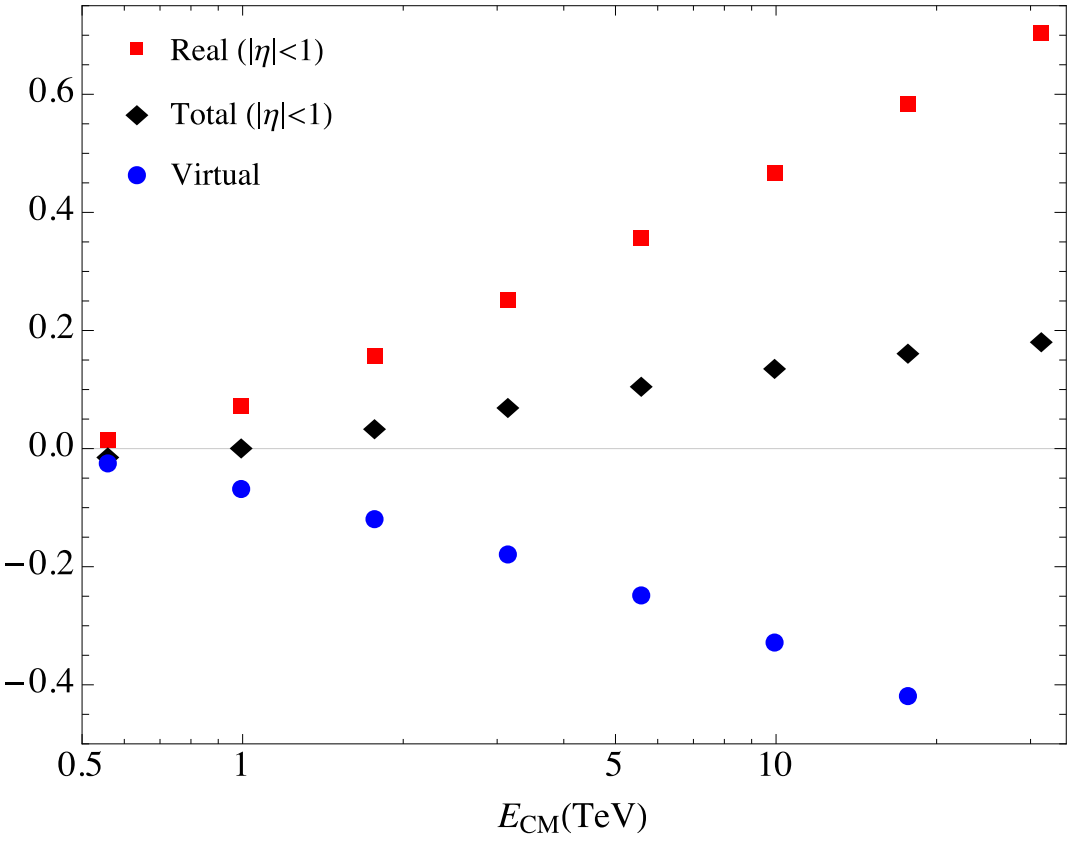

Figure 3.8: Plot of the real and virtual corrections to $gg \to q\bar{q}$ for $q = t, b$ for $m_b = 100\,\text{GeV}$ with an $|\eta| < 1$ cut. The virtual corrections are blue dots, the total real emission rate is shown as red squares, and the total radiative correction is shown as black diamonds. All rates are normalized to the $gg \to u\bar{u}$ rate. The total rate levels off beyond 30 TeV.

and $b\bar{b}$ production are given in Eq. (3.12). The real rates are computed using MadGraph5_aMC@NLO. All rates are divided by the corresponding $gg \to u\bar{u}$ rate to remove an overall $1/s$ normalization factor. The tree-level rates $gg \to t\bar{t}$ and $gg \to b\bar{b}$ are essentially equal to $gg \to u\bar{u}$ except very close to $t\bar{t}$ threshold, so each of these tree-level rates are 1 in the normalization of the plot, and have not been shown.

The real and virtual corrections are shown in Fig. 3.7 for the $|\eta| < 1$ cut. The $|\eta| < 3$ plots are very similar, with a small offset from the $|\eta| < 1$ curves, as for the u, d case in Fig. 3.6. The $t\bar{b}W^-$ emission rate is the sum of the rates for transversely and longitudinally polarized gauge bosons. The rate for transversely polarized gauge bosons at high energies is the same as that for $u\bar{d}W^-$ production, since fermion mass effects are power suppressed. The rate for longitudinally polarized gauge bosons is the same as for emission of the unphysical scalar (by the equivalence theorem), and is related to the Higgs emission rate. The real and virtual rates can be written in terms of the $u\bar{d}W^-$ rate and the rate σ_S to emit a scalar with unit Yukawa coupling,

$$\begin{aligned}
\sigma(t\bar{b}W^-) &\to \sigma(u\bar{d}W^-) + 2(y_t^2 + y_b^2)\sigma_S \\
\sigma(t\bar{t}Z) &\to \frac{1}{2}\sigma(u\bar{d}W^-) + 2y_t^2\sigma_S \\
\sigma(b\bar{b}Z) &\to \frac{1}{2}\sigma(u\bar{d}W^-) + 2y_b^2\sigma_S \\
\sigma(t\bar{t}H) &\to 2y_t^2\sigma_S \\
\sigma(b\bar{b}H) &\to 2y_b^2\sigma_S \\
\sigma_V(t\bar{t}) &\to (v_W + 3v_t + v_b)\,\sigma(u\bar{u}) \\
\sigma_V(b\bar{b}) &\to (v_W + v_t + 3v_b)\,\sigma(u\bar{u})
\end{aligned} \tag{3.15}$$

The $\sigma(u\bar{d}W^-)$ terms in $\sigma(t\bar{b}W^-)$, etc., are for transverse W and Z emission and the σ_S terms are for longitudinal W and Z emission.[2] One can verify that the real emission curves in Fig. 3.7 satisfy Eq. (3.15), so that five curves are given in terms of two quantities, $\sigma(u\bar{d}W^-)$ determined already in Sec. 3.4.1, and σ_S. The Higgs

[2]Remember that $Z = W^3$ since we are in a pure $SU(2)_W$ theory. Otherwise, the Z rates would have additional factors of $1/\cos^2\theta_W$.

emission curves $\sigma(t\bar{t}H), \sigma(b\bar{b}H)$ are linear, which means they contain L terms but no L^2 terms.

The sum of all the real radiation rates, as well as the total cross section, are shown in Fig. 3.8. The total cross section levels out at high energy (we have verified this by continuing the plot to even higher center of mass energies), which shows numerically that the L^2 and L terms cancel between the real and virtual corrections. The total real emission rate is

$$\begin{aligned}\sigma_R &= 2\sigma(t\bar{b}W^-) + \sigma(t\bar{t}Z) + \sigma(b\bar{b}Z) + \sigma(t\bar{t}H) + \sigma(b\bar{b}H) \\ &\to 3\sigma(u\bar{d}W^-) + 8(y_t^2 + y_b^2)\sigma_S \end{aligned} \tag{3.16}$$

and the total virtual rate is

$$\sigma_V = \sigma_V(t\bar{t}) + \sigma_V(b\bar{b}) = (2v_W + 4v_t + 4v_b)\,\sigma(u\bar{u}) \tag{3.17}$$

The cancellation $\sigma_R + \sigma_V \to 0$ implies that

$$3\sigma(u\bar{d}W^-) + 8(y_t^2 + y_b^2)\sigma_S + (2v_W + 4v_t + 4v_b)\,\sigma(u\bar{u}) \to 0. \tag{3.18}$$

The gauge and Higgs parts cancel separately. The gauge part cancels using Eq. (3.14), and

$$8(y_t^2 + y_b^2)\sigma_S + (4v_t + 4v_b)\,\sigma(u\bar{u}) \to 0. \tag{3.19}$$

From Eq. (3.13), we see that $v_{t,b}$ are linear in L, which explains the linearity of the Higgs emission cross section σ_S.

3.4.3 t, b Quark Production with $m_b = 4.7\,\mathrm{GeV}$

Finally, we study the case of a physical b quark with $m_b = 4.7\,\mathrm{GeV}$ and an unstable t quark. The virtual corrections are still given by Eq. (3.12). There is, however, an important change in the $t\bar{b}W^-$ decay rate because the process $gg \to t\bar{t}$ followed by $\bar{t} \to \bar{b}W^-$ contributes to this rate. The $t\bar{b}W^-$ differential decay rate has a singularity when $(p_{\bar{b}} + p_{W^-})^2 = m_t^2$, and the cross section diverges when integrated over final state phase space. The standard way to resolve this

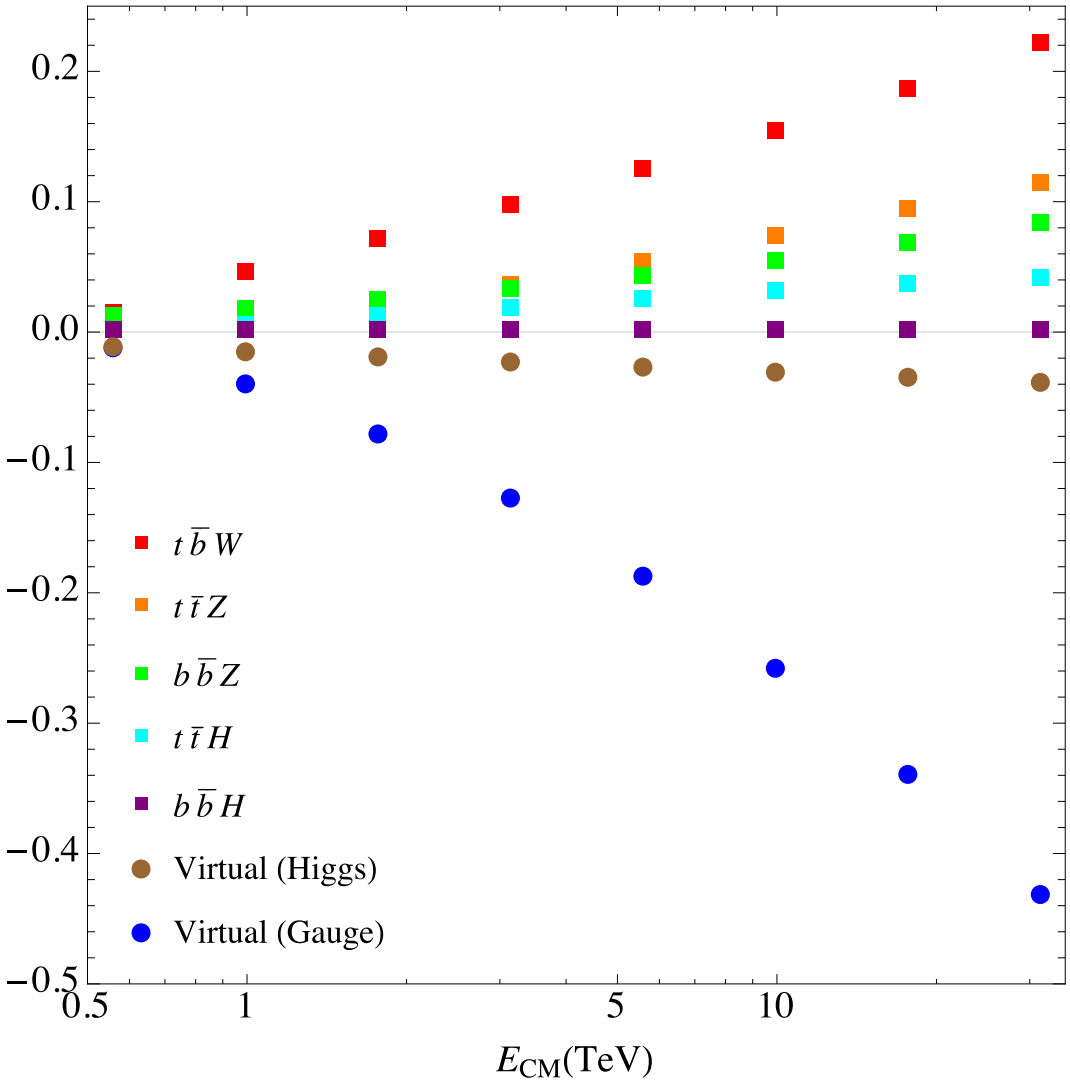

Figure 3.9: Same as Fig. 3.7, but for $m_b = 4.7\,\text{GeV}$.

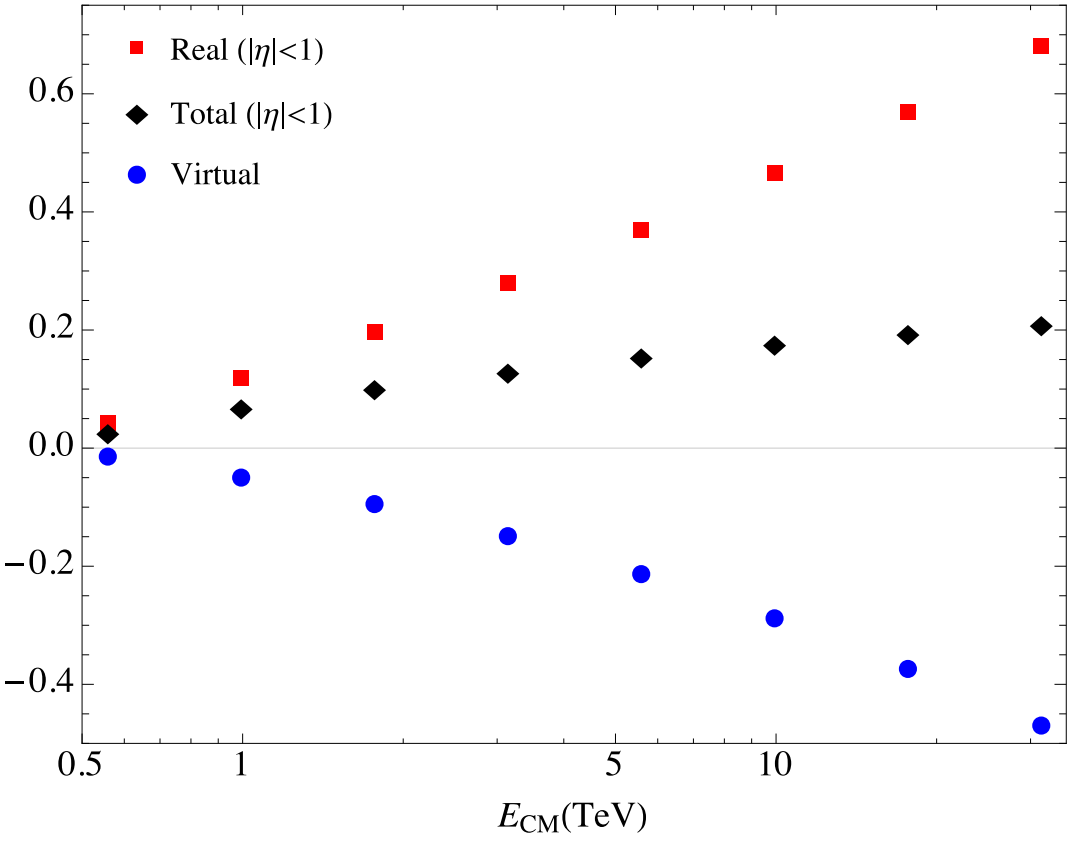

Figure 3.10: Same as Fig. 3.8, but for $m_b = 4.7\,\text{GeV}$.

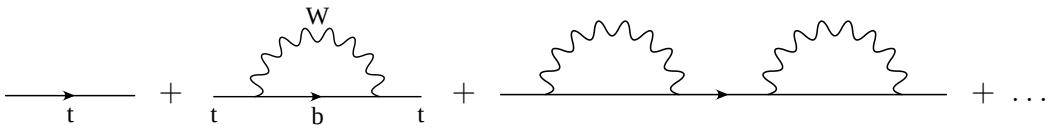

Figure 3.11: Graphs that are summed in the narrow width approximation. In Eq. (3.20), only the imaginary part of each loop is included.

singularity is to regulate it by the t-quark width using the replacement (the narrow width approximation, which is what is used in MadGraph5_aMC@NLO)

$$\frac{1}{p^2 - m_t^2 + i\epsilon} \to \frac{1}{p^2 - m_t^2 + i m_t \Gamma_t} \tag{3.20}$$

for the t-quark propagator, where Γ_t is the t-quark width. This is equivalent to summing a class of diagrams, the imaginary parts of W corrections to the t-quark propagator, shown in Fig. 3.11. This is not gauge invariant, and also formally mixes different orders in the α_W expansion, since the t-quark width is $\mathcal{O}(\alpha_W m_t)$. The cut in the second graph of Fig. 3.1 is the same cut as occurs in summing the imaginary parts of Fig. 3.11, and the two cuts cannot be treated separately, as is done in the narrow width approximation.

If the $t \to bW^-$ decay is kinematically forbidden, the $t\bar{b}W^-$ real emission rate is order α_W. When the decay is kinematically allowed, the $t\bar{b}W^-$ rate becomes order 1. The reason is that in the resonance region, the rate is enhanced by a factor of $1/\Gamma_t$. The total $t\bar{b}W^-$ rate includes what, in the kinematically forbidden case, is the $\mathcal{O}(1)$ $t\bar{t}$ rate. Once the $t\bar{b}W^-$ decay is kinematically allowed, the approximation Eq. (3.20), while getting the correct $\mathcal{O}(1)$ rate, does not get the correct $\mathcal{O}(\alpha_W)$ piece.

To understand how the infrared divergence cancellation occurs for an unstable t quark, consider the simpler case of $t\bar{t}$ production by a current J, as in Sec. 3.3. The α_W correction to the total rate can be computed from the imaginary part of the vacuum polarization graphs in Fig. 3.1. The vacuum polarization $\Pi(q^2)$ has no singularities for Euclidean q^2 even if $m_t > m_b + m_W$, so the analytic continuation to timelike q^2 does not either. The imaginary part for timelike q^2 is given by the real emission and virtual correction cuts shown in Fig. 3.1, so the two contributions combined have no infrared divergence.

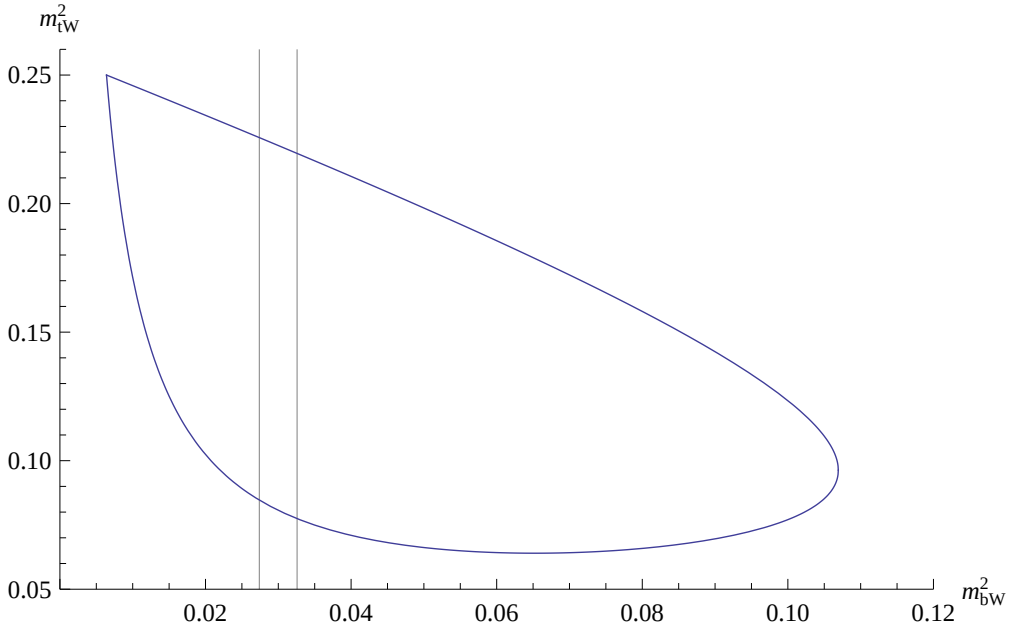

Figure 3.12: Phase space region for $t\bar{b}W$ production for $E_{\rm CM} = 500\,{\rm GeV}$. The vertical band is the region where $(m_t - 5\Gamma_t)^2 \le m^2_{bW} \le (m_t + 5\Gamma_t)^2$. The axes are in $({\rm TeV})^2$.

The graphs in Fig. 3.1 are all order α_W, and their total gives the $\mathcal{O}(\alpha_W)$ correction to the total rate. The graphs are computed with the t-quark propagator on the l.h.s. of Eq. (3.20), rather than the narrow width approximation on the r.h.s. The real emission graph is singular because the $t \to bW^-$ decay is kinematically allowed. A careful calculation shows that the virtual correction is also singular, and the sum is finite. The cancellation can be checked using the l.h.s. of Eq. (3.20) with the $i\epsilon$ term acting as a regulator. The real and virtual graphs each have a piece proportional to $1/\epsilon$, which cancels in the sum.

The $t\bar{b}W^-$ rate can be computed by adding the rates for two regions: A, which is a small region around where the t-quark is on-shell, and A', which is the rest of phase space. In terms of the final state phase space variables $m^2_{bW} = (p_b + p_W)^2$, $m^2_{tW} = (p_t + p_W)^2$ needed for three-body decay, A is the region $m_t^2 - \Delta \le m^2_{bW} < m_t^2 + \Delta$, and A' is the remaining region. The phase space region is shown in Fig. 3.12, with A the region within the vertical band, and A' outside. For a stable t-quark, the vertical band moves outside the allowed phase space region, and there is no singularity in the phase space integral. For an unstable t-quark, the

rate is non-singular in region A', and can be computed by the propagator on the l.h.s. of Eq. (3.20). To correctly compute the $\mathcal{O}(\alpha_W)$ terms, one must also use the propagator on the l.h.s. of Eq. (3.20), rather than the narrow width approximation on the r.h.s., for the integral over the singular region A.

The region A contribution has a singular $1/\epsilon$ piece that must be subtracted, keeping only the finite $\mathcal{O}(\alpha_W)$ part. The $1/\epsilon$ singular part of the rate becomes the $\mathcal{O}(1)$ contribution in the narrow width approximation, and the subleading $\mathcal{O}(\alpha_W)$ is, unfortunately, not given correctly by the narrow width approximation.

The phase space integral of the decay distribution over A has the form

$$I = \int_{m_t^2-\Delta}^{m_t^2+\Delta} \mathrm{d}m_{bW}^2 \; \frac{f(m_{bW}^2)}{(m_{bW}^2 - m_t^2)^2 + \epsilon^2} \tag{3.21}$$

where the denominator is from the absolute value squared of the propagator in Eq. (3.20), f contains all non-singular factors in the decay distribution, and Δ is the width of the integration region. Expanding around m_t^2,

$$f(m_{bW}^2) = f_0 + (m_{bW}^2 - m_t^2) f_1 + (m_{bW}^2 - m_t^2)^2 f_2 + \ldots \tag{3.22}$$

gives

$$I = \frac{\pi}{\epsilon} f_0 + 2\Delta f_2 + \ldots \tag{3.23}$$

The first term is the singular $1/\epsilon$ piece that must be subtracted, and the remaining terms are the finite $\mathcal{O}(\alpha_W)$ terms. Relative to the contribution from region A', they are smaller by a factor Δ, i.e. the width of the vertical band relative to the width of the full phase space region. Since we are only interested in the $\mathcal{O}(\alpha_W)$ contribution to the rate, we can get a good estimate of this by simply using the contribution from region A', and ignoring A. The $\mathcal{O}(\alpha_W)$ term from A is a small correction, since the size of A is much smaller than A'. A practical way to do this in MadGraph5_aMC@NLO is to use the `$t` tag, which excludes a region of width $15\Gamma_t$ around the on-shell t-quark.

The results of this computation are shown in Figs. (3.9,3.10), and are very similar to those for $m_b = 100\,\mathrm{GeV}$. The main difference is the Yukawa correction is smaller, since y_b is now almost zero. The entire discussion of Sec. 3.4.2 holds, and will not be repeated again.

3.5 Discussion and Conclusions

We have presented the electroweak radiative corrections to $gg \to t\bar{t}, gg \to b\bar{b}$ production in Sec. 3.4. The individual processes that contribute have large electroweak corrections that depend on L^2 and L, but these cancel in the total rate. The virtual corrections are around -10% for $E_{\rm CM} \sim 2\,\text{TeV}$, and grow with energy.

The electroweak corrections to the individual processes are relevant for measurements at the LHC. For example, suppose one is interested in measuring the $t\bar{t}$ production rate. The virtual corrections to $t\bar{t}$ contribute to this rate. If one has a perfect detector, then one can exclude the real emission final states $t\bar{b}W$, $t\bar{t}Z$, $b\bar{b}Z$, $t\bar{t}H$, $b\bar{b}H$. In this case, the cross section is given by the blue dots in Fig. 3.9, and there are large electroweak radiative corrections. In a more realistic case, there will be some leakage from the real radiation processes into the $t\bar{t}$ channel. For example $t\bar{t}Z$ with $Z \to \nu\bar{\nu}$ could be mistaken for $t\bar{t}$, or $t\bar{t}Z$ with $Z \to q\bar{q}$, where the Z decay products cannot be separated from the t-quark decay jets. If some fraction of the real radiation is included, then there will be some cancellation with the electroweak corrections to the virtual rate, so that the overall electroweak correction is somewhat smaller. A realistic calculation of the measured rates is beyond the scope of this work. To do such a calculation requires taking the corrections discussed in this paper, integrating over the gluon PDFs, and then putting the parton processes through a showering algorithm and detector cuts. In addition, one should also include the quark production rates $q\bar{q} \to t\bar{t}$, which were included in the analysis of Ref. [63]. As noted earlier, the electroweak corrections to $q\bar{q} \to t\bar{t}$ do not cancel even for the totally inclusive rate. It should be clear that even in a complete calculation, the electroweak corrections do not cancel, and a significant correction remains.

The electroweak radiative corrections start to become measurable at LHC energies, and their importance grows with energy. We have numerically studied the $gg \to t\bar{t}$ process in this paper. Most processes have much larger electroweak corrections than this process, because they typically contain more particles with electroweak interactions. (The gluon does not have electroweak interactions at

leading order.) The corrections for $q\bar{q} \to t\bar{t}$ are approximately twice as large, because the initial and final states both have electroweak interactions. Processes such as $q\bar{q} \to WW$ which involve electroweak gauge bosons have even larger corrections, since the group theory factor $C_F = 3/4$ is replaced by $C_A = 2$ in the amplitude.

The effective theory method breaks the electroweak correction into the high-scale matching C, the running γ and the low-scale matching D. The L^2 term arise from γ, and the L terms from γ and D. All terms are known to NLL order, as are the most important terms at NNLL order (see appendix).

In addition to the electroweak corrections, there are of course, QCD corrections, which are much larger, and have been included in existing calculations and implemented in Monte Carlo code. The QCD and electroweak corrections factor in A and D_L to two-loop order and in B, D_0 and C to one-loop order [33, 38], so that the total radiative correction to NLL order can be written as the product $R_{\rm QCD}R_{\rm EW}$. $R_{\rm QCD}$ has been included in existing calculations, so the electroweak corrections can be included to NLL order simply by reweighing the QCD results by $R_{\rm EW}$. This has to be done before integrating over the final state phase space, since $R_{\rm EW}$ can depend on kinematic variables such as scattering angles. One complication is that $R_{\rm EW}$ depends on the helicities of the partons, since the weak interactions are chiral.

The experimental energy reach at the LHC is high enough that electroweak corrections should be included in measurements that are approaching 10% accuracy. Recently, there have been studies of a possible 100 TeV hadron collider. At these high energies, the electroweak corrections are large, and must be resummed to have reliable cross sections.

Chapter 3, in full, is a reprint of the material as it appears in *Phys. Lett. B* **740** 179 (2015). A. Manohar, B. Shotwell, C. Bauer, and S. Turczyk. The dissertation author and the Ph.D. committee chair were the principal investigators and co-authors of this paper.

Chapter 4

Baryon Number Violation

We calculate the one-loop anomalous dimension matrix for the dimension-six baryon number violating operators of the Standard Model effective field theory, including right-handed neutrino fields. We discuss the flavor structure of the renormalization group evolution in the contexts of minimal flavor violation and unification.

4.1 Introduction

The baryon asymmetry of the universe hints at baryon number violating (BNV) interactions beyond the Standard Model (SM) of particle physics. Baryon number is an accidental symmetry of the SM violated by quantum effects [64], and there is no fundamental reason why it cannot be violated in extensions of the SM. Indeed, well-motivated theories like grand unified theories [65–67] violate baryon number at tree level through the exchange of very massive gauge bosons.

There has been no direct experimental observation of baryon number violation to date. The large lower bound for the lifetime of the proton [68, 69] requires that the scale of baryon number violation $M_{\not B}$ be much greater than accessible energy scales, and, in particular, much greater than the SM electroweak scale M_Z. The decay of baryons (such as the proton) can then be computed using an Effective Field Theory (EFT) formalism. In the model-independent treatment of EFT, the SM Lagrangian is extended by higher dimensional non-renormalizable operators

($d \geq 5$) suppressed by inverse powers of the new physics scale.

The leading order BNV operators arise at dimension $d = 6$. The most general dimension-six Lagrangian can be cast in 63 independent operators [70–74]. Out of these 63 operators, 59 operators preserve baryon number, and the complete set of one-loop renormalization group equations for these 59 operators was recently computed in Refs. [75–78]. In the present work, we focus on the four BNV operators [72–74], and we extend the one-loop renormalization group evolution (RGE) analysis to these remaining dimension-six operators.

The four BNV operators can be written[1] as [74]

$$\begin{aligned} Q^{duq\ell}_{prst} &= \epsilon_{\alpha\beta\gamma}\epsilon_{ij}(d^{\alpha}_{p}Cu^{\beta}_{r})(q^{i\gamma}_{s}C\ell^{j}_{t})\,, \\ Q^{qque}_{prst} &= \epsilon_{\alpha\beta\gamma}\epsilon_{ij}(q^{i\alpha}_{p}Cq^{j\beta}_{r})(u^{\gamma}_{s}Ce_{t})\,, \\ Q^{qqq\ell}_{prst} &= \epsilon_{\alpha\beta\gamma}\epsilon_{il}\epsilon_{jk}(q^{i\alpha}_{p}Cq^{j\beta}_{r})(q^{k\gamma}_{s}C\ell^{l}_{t})\,, \\ Q^{duue}_{prst} &= \epsilon_{\alpha\beta\gamma}(d^{\alpha}_{p}Cu^{\beta}_{r})(u^{\gamma}_{s}Ce_{t})\,, \end{aligned} \tag{4.1}$$

where C is the Dirac matrix of charge conjugation, q and ℓ are the quark and lepton left-handed doublets, and we use u, d and e for up-type, down-type, and charged lepton right-handed fermions. Greek letters denote $SU(3)_c$ color indices and Roman letters from i to l refer to $SU(2)_L$ indices. Roman letters towards the end of the alphabet p-w refer to flavor (generation) indices and take on values from $1, \ldots, n_g = 3$.

In this work, we also will accommodate neutrino masses for the light neutrinos by including singlet fermions N (right-handed neutrinos) under the SM gauge group. Including singlet N fields, two additional dimension-six BNV operators can be constructed:

$$\begin{aligned} Q^{qqdN}_{prst} &= \epsilon_{\alpha\beta\gamma}\epsilon_{ij}(q^{i\alpha}_{p}Cq^{j\beta}_{r})(d^{\gamma}_{s}CN_{t})\,, \\ Q^{uddN}_{prst} &= \epsilon_{\alpha\beta\gamma}(u^{\alpha}_{p}Cd^{\beta}_{r})(d^{\gamma}_{s}CN_{t}). \end{aligned} \tag{4.2}$$

The singlet neutrinos N, in contrast to the SM fermions, are allowed a Majorana mass M_N by the SM gauge symmetry. M_N can range from a very high scale as in the standard type-I seesaw model [79–82] to the Dirac neutrino limit for which it vanishes — see Ref. [83] for a general parametrization in terms of light masses and

[1] The connection with the basis of Ref. [72] is given in Appendix D.

mixing angles. Even in the case of a very high Majorana mass scale M_N, naïve estimates of proton decay and light neutrino masses imply that $M_N < M_{\not B}$. This hierarchy of scales implies that an EFT with the operators in Eq. (4.2) holds in the energy regime $M_N < \mu < M_{\not B}$. Below the scale M_N, one integrates out the N fields, matching onto the EFT containing only the four operators of Eq. (4.1), and drops the terms of Eq. (4.2) in the renormalization group equations.

We will use the conventions of Ref. [75], generalized to include singlet fermions N *at energies above* M_N. Specifically, for $\mu > M_N$, the $\mathcal{L}_{d\leq 4}$ SM Lagrangian includes a Majorana mass term M_N for the N fermions as well as Yukawa couplings Y_N for the N and ℓ fermions to the electroweak Higgs doublet H. For $\mu < M_N$, the N fields are integrated out of the EFT, and $\mathcal{L}_{d\leq 4}$ reduces to the conventional SM Lagrangian.

Baryon number is an (anomalous) symmetry that is preserved by the one-loop renormalization group equations, so the dimension-six BNV operators only mix among themselves. The gauge contribution to the anomalous dimensions of Eq. (4.1) was computed in Ref. [74], and we agree with those results. In addition, we compute the anomalous dimensions of Eq. (4.2), and the Yukawa terms. We also classify the operators in terms of representations of the permutation group, which diagonalizes the gauge contributions to the anomalous dimension matrix.

4.2 Results

The one-loop anomalous dimension matrix of the BNV operators decomposes into a sum of gauge and Yukawa terms. The gauge anomalous dimension matrix of the operators in Eq. (4.1) was computed in Ref. [74]. The gauge terms for Eq. (4.2) have not been computed previously. The Yukawa terms are generated by the diagram in Fig. 4.1, where all the fermion lines are incoming, because of the chiral structure of the BNV operators. The gauge coupling dependence is obtained from an analogous diagram with the scalar replaced by a gauge boson.

The calculation is done using dimensional regularization in $d = 4-2\epsilon$ dimensions in a general ξ gauge. Cancellation of the gauge parameter ξ provides a check

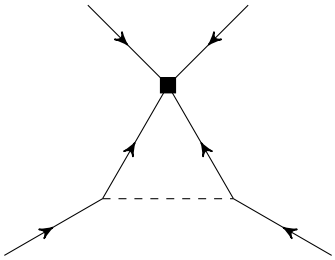

Figure 4.1: The one-loop Yukawa renormalization graph.

on the calculation. The sum of the hypercharges y_i of the four fermions for each operator is constrained to be equal to zero for the ξ-dependence to cancel. Furthermore, the number of colors $N_c = 3$ for the operator to be $SU(3)$ gauge invariant. The RGE for the operator coefficients $\mathcal{L} = \sum_i C^i Q^i$ are ($\dot{C} \equiv 16\pi^2 \mu \, \mathrm{d}C/\mathrm{d}\mu$):

$$
\begin{aligned}
\dot{C}^{duq\ell}_{prst} =& - C^{duq\ell}_{prst}\left[4g_3^2 + \frac{9}{2}g_2^2 - 6(\mathsf{y}_d\mathsf{y}_u + \mathsf{y}_q\mathsf{y}_l)g_1^2\right] - C^{duq\ell}_{vrwt}(Y_d)_{vs}(Y_d^\dagger)_{wp} \\
& - C^{duq\ell}_{pvwt}(Y_u)_{vs}(Y_u^\dagger)_{wr} + \left\{2C^{duue}_{prwv} + C^{duue}_{pwrv}\right\}(Y_e)_{vt}(Y_u)_{ws} \\
& - 2C^{qqdN}_{swpv}(Y_N)_{vt}(Y_u^\dagger)_{wr} + \left\{2C^{uddN}_{rpwv} + C^{uddN}_{rwpv}\right\}(Y_N)_{vt}(Y_d)_{ws} \\
& + \left\{2C^{qqq\ell}_{vwst} + 2C^{qqq\ell}_{wvst} - C^{qqq\ell}_{vswt} - C^{qqq\ell}_{wsvt} + 2C^{qqq\ell}_{svwt} + 2C^{qqq\ell}_{swvt}\right\}(Y_d^\dagger)_{vp}(Y_u^\dagger)_{wr} \\
& + 2C^{qque}_{wsrv}(Y_d^\dagger)_{wp}(Y_e)_{vt} + C^{duq\ell}_{vrst}(Y_d Y_d^\dagger)_{vp} + C^{duq\ell}_{pvst}(Y_u Y_u^\dagger)_{vr} \\
& + \frac{1}{2}C^{duq\ell}_{prvt}(Y_u^\dagger Y_u + Y_d^\dagger Y_d)_{vs} + \frac{1}{2}C^{duq\ell}_{prsv}(Y_N^\dagger Y_N + Y_e^\dagger Y_e)_{vt}
\end{aligned}
\tag{4.3}
$$

$$
\begin{aligned}
\dot{C}^{qque}_{prst} =& - C^{qque}_{prst}\left[4g_3^2 + \frac{9}{2}g_2^2 - 6(\mathsf{y}_q^2 + \mathsf{y}_u\mathsf{y}_e)g_1^2\right] - C^{qque}_{pwvt}(Y_u)_{vr}(Y_u^\dagger)_{ws} \\
& - C^{qque}_{rwvt}(Y_u)_{vp}(Y_u^\dagger)_{ws} + \frac{1}{2}C^{duq\ell}_{vspw}(Y_e^\dagger)_{wt}(Y_d)_{vr} + \frac{1}{2}C^{duq\ell}_{vsrw}(Y_e^\dagger)_{wt}(Y_d)_{vp} \\
& - \frac{1}{2}\left\{2C^{duue}_{vwst} + C^{duue}_{vswt}\right\}\left[(Y_d)_{vp}(Y_u)_{wr} + (Y_d)_{vr}(Y_u)_{wp}\right] \\
& + \frac{1}{2}\left\{-2C^{qqq\ell}_{prwv} - 2C^{qqq\ell}_{rpwv} + C^{qqq\ell}_{pwrv} + C^{qqq\ell}_{rwpv} - 2C^{qqq\ell}_{wprv} - 2C^{qqq\ell}_{wrpv}\right\}(Y_u^\dagger)_{ws}(Y_e^\dagger)_{vt} \\
& + \frac{1}{2}C^{qque}_{vrst}(Y_u^\dagger Y_u + Y_d^\dagger Y_d)_{vp} + \frac{1}{2}C^{qque}_{pvst}(Y_u^\dagger Y_u + Y_d^\dagger Y_d)_{vr} \\
& + C^{qque}_{prvt}(Y_u Y_u^\dagger)_{vs} + C^{qque}_{prsv}(Y_e Y_e^\dagger)_{vt}
\end{aligned}
\tag{4.4}
$$

$$\begin{aligned}\dot{C}^{qqdN}_{prst} =& - C^{qqdN}_{prst}\left[4g_3^2+\frac{9}{2}g_2^2-6\mathsf{y}_q^2g_1^2\right] - C^{qqdN}_{vrwt}(Y_d^\dagger)_{vs}(Y_d)_{wp} - C^{qqdN}_{vpwt}(Y_d^\dagger)_{vs}(Y_d)_{wr}\\ &- \frac{1}{2}C^{duq\ell}_{swrv}(Y_N^\dagger)_{vt}(Y_u)_{wp} - \frac{1}{2}C^{duq\ell}_{swpv}(Y_N^\dagger)_{vt}(Y_u)_{wr}\\ &+ \frac{1}{2}\left\{2C^{uddN}_{vwst}+C^{uddN}_{vswt}\right\}\left[(Y_u)_{vp}(Y_d)_{wr}+(Y_u)_{vr}(Y_d)_{wp}\right]\\ &+ \frac{1}{2}\left\{2C^{qqq\ell}_{prwv}+2C^{qqq\ell}_{rpwv}-C^{qqq\ell}_{pwrv}-C^{qqq\ell}_{rwpv}+2C^{qqq\ell}_{wprv}+2C^{qqq\ell}_{wrpv}\right\}(Y_d^\dagger)_{ws}(Y_N^\dagger)_{vt}\\ &+ \frac{1}{2}C^{qqdN}_{vrst}(Y_u^\dagger Y_u+Y_d^\dagger Y_d)_{vp}+\frac{1}{2}C^{qqdN}_{pvst}(Y_u^\dagger Y_u+Y_d^\dagger Y_d)_{vr}\\ &+ C^{qqdN}_{prvt}(Y_dY_d^\dagger)_{vs}+C^{qqdN}_{prsv}(Y_NY_N^\dagger)_{vt}\end{aligned} \tag{4.5}$$

$$\begin{aligned}\dot{C}^{qqq\ell}_{prst} =& - C^{qqq\ell}_{prst}\left[4g_3^2+3g_2^2-6(\mathsf{y}_q^2+\mathsf{y}_q\mathsf{y}_l)g_1^2\right] - 4\left\{C^{qqq\ell}_{rpst}+C^{qqq\ell}_{srpt}+C^{qqq\ell}_{psrt}\right\}g_2^2\\ &- 4C^{qque}_{prwv}(Y_e)_{vt}(Y_u)_{ws}+4C^{qqdN}_{prwv}(Y_N)_{vt}(Y_d)_{ws}\\ &+ 2C^{duq\ell}_{vwst}\left[(Y_d)_{vp}(Y_u)_{wr}+(Y_d)_{vr}(Y_u)_{wp}\right]\\ &+ \frac{1}{2}C^{qqq\ell}_{vrst}(Y_u^\dagger Y_u+Y_d^\dagger Y_d)_{vp}+\frac{1}{2}C^{qqq\ell}_{pvst}(Y_u^\dagger Y_u+Y_d^\dagger Y_d)_{vr}\\ &+ \frac{1}{2}C^{qqq\ell}_{prvt}(Y_u^\dagger Y_u+Y_d^\dagger Y_d)_{vs}+\frac{1}{2}C^{qqq\ell}_{prsv}(Y_N^\dagger Y_N+Y_e^\dagger Y_e)_{vt}\end{aligned} \tag{4.6}$$

$$\begin{aligned}\dot{C}^{duue}_{prst} =& - C^{duue}_{prst}\left[4g_3^2-2\left(2\mathsf{y}_d\mathsf{y}_u+2\mathsf{y}_e\mathsf{y}_u+\mathsf{y}_u^2+\mathsf{y}_e\mathsf{y}_d\right)g_1^2\right]\\ &+ 4C^{duue}_{psrt}\left((\mathsf{y}_d+\mathsf{y}_e)\mathsf{y}_u-\mathsf{y}_u^2-\mathsf{y}_e\mathsf{y}_d\right)g_1^2\\ &+ 4C^{duq\ell}_{prwv}(Y_u^\dagger)_{ws}(Y_e^\dagger)_{vt}-8C^{qque}_{vwst}(Y_d^\dagger)_{vp}(Y_u^\dagger)_{wr}\\ &+ C^{duue}_{vrst}(Y_dY_d^\dagger)_{vp}+C^{duue}_{pvst}(Y_uY_u^\dagger)_{vr}+C^{duue}_{prvt}(Y_uY_u^\dagger)_{vs}+C^{duue}_{prsv}(Y_eY_e^\dagger)_{vt}\end{aligned} \tag{4.7}$$

$$\begin{aligned}\dot{C}^{uddN}_{prst} =& - C^{uddN}_{prst}\left[4g_3^2-2\left(2\mathsf{y}_u\mathsf{y}_d+\mathsf{y}_d^2\right)g_1^2\right]+4C^{uddN}_{psrt}\left(\mathsf{y}_u\mathsf{y}_d-\mathsf{y}_d^2\right)g_1^2\\ &+ 4C^{duq\ell}_{rpwv}(Y_d^\dagger)_{ws}(Y_N^\dagger)_{vt}+8C^{qqdN}_{vwst}(Y_u^\dagger)_{vp}(Y_d^\dagger)_{wr}\\ &+ C^{uddN}_{vrst}(Y_uY_u^\dagger)_{vp}+C^{uddN}_{pvst}(Y_dY_d^\dagger)_{vr}+C^{uddN}_{prvt}(Y_dY_d^\dagger)_{vs}+C^{uddN}_{prsv}(Y_NY_N^\dagger)_{vt}\end{aligned} \tag{4.8}$$

A non-trivial check on these equations is provided by the custodial symmetry limit ($Y_{u(N)} \to Y_{d(e)}, g_1 \to 0$). In order to respect the custodial symmetry, the

BNV operator coefficients have to satisfy certain relations given in appendix A, and the RGE flow should preserve these relations. Remarkably, the construction of custodial invariant operators is compatible with $U(1)_Y$ invariance.

The structure of the anomalous dimensions can be clarified by studying the symmetry properties of the BNV operators. The operators Q^{qque} and Q^{qqdN} are symmetric in the two q indices [74],

$$Q^{qque}_{prst} = Q^{qque}_{rpst}\,, \qquad\qquad Q^{qqdN}_{prst} = Q^{qqdN}_{rpst}\,. \tag{4.9}$$

The operator $Q^{qqq\ell}$ satisfies the relation [74],

$$Q^{qqq\ell}_{prst} + Q^{qqq\ell}_{rpst} = Q^{qqq\ell}_{sprt} + Q^{qqq\ell}_{srpt}\,. \tag{4.10}$$

$Q^{qqq\ell}$ has three q indices, and so transforms like $\square \otimes \square \otimes \square$, which gives one completely symmetric, one completely antisymmetric, and two mixed symmetry tensors. Eq. (4.10) implies that one of the mixed symmetry tensors vanishes. The allowed representations of the BNV operators are shown in Table 4.1.

The coefficients C^{duue}_{prst} and C^{uddN}_{prst} can be decomposed into the symmetric and antisymmetric combinations,

$$\begin{aligned} C^{duue\,(\pm)}_{prst} &= \frac{1}{2}\left[C^{duue}_{prst} \pm C^{duue}_{psrt}\right]\,, \\ C^{uddN\,(\pm)}_{prst} &= \frac{1}{2}\left[C^{uddN}_{prst} \pm C^{uddN}_{psrt}\right]\,. \end{aligned} \tag{4.11}$$

The coefficient $C^{qqq\ell}_{prst}$ can be decomposed into terms with definite symmetry under permutations,

$$C^{qqq\ell}_{prst} = S^{qqq\ell}_{prst} + A^{qqq\ell}_{prst} + M^{qqq\ell}_{prst} + N^{qqq\ell}_{prst}\,, \tag{4.12}$$

where $S^{qqq\ell}_{prst}$ is totally symmetric in (p,r,s), $A^{qqq\ell}_{prst}$ is totally antisymmetric in (p,r,s), and $M^{qqq\ell}_{prst}$ and $N^{qqq\ell}_{prst}$ have mixed symmetry.

A convenient choice of basis is

$$\begin{aligned} S^{qqq\ell}_{prst} &= \frac{1}{6}\left[C^{qqq\ell}_{prst} + C^{qqq\ell}_{sprt} + C^{qqq\ell}_{rspt} + C^{qqq\ell}_{psrt} + C^{qqq\ell}_{srpt} + C^{qqq\ell}_{rpst}\right]\,, \\ A^{qqq\ell}_{prst} &= \frac{1}{6}\left[C^{qqq\ell}_{prst} + C^{qqq\ell}_{sprt} + C^{qqq\ell}_{rspt} - C^{qqq\ell}_{psrt} - C^{qqq\ell}_{srpt} - C^{qqq\ell}_{rpst}\right]\,, \\ M^{qqq\ell}_{prst} &= \frac{1}{3}\left[C^{qqq\ell}_{prst} - C^{qqq\ell}_{rspt} - C^{qqq\ell}_{rpst} + C^{qqq\ell}_{srpt}\right]\,, \\ N^{qqq\ell}_{prst} &= \frac{1}{3}\left[C^{qqq\ell}_{prst} - C^{qqq\ell}_{sprt} + C^{qqq\ell}_{rpst} - C^{qqq\ell}_{srpt}\right]. \end{aligned} \tag{4.13}$$

Table 4.1: Flavor representations of the BNV operators, and their dimensions. There are 273 operators in Eq. (4.1) and 135 in Eq. (4.2), for a total of 408 $\Delta B = 1$ operators with complex coefficients. One coefficient can be made real by a phase rotation of fields proportional to baryon number.

	dim	$SU(n_g)_q$	$SU(n_g)_u$	$SU(n_g)_d$	$SU(n_g)_l$	$SU(n_g)_e$	$SU(n_g)_N$
$Q^{duq\ell}_{prst}$	n_g^4	$\square$	$\square$	$\square$	$\square$	1	1
Q^{que}_{prst}	$\frac{1}{2}n_g^3(n_g+1)$	$\square\square$	$\square$	1	1	$\square$	1
Q^{qqdN}_{prst}	$\frac{1}{2}n_g^3(n_g+1)$	$\square\square$	1	$\square$	1	1	$\square$
$Q^{qqq\ell}_{prst}$	$\frac{1}{6}n_g^2(n_g+1)(n_g+2)$	$\square\square\square$	1	1	$\square$	1	1
	$\frac{1}{3}n_g^2(n_g^2-1)$	$\begin{array}{ll}\square&\square\\\square&\end{array}$	1	1	$\square$	1	1
	$\frac{1}{6}n_g^2(n_g-1)(n_g-2)$	$\begin{array}{l}\square\\\square\\\square\end{array}$	1	1	$\square$	1	1
Q^{duue}_{prst}	$\frac{1}{2}n_g^3(n_g+1)$	1	$\square\square$	$\square$	1	$\square$	1
	$\frac{1}{2}n_g^3(n_g-1)$	1	$\begin{array}{l}\square\\\square\end{array}$	$\square$	1	$\square$	1
Q^{uddN}_{prst}	$\frac{1}{2}n_g^3(n_g+1)$	1	$\square$	$\square\square$	1	1	$\square$
	$\frac{1}{2}n_g^3(n_g-1)$	1	$\square$	$\begin{array}{l}\square\\\square\end{array}$	1	1	$\square$

The coefficient $M^{qqq\ell}_{prst}$ is obtained by first anti-symmetrizing $C^{qqq\ell}_{prst}$ in (p,r), and then symmetrizing in (p,s). Likewise, $N^{qqq\ell}_{prst}$ is obtained by first anti-symmetrizing in (p,s), and then symmetrizing in (p,r). Eq. (4.10) implies that $N^{qqq\ell}_{prst}$ vanishes.

The gauge contributions to the anomalous dimensions respect the flavor symmetry of the operators. With the decomposition Eq. (4.13), the gauge contribution to the anomalous dimension matrix diagonalizes,

$$\begin{aligned}
\dot{C}^{duue\,(\pm)}_{prst} &= -\left[4g_3^2 + \left(2 \pm \frac{20}{3}\right) g_1^2\right] C^{duue\,(\pm)}_{prst} + \ldots \\
\dot{C}^{uddN\,(\pm)}_{prst} &= -\left[4g_3^2 + \left(\frac{2}{3} \pm \frac{4}{3}\right) g_1^2\right] C^{uddN\,(\pm)}_{prst} + \ldots \\
\dot{S}^{qqq\ell}_{prst} &= -\left[4g_3^2 + 15g_2^2 + \frac{1}{3}g_1^2\right] S^{qqq\ell}_{prst} + \ldots \\
\dot{A}^{qqq\ell}_{prst} &= -\left[4g_3^2 - 9g_2^2 + \frac{1}{3}g_1^2\right] A^{qqq\ell}_{prst} + \ldots \\
\dot{M}^{qqq\ell}_{prst} &= -\left[4g_3^2 + 3g_2^2 + \frac{1}{3}g_1^2\right] M^{qqq\ell}_{prst} + \ldots .
\end{aligned} \tag{4.14}$$

The "$\ldots$" refers to the Yukawa contributions, which can mix different permutation representations.

4.3 Discussion

The renormalization group equations presented here have an involved flavor structure; to better understand the generic features, we turn now to certain simplifying hypotheses and models that produce a simple subclass of BNV operators.

4.3.1 Minimal Flavor Violation

The SM has an $SU(3)^5$ flavor symmetry for the q, u, d, l, and e fields, broken only by the Higgs Yukawa interactions. The symmetry is preserved if we promote the Yukawa coupling matrices to spurions that transform appropriately under the flavor group. Minimal flavor violation (MFV) [84, 85] is the hypothesis that any new physics beyond the SM preserves this symmetry, so the Yukawa coupling matrices are the only spurions.

Dimension-six BNV operators do not satisfy naïve minimal flavor violation because of triality. The argument proceeds as follows: under every $SU(3)_i$ flavor transformation, each BNV operator transforms as a representation of $SU(3)_i$ with n_i upper indices and m_i lower indices. All BNV operators satisfy $\sum_{i=1}^{5}(n_i - m_i) \equiv 1 \pmod 3$. No combination of Yukawa matrices (or other invariant tensors) can change this into a singlet, as they all have $(n - m) \equiv 0 \pmod 3$.

In extensions of the MFV hypothesis to account for massive neutrinos [86–88], a Majorana mass term introduces a spurion with $(n - m) \equiv 2 \pmod 3$. This in turn allows for the implementation of MFV, as pointed out in Ref. [89]. Note also that if the Yukawa spurions are built out of objects with simpler flavor-transformation properties [90], a variant of minimal flavor violation is possible without Lepton number violation.

Finally, there is the possibility that the fermion fields do not each separately have an $SU(3)$ flavor symmetry, but that some transform simultaneously [91]. The latter is an attractive option that is realized in Grand Unified Theories (GUTs), and we explore this possibility in the next subsection.

4.3.2 Grand Unified Theories

The Georgi-Glashow $SU(5)$ theory [65] places u^c, q, and e^c in a **10** representation of $SU(5)$, and d^c and l in a $\overline{\mathbf{5}}$. In the context of the type-I seesaw, N is a **1**. The flavor group in this case cannot be that of putative MFV since the fields in each $SU(5)$ representation must transform simultaneously. The flavor symmetry is instead $SU(3)^3 = SU(3)_{\mathbf{10}} \otimes SU(3)_{\bar{\mathbf{5}}} \otimes SU(3)_{\mathbf{1}}$, where each $SU(3)$ stands for transformations in flavor space of the corresponding $SU(5)$ representation [91]. The fermions and spurions then fall into the representations

$$\begin{aligned} u^c, q, e^c &\sim (\mathbf{3}, \mathbf{1}, \mathbf{1})\,, & Y_u &\sim (\bar{\mathbf{6}}, \mathbf{1}, \mathbf{1})\,, \\ d^c, l &\sim (\mathbf{1}, \mathbf{3}, \mathbf{1})\,, & Y_d, Y_e^T &\sim (\bar{\mathbf{3}}, \bar{\mathbf{3}}, \mathbf{1})\,, \\ N^c &\sim (\mathbf{1}, \mathbf{1}, \mathbf{3})\,, & Y_N &\sim (\mathbf{1}, \bar{\mathbf{3}}, \bar{\mathbf{3}})\,, \\ & & M_N &\sim (\mathbf{1}, \mathbf{1}, \mathbf{6})\,, \end{aligned} \tag{4.15}$$

where the right-handed neutrino Majorana mass M_N also needs to be promoted to

a spurion. Note that the triality argument given previously does not apply to the Yukawa matrices in this scenario. With the $SU(5)$ GUT in mind, we will relabel the Yukawas $Y_u \to Y_{10}$, $(Y_d, Y_e^T) \to Y_5$, and $Y_N \to Y_1$.

The operators transform as

$$\begin{aligned}
Q^{duq\ell} &\sim (\mathbf{3}\otimes\bar{\mathbf{3}}, \mathbf{3}\otimes\bar{\mathbf{3}}, \mathbf{1}),\\
Q^{qqq\ell} &\sim (\mathbf{3}\otimes\mathbf{3}\otimes\mathbf{3}, \mathbf{3}, \mathbf{1}),\\
Q^{uddN} &\sim (\bar{\mathbf{3}}, \bar{\mathbf{3}}\otimes\bar{\mathbf{3}}, \bar{\mathbf{3}}),\\
Q^{duue} &\sim (\bar{\mathbf{3}}\otimes\bar{\mathbf{3}}\otimes\bar{\mathbf{3}}, \bar{\mathbf{3}}, \mathbf{1}),\\
Q^{qqdN} &\sim (\mathbf{3}\otimes\mathbf{3}, \bar{\mathbf{3}}, \bar{\mathbf{3}}),\\
Q^{qque} &\sim (\mathbf{3}\otimes\bar{\mathbf{3}}\otimes\mathbf{3}\otimes\bar{\mathbf{3}}, \mathbf{1}, \mathbf{1}),
\end{aligned} \tag{4.16}$$

which now can be combined with Yukawa couplings to build up invariant terms in the Lagrangian. Explicitly, the coefficients of the operators in terms of Yukawa matrices up to second order are

$$\begin{aligned}
C^{duq\ell} &\sim 1 \oplus Y_{10}^\dagger Y_{10} \oplus Y_5^\dagger Y_5\,,\\
C^{qqq\ell} &\sim Y_{10}\otimes Y_5\,,\\
C^{uddN} &\sim Y_5^\dagger \otimes Y_1^\dagger\,,\\
C^{duue} &\sim Y_{10}^\dagger \otimes Y_5^\dagger\,,\\
C^{qqdN} &\sim Y_{10}\otimes Y_1^\dagger\,,\\
C^{qque} &\sim 1 \oplus Y_{10}Y_{10}^\dagger \oplus Y_{10}\otimes Y_{10}^\dagger\,.
\end{aligned} \tag{4.17}$$

Notice that only $C^{duq\ell}$ and C^{qque} can be constructed out of flavor singlets. These are the only two operators that can be generated by integrating out heavy gauge bosons in the context of $SU(5)$ or, in general, by flavor-blind $SU(5)$ invariant dynamics. In addition, these are the only two coefficients that remain in the limit $Y_5, Y_1 \to 0$ ($Y_d, Y_e, Y_N \to 0$).

To close this section, let us comment on the implications for supersymmetric GUTs in our framework. BNV dimension-five operators are produced by integrating out GUT particles in supersymmetric theories in the absence of selection rules like R-parity [92–94]. Below the supersymmetry breaking scale, these

will translate into the operators $Q^{qqq\ell}$, Q^{duue} and Q^{uddN} in terms of the SM EFT Lagrangian, being only suppressed by one power of the BNV scale: $1/(M_{\not B} M_{\rm SUSY})$. A feature of this scenario is that, as a result of the supersymmetric origin of the operators, all diagonal entries in flavor vanish [93], so that proton decay would require a strange particle. The renormalization group equations presented here only apply in the regime $\mu < M_{\rm SUSY}$ since they depend on the spectrum of the theory, and we have assumed only dynamical SM particles. See Ref. [95] for a RGE study of BNV effects in the context of supersymmetry.

4.3.3 Magnitude of Effects

In this subsection, we simplify the RGE to estimate the magnitude of running a BNV operator coefficient from the GUT scale to the electroweak scale. Working in the context of a MFV GUT discussed in Sec. 4.3.2, we set $Y_d = Y_e = Y_N = 0$, assuming top-Yukawa dominance. In that limit, the only two non-vanishing operators are $Q^{duq\ell}_{prst}$ and Q^{qque}_{prst}, whose RGE equations decouple. The coefficients of these two operators are given by appropriate combinations of Y_{10} which transforms as the symmetric representation, $\bar{\mathbf{6}}$.

As an example, we focus on $Q^{duq\ell}_{prst}$, whose coefficient takes on a simple form:

$$C^{duq\ell}_{prst} = C^{duq\ell}_{rs}\delta_{pt}, \quad \text{where} \quad C^{duq\ell}_{rs} = f(Y_{10}^\dagger Y_{10})_{rs}\,, \tag{4.18}$$

and $f(0)_{rs} \propto \delta_{rs}$. The RGE of this coefficient becomes

$$\dot{C}^{duq\ell}_{rs} \to \left[\frac{1}{2}Y_{10}^\dagger Y_{10} - 4g_3^2 - \frac{9}{2}g_2^2 - \frac{11}{6}g_1^2\right]_{rw} C^{duq\ell}_{ws}. \tag{4.19}$$

We can now choose the basis $Y_{10} = Y_u = \mathrm{diag}(0,0,y_t)$, where y_t is the top-quark Yukawa coupling and lighter up-type quark masses are neglected. With this simplification, $C^{duq\ell}_{rs}$ is a diagonal matrix. Setting $M_{GUT} \approx 10^{15}\,\mathrm{GeV}$, the $C^{duq\ell}$ coefficients at the electroweak and GUT scales are related by

$$\begin{aligned} C^{duq\ell}_{33}(M_Z) &\approx (2.26)(0.96)\, C^{duq\ell}_{33}(M_{\rm GUT})\,, \\ C^{duq\ell}_{22\,(11)}(M_Z) &\approx (2.26)\, C^{duq\ell}_{22\,(11)}(M_{\rm GUT})\,. \end{aligned} \tag{4.20}$$

The first factor in parentheses comes from the gauge contribution alone, is dominated by the QCD coupling, and is common to all flavor coefficients. The second factor is the extra correction from including the Yukawa contribution, with only the top entry sizeable. Whereas the gauge contribution to the RGE enhances the $C_{rs}^{duq\ell}$ coefficient at lower energy scales, the Yukawa contribution gives a small suppression.

The Yukawa-induced running will in general be negligible for the lightest generation coefficients and processes like proton or neutron decay are unaffected. The Yukawa running gives a small correction for heavier generations. Note that the relatively small correction from Yukawa running compared to gauge-induced running stems from the different numerical coefficients of the anomalous dimension, since $g_3 \sim y_t$. For example, in Eq. (4.19), the color and $SU(2)_L$ gauge contributions have *each* a pre-factor ~ 8 times that of the Yukawas. These numerical factors cannot be estimated and require the explicit computation presented here.

The Yukawa running studied in this section have the most impact in heavy flavor BNV transitions, which are searched for experimentally [96, 97]. In this regard, the fact that W boson exchange below the electroweak symmetry-breaking scale produces flavor mixing is relevant. In particular, at two-loop order, proton or neutron decay is sensitive to BNV operators with arbitrary flavor. Even though a two-loop effect, this places a strong bound on heavy flavor BNV. Discussions of heavy BNV transitions taking into account these effects can be found in Refs. [98–100].

4.4 Conclusions

In this chapter, we have included the Yukawa contribution to the anomalous dimension matrix of baryon number violating operators and have thus completed the one-loop renormalization group evolution. Together with the computation of Refs. [75–77], this completes the anomalous dimension matrix for the totality of dimension-six operators of the SM. We included right-handed neutrinos and therefore two new BNV operators, and classified all the operators under flavor

symmetry. None of the operators satisfies $SU(3)^5$ minimal flavor violation, but it is possible to impose a weaker grand unified theory variant of MFV. The Yukawa coupling corrections only give small corrections to the operator evolution.

Chapter 4, in full, is a reprint of the material as it appears in *Phys. Lett. B* **734** 302 (2014). R. Alonso, H.-M. Chang, E. Jenkins, A. Manohar, and B. Shotwell. The dissertation author was co-author of this paper.

Appendix A

Dimensional Regularization Formulae

The following integrals (Eq. (A.1) – (A.2)) come from Chapter 1 of Ref. [12]. "Feynman Parameterization" often refers to the formula ($M \equiv \sum_{i=1}^{n} m_i$)

$$\frac{1}{a_1^{m_1} \cdots a_n^{m_n}} = \frac{\Gamma(M)}{\Gamma(m_1) \cdots \Gamma(m_n)} \int_0^1 dx_1 x_1^{m_1 - 1} \cdots \int_0^1 dx_n x_n^{m_n - 1} \frac{\delta\left(1 - \sum_{i=1}^{n} x_i\right)}{[x_1 a_1 + \cdots + x_n a_n]^M} \tag{A.1}$$

A very useful formula for integrals in Dimensional Regularization is

$$\int \underbrace{\frac{d^d \ell}{(2\pi)^d}}_{\equiv \bar{d}^d \ell} \frac{(\ell^2)^\alpha}{(\ell^2 - \Delta)^\beta} = \frac{i}{(4\pi)^{d/2}} (-1)^{\alpha+\beta} (\Delta)^{\alpha - \beta + d/2} \frac{\Gamma(\alpha + d/2)\Gamma(\beta - \alpha - d/2)}{\Gamma(d/2)\Gamma(\beta)} \tag{A.2}$$

For example, for $d = 4 - 2\epsilon$ and $\beta - \alpha - 2 = 0$, the integral gives:

$$\mu^{2\epsilon} \int \frac{d^d \ell}{(2\pi)^d} \frac{(\ell^2)^\alpha}{(\ell^2 - \Delta)^\beta} = \frac{i}{(16\pi^2)} \left(\frac{1}{\epsilon} - \log\left(\frac{\Delta}{4\pi e^{-\gamma} \mu^2} \right) + 1 - \sum_{n=1}^{\beta - 1} \frac{1}{n} + \mathcal{O}(\epsilon) \right) \tag{A.3}$$

where $\beta \in \mathbb{Z}$ and $\beta \geq 2$.

Appendix B

Plus Distributions

The *Plus Distribution* $f(x)_+$ on $x \in [0,1]$ is defined to have the following properties:

1. $f(x)_+ = f(x)$ for all x such that $f(x)$ is finite.
2. $\int_0^1 f(x)_+ = 0$.

Plus distributions, like delta-function distributions, serve as integral transforms; often they are used to make a kernel out of a non-integrable function $f(x)$. One can manipulate terms involving plus distributions to extract or absorb divergences via delta-functions. For example,

$$\int_0^1 \frac{1+z^2}{(1-z)_+}dz = \int_0^1 \frac{1+z^2-2+2}{(1-z)_+}dz = -\int_0^1 (z+1)dz + 0 = -\frac{3}{2} \qquad \text{(B.1)}$$

This implies $\left(\frac{1+z^2}{1-z}\right)_+ = \frac{1+z^2}{(1-z)_+} + \frac{3}{2}\delta(1-z)$ (used in Eq. (2.80)).

In addition, the following plus distribution identity is used in Chapter 2:

$$\frac{1}{(1-z)^{1+\epsilon}} = -\frac{1}{\epsilon}\delta(1-z) + \frac{1}{(1-z)_+} - \epsilon\left(\frac{\ln(1-z)}{1-z}\right)_+ + \mathcal{O}(\epsilon^2) \qquad \text{(B.2)}$$

Appendix C

Summary of $\mathbf{SCET_{EW}}$ Results

We now summarize the results of Refs. [33–40] for the electroweak corrections.

1. At a high scale μ_h of order s, the scattering amplitudes are matched onto $SU(3) \times SU(2) \times U(1)$ gauge invariant local operators O_i with coefficients C_i which can be computed perturbatively in a power series in $\alpha(\mu_h)$. The calculations in Refs. [33–40] include QCD as well as electroweak corrections, so α denotes any of the three gauge coupling constants in the Standard Model (SM). As an example, for $g(p_1) + g(p_2) \to q(p_3) + \overline{q}(p_4)$, the operators are

$$\begin{aligned} O_1 &= \bar{q}_4 q_3 A_2^A A_1^A \\ O_2 &= d^{ABC} \bar{q}_4 T^C q_3 A_2^A A_1^B \\ O_3 &= i f^{ABC} \bar{q}_4 T^C q_3 A_2^A A_1^B \,. \end{aligned} \tag{C.1}$$

   which give the possible color structures of the amplitude. The subscripts $1, 2, 3, 4$ label the different particle momenta.

2. The coefficients C_i are evolved using renormalization group equations (RGE) down to a low scale μ_l of order M_W. The anomalous dimensions can be computed in the unbroken $SU(3) \times SU(2) \times U(1)$ theory.

3. At the scale μ_l, the W, Z, H and t are integrated out. This calculation must be done in the broken theory. A single gauge invariant operator breaks up

into different components because the weak interaction symmetry is broken. For example, each of the operators O_i in Eq. (C.1) breaks up into an $SU(3)$ invariant $gg \to t\bar{t}$ and $gg \to b\bar{b}$ operator.

4. The operators in the theory below μ_l are then used to compute the scattering cross sections.

The final result is that the scattering amplitudes $\mathcal{M}$ can be written as

$$\begin{aligned}\mathcal{M} = &\exp\left[D_C(\mu_l, \mathsf{L_M}, \bar{n}\cdot p)\right] d_S(\mu_l, \mathsf{L_M}) \\ &\times P\,\exp\left[\int_{\mu_h}^{\mu_l} \frac{\mathrm{d}\mu}{\mu}\gamma(\mu, \bar{n}\cdot p)\right] C(\mu_h, \mathsf{L_Q})\end{aligned} \tag{C.2}$$

Eq. (C.2) gives the scattering amplitude in resummed form. Explicit formulæ for all the pieces can be found in Ref. [34].

The high-scale matching $C(\mu_h, \mathsf{L_Q})$ is an n dimensional column vector with a perturbative expansion in $\alpha_i(\mu_h)$, with $i = 1, 2, 3$ being the $U(1)$, $SU(2)$ and $SU(3)$ couplings. It also depends on $\mathsf{L_Q} = \ln s/\mu_h^2$, which is not a large logarithm if one picks $\mu_h^2 \sim s$. For Eq. (C.1), $n = 3$ since there are 3 gauge invariant amplitudes.

The SCET anomalous dimension $\gamma(\mu)$ is an $n \times n$ anomalous dimension matrix which can be written as the sum of a collinear and soft part

$$\gamma(\mu, \bar{n}\cdot p) = \gamma_C(\mu, \bar{n}\cdot p) + \gamma_S(\mu) \tag{C.3}$$

where the collinear part is diagonal

$$\gamma_C(\mu, \bar{n}\cdot p) = \mathbb{1}\sum_r \left[A_r(\mu)\ln\frac{2E_r}{\mu} + B_r(\mu)\right] \tag{C.4}$$

and linear in $\log \bar{n}_r \cdot p_r = E_r$, the energy of the parton, to all orders in perturbation theory [18,33]. The sum on r is over all partons in the scattering process, and $A_r(\mu)$ and $B_r(\mu)$ have a perturbative expansion in $\alpha_i(\mu)$. γ_S at one-loop order is

$$\gamma_S(\mu) = -\sum_{\langle rs\rangle, i} \frac{\alpha_i(\mu)}{\pi} T_r^{(i)} \cdot T_s^{(i)} \ln\frac{-n_r\cdot n_s + i0^+}{2} \tag{C.5}$$

where the sum is over all parton pairs $\langle rs\rangle$, and $n_r = (1, \mathbf{n}_r)$ is a null vector in the direction of parton r for each incoming parton, and $n_r = -(1, \mathbf{n}_r)$ for each outgoing parton. $T_r^{(i)}$ is the gauge generator for the i^{th} gauge group acting on parton r.

The low-scale matching has a collinear part D_C and a soft part d_S. The soft part d_S is an $m \times n$ matrix, where m is the number of amplitudes produced after $SU(2) \times U(1)$ breaking. In $gg \to q\overline{q}$, if q is an electroweak doublet of left-handed quarks $(t, b)_L$, then starting with the operators in Eq. (C.1) gives $m = 6$ operators after $SU(2) \times U(1)$ breaking, where $\overline{q}_4 q_3 \to \overline{t}_4 t_3$, or $\overline{q}_4 q_3 \to \overline{b}_4 b_3$. If q in Eq. (C.1) is an electroweak singlet, such as b_R or t_R, then $m = 3$. $d_S(\mu, \mathsf{L_M})$ has an expansion in $\alpha_{S,W,\mathrm{EM}}(\mu_l)$, and can depend on electroweak scale masses and μ_l via dimensionless ratios such as M_W/M_Z and $\mathsf{L_M} = \ln M_Z/\mu_l$. The logarithms are small if one chooses $\mu_l \sim M_Z$.

The collinear matching D_C is an $m \times m$ diagonal matrix given by

$$[D_C(\mu, \bar{n} \cdot p, \mathsf{L_M})]_{ii} = \sum_r \left[J_r(\mu, \mathsf{L_M}) \ln \frac{2E_r}{\mu} + H_r(\mu, \mathsf{L_M}) \right] \tag{C.6}$$

and J_r and H_r are functions of $\alpha_{S,W,\mathrm{EM}}(\mu_l)$, and can depend on electroweak scale masses and μ_l via dimensionless ratios such as M_W/M_Z and $\mathsf{L_M} = \ln M_Z/\mu_l$. The sum on r is over all particles in operator O_i produced after electroweak symmetry breaking, and D_C is linear in $\ln \bar{n} \cdot p$ to all orders in perturbation theory [18, 33].

The exponent contains at most a double-log given by integrating the A_i terms in the collinear anomalous dimension. The low-scale matching contains a single-log term. This a new feature of $\mathrm{SCET_{EW}}$ first pointed out in Ref. [36]. One can show that the low-scale matching contains at most a single-log to all orders in perturbation theory [34, 36]. As a consequence, resummed perturbation theory remains valid even at high energy, because $\alpha^n \ln s/M_W^2 \ll 1$ for large enough n. A_i, γ_S, and J_i are related to the cusp anomalous dimension.

The log term in the matching Eq. (C.6) is needed for proper factorization of scales. A typical Sudakov double-log term at one loop has the form (dropping the overall α)

$$\ln^2 \frac{Q^2}{M^2} = \ln^2 \frac{Q^2}{\mu_h^2} + \left[\ln^2 \frac{Q^2}{\mu_l^2} - \ln^2 \frac{Q^2}{\mu_h^2} \right] + \left[\ln^2 \frac{M^2}{\mu_l^2} - 2 \ln \frac{Q^2}{\mu_l^2} \ln \frac{M^2}{\mu_l^2} \right] \tag{C.7}$$

The first term is the high-scale matching C, the second term arises from integrating the $\ln Q^2/\mu^2$ anomalous dimension from μ_h to μ_l, and the third term is the low-scale matching D. The existence of the log term in the matching also follows from

the consistency condition that the theory is independent of μ_l. Since changes in the running between μ_h and μ_l contain a single log from the anomalous dimension, there must be a single log in the matching. What is non-trivial is that Eq. (C.2) only requires a single-log in the matching to all orders in perturbation theory [34, 36].

The resummed electroweak corrections can be grouped as LL, NLL, etc., in the usual way, and the precise definition for $\mathrm{SCET}_{\mathrm{EW}}$ can be found in Ref. [33]. All terms needed for a NLL computation are known, so *all* processes can be computed to resummed NLL order. Refs. [34,35] computed the one-loop d_S and C terms, for all $2 \to 2$ processes.

The three-loop cusp anomalous dimension A and two-loop non-cusp anomalous B are known, except for the scalar Higgs contributions, which are numerically small. The two-loop contribution to D_C is not known. The NNLL results are known, with the exception of these terms.

Appendix D

Operator Relations and Custodial Symmetry

Refs. [71, 72] split the $Q^{qqq\ell}$ operator into two operators

$$\begin{aligned} Q_{prst}^{qqq\ell\,(1)} &= \epsilon_{\alpha\beta\gamma}\epsilon_{ij}\epsilon_{kl}(q_p^{i\alpha}Cq_r^{j\beta})(q_s^{\gamma k}Cl_t^l)\,, \\ Q_{prst}^{qqq\ell\,(3)} &= \epsilon_{\alpha\beta\gamma}(\tau^I\epsilon)_{ij}(\tau^I\epsilon)_{kl}(q_p^{i\alpha}Cq_r^{j\beta})(q_s^{\gamma k}Cl_t^l)\,, \end{aligned} \tag{D.1}$$

where τ^I is an $SU(2)_L$ generator. These operators can be written in terms of $Q_{prst}^{qqq\ell}$ [74]

$$\begin{aligned} Q_{prst}^{qqq\ell\,(1)} &= -(Q_{prst}^{qqq\ell} + Q_{rpst}^{qqq\ell})\,, \\ Q_{prst}^{qqq\ell\,(3)} &= -(Q_{prst}^{qqq\ell} - Q_{rpst}^{qqq\ell})\,, \end{aligned} \tag{D.2}$$

$Q_{prst}^{qqq\ell\,(1)}$ and $Q_{prst}^{qqq\ell\,(3)}$ are symmetric and antisymmetric in the first two flavor indices, respectively, and transform as symmetric plus mixed, and antisymmetric plus mixed representations under permutation of the three q indices. Since there is only one mixed symmetry tensor in $Q^{qqq\ell}$ by Eq. (4.10), the mixed symmetry tensors in $Q^{qqq\ell\,(1,3)}$ are the same, and the two operators are not independent.

The custodial $SU(2)_L \times SU(2)_R$ symmetry is preserved in the SM for $g_1 \to 0$ and $Y_{u(N)} \to Y_{d(e)}$. It can be implemented in the BNV operators by arranging the right-handed fermions in doublets, $q_R = (u_R, d_R)^T$ and $\ell_R = (N_R, e_R)^T$. By construction, $Q^{qqq\ell}$ is already custodial invariant and the five remaining operators

are grouped into the custodial $SU(2)$ invariant combinations

$$\begin{aligned}
\epsilon_{ij}\epsilon_{kl}(q^i_{R\,p}Cq^j_{R\,r})(q^k_s C\ell^l_t) &= -Q^{duq\ell}_{prst} - Q^{duq\ell}_{rpst}\,, \\
\epsilon_{ij}\epsilon_{kl}(q^i_p Cq^j_r)(q^k_{R\,s}C\ell^l_{R\,t}) &= Q^{qque}_{prst} - Q^{qqdN}_{prst}\,, \\
\epsilon_{ij}\epsilon_{kl}(q^i_{R\,p}Cq^j_{R\,r})(q^k_{R\,s}C\ell^l_{R\,t}) &= -Q^{uddN}_{prst} - Q^{uddN}_{rpst} - Q^{duue}_{prst} - Q^{duue}_{rpst}\,,
\end{aligned} \tag{D.3}$$

where color indices are implicit. The component fields of q_R and ℓ_R have different hypercharges, but the custodial invariant operators *are* $U(1)_Y$ invariant. The above equations imply extra relations for the operator coefficients

$$\begin{aligned}
C^{duq\ell}_{prst} &= C^{duq\ell}_{rpst}\,, \\
C^{qque}_{prst} &= -C^{qqdN}_{prst}\,, \\
C^{duue}_{prst} &= C^{duue}_{rpst}\,, \\
C^{duue}_{prst} &= C^{uddN}_{prst}\,,
\end{aligned} \tag{D.4}$$

in the custodial $SU(2)$ limit.

Bibliography

[1] Aneesh V. Manohar. Effective field theories. 1995.

[2] Christian W. Bauer, Sean Fleming, and Michael E. Luke. Summing Sudakov logarithms in $B \to X(s\gamma)$ in effective field theory. *Phys.Rev.*, D63:014006, 2000.

[3] Christian W. Bauer, Sean Fleming, Dan Pirjol, and Iain W. Stewart. An Effective field theory for collinear and soft gluons: Heavy to light decays. *Phys.Rev.*, D63:114020, 2001.

[4] Christian W. Bauer and Iain W. Stewart. Invariant operators in collinear effective theory. *Phys.Lett.*, B516:134–142, 2001.

[5] Christian W. Bauer, Dan Pirjol, and Iain W. Stewart. Soft collinear factorization in effective field theory. *Phys.Rev.*, D65:054022, 2002.

[6] Michael J. Dugan and Benjamin Grinstein. QCD basis for factorization in decays of heavy mesons. *Phys.Lett.*, B255:583–588, 1991.

[7] Benjamin Grinstein. The Static Quark Effective Theory. *Nucl.Phys.*, B339:253–268, 1990.

[8] Estia Eichten and Brian Russell Hill. An Effective Field Theory for the Calculation of Matrix Elements Involving Heavy Quarks. *Phys.Lett.*, B234:511, 1990.

[9] Howard Georgi. An Effective Field Theory for Heavy Quarks at Low-energies. *Phys.Lett.*, B240:447–450, 1990.

[10] Ambar Jain, Massimiliano Procura, Brian Shotwell, and Wouter J. Waalewijn. Fragmentation with a Cut on Thrust: Predictions for B-factories. *Phys.Rev.*, D87(7):074013, 2013.

[11] Edward Farhi. A QCD Test for Jets. *Phys.Rev.Lett.*, 39:1587–1588, 1977.

[12] Aneesh V. Manohar and Mark B. Wise. Heavy quark physics. *Camb.Monogr.Part.Phys.Nucl.Phys.Cosmol.*, 10:1–191, 2000.

[13] John C. Collins, Aneesh V. Manohar, and Mark B. Wise. Renormalization of the vector current in QED. *Phys.Rev.*, D73:105019, 2006.

[14] Ambar Jain, Massimiliano Procura, and Wouter J. Waalewijn. Parton Fragmentation within an Identified Jet at NNLL. *JHEP*, 1105:035, 2011.

[15] Guido Altarelli, R. Keith Ellis, G. Martinelli, and So-Young Pi. Processes Involving Fragmentation Functions Beyond the Leading Order in QCD. *Nucl.Phys.*, B160:301, 1979.

[16] G. Curci, W. Furmanski, and R. Petronzio. Evolution of Parton Densities Beyond Leading Order: The Nonsinglet Case. *Nucl.Phys.*, B175:27, 1980.

[17] E.G. Floratos, C. Kounnas, and R. Lacaze. Higher Order QCD Effects in Inclusive Annihilation and Deep Inelastic Scattering. *Nucl.Phys.*, B192:417, 1981.

[18] Aneesh V. Manohar. Deep inelastic scattering as $x \to 1$ using soft collinear effective theory. *Phys.Rev.*, D68:114019, 2003.

[19] Matthew D. Schwartz. Quantum Field Theory and the Standard Model. 2013.

[20] Guido Altarelli and G. Parisi. Asymptotic Freedom in Parton Language. *Nucl.Phys.*, B126:298, 1977.

[21] Massimiliano Procura and Iain W. Stewart. Quark Fragmentation within an Identified Jet. *Phys.Rev.*, D81:074009, 2010.

[22] **Belle Collaboration** Collaboration, R. Seidl et al. Measurement of Azimuthal Asymmetries in Inclusive Production of Hadron Pairs in e+e- Annihilation at $\sqrt{s} = 10.58\,\mathrm{GeV}$. *Phys.Rev.*, D78:032011, 2008.

[23] M. Hirai, S. Kumano, T.-H. Nagai, and K. Sudoh. Determination of fragmentation functions and their uncertainties. *Phys.Rev.*, D75:094009, 2007.

[24] Massimiliano Procura and Wouter J. Waalewijn. Fragmentation in Jets: Cone and Threshold Effects. *Phys.Rev.*, D85:114041, 2012.

[25] Riccardo Abbate, Michael Fickinger, Andre Hoang, Vicent Mateu, and Iain W. Stewart. Thrust distribution at N^3LL with power corrections and precision determination of $\alpha_s(M_Z)$. *PoS*, DIS2010:124, 2010.

[26] Marcello Ciafaloni, Paolo Ciafaloni, and Denis Comelli. Bloch-Nordsieck violating electroweak corrections to inclusive TeV scale hard processes. *Phys. Rev. Lett.*, 84:4810–4813, 2000.

[27] P. Ciafaloni and D. Comelli. Sudakov enhancement of electroweak corrections. *Phys. Lett.*, B446:278–284, 1999.

[28] P. Ciafaloni and D. Comelli. Electroweak Sudakov form factors and nonfactorizable soft QED effects at NLC energies. *Phys. Lett.*, B476:49–57, 2000.

[29] Paolo Ciafaloni and Denis Comelli. The Importance of weak bosons emission at LHC. *JHEP*, 0609:055, 2006.

[30] U. Baur. Weak Boson Emission in Hadron Collider Processes. *Phys.Rev.*, D75:013005, 2007.

[31] G. Bell, J.H. Kuhn, and J. Rittinger. Electroweak Sudakov Logarithms and Real Gauge-Boson Radiation in the TeV Region. *Eur.Phys.J.*, C70:659–671, 2010.

[32] S. Frixione, V. Hirschi, D. Pagani, H. S. Shao, and M. Zaro. Weak corrections to Higgs hadroproduction in association with a top-quark pair. 2014.

[33] Jui-yu Chiu, Andreas Fuhrer, Randall Kelley, and Aneesh V. Manohar. Factorization Structure of Gauge Theory Amplitudes and Application to Hard Scattering Processes at the LHC. *Phys.Rev.*, D80:094013, 2009.

[34] Jui-yu Chiu, Andreas Fuhrer, Randall Kelley, and Aneesh V. Manohar. Soft and Collinear Functions for the Standard Model. *Phys.Rev.*, D81:014023, 2010.

[35] Andreas Fuhrer, Aneesh V. Manohar, Jui-yu Chiu, and Randall Kelley. Radiative Corrections to Longitudinal and Transverse Gauge Boson and Higgs Production. *Phys.Rev.*, D81:093005, 2010.

[36] Jui-yu Chiu, Frank Golf, Randall Kelley, and Aneesh V. Manohar. Electroweak Sudakov corrections using effective field theory. *Phys.Rev.Lett.*, 100:021802, 2008.

[37] Jui-yu Chiu, Frank Golf, Randall Kelley, and Aneesh V. Manohar. Electroweak Corrections in High Energy Processes using Effective Field Theory. *Phys.Rev.*, D77:053004, 2008.

[38] Jui-yu Chiu, Randall Kelley, and Aneesh V. Manohar. Electroweak Corrections using Effective Field Theory: Applications to the LHC. *Phys.Rev.*, D78:073006, 2008.

[39] Jui-yu Chiu, Andreas Fuhrer, Andre H. Hoang, Randall Kelley, and Aneesh V. Manohar. Using SCET to calculate electroweak corrections in gauge boson production. *PoS*, EFT09:009, 2009.

[40] Jui-yu Chiu, Andreas Fuhrer, Andre H. Hoang, Randall Kelley, and Aneesh V. Manohar. Soft-Collinear Factorization and Zero-Bin Subtractions. *Phys.Rev.*, D79:053007, 2009.

[41] Andreas Fuhrer, Aneesh V. Manohar, and Wouter J. Waalewijn. Electroweak radiative Corrections to Higgs Production via Vector Boson Fusion using Soft-Collinear Effective Theory. *Phys.Rev.*, D84:013007, 2011.

[42] Victor S. Fadin, L. N. Lipatov, Alan D. Martin, and M. Melles. Resummation of double logarithms in electroweak high energy processes. *Phys. Rev.*, D61:094002, 2000.

[43] Johann H. Kuhn, A. A. Penin, and Vladimir A. Smirnov. Summing up subleading Sudakov logarithms. *Eur. Phys. J.*, C17:97–105, 2000.

[44] Bernd Feucht, Johann H. Kuhn, Alexander A. Penin, and Vladimir A. Smirnov. Two-loop Sudakov form factor in a theory with mass gap. *Phys. Rev. Lett.*, 93:101802, 2004.

[45] Bernd Jantzen, Johann H. Kuhn, Alexander A. Penin, and Vladimir A. Smirnov. Two-loop electroweak logarithms. *Phys. Rev.*, D72:051301, 2005.

[46] Bernd Jantzen, Johann H. Kuhn, Alexander A. Penin, and Vladimir A. Smirnov. Two-loop electroweak logarithms in four-fermion processes at high energy. *Nucl. Phys.*, B731:188–212, 2005.

[47] M. Beccaria, F. M. Renard, and C. Verzegnassi. Top quark production at future lepton colliders in the asymptotic regime. *Phys. Rev.*, D63:053013, 2001.

[48] Ansgar Denner and Stefano Pozzorini. One-loop leading logarithms in electroweak radiative corrections. I: Results. *Eur. Phys. J.*, C18:461–480, 2001.

[49] Ansgar Denner and Stefano Pozzorini. One-loop leading logarithms in electroweak radiative corrections: II. Factorization of collinear singularities. *Eur. Phys. J.*, C21:63–79, 2001.

[50] M. Hori, H. Kawamura, and J. Kodaira. Electroweak Sudakov at two loop level. *Phys. Lett.*, B491:275–279, 2000.

[51] W. Beenakker and A. Werthenbach. Electroweak two-loop Sudakov logarithms for on-shell fermions and bosons. *Nucl. Phys.*, B630:3–54, 2002.

[52] Ansgar Denner, M. Melles, and S. Pozzorini. Two-loop electroweak angular-dependent logarithms at high energies. *Nucl. Phys.*, B662:299–333, 2003.

[53] S. Pozzorini. Next-to-leading mass singularities in two-loop electroweak singlet form factors. *Nucl. Phys.*, B692:135–174, 2004.

[54] Bernd Jantzen and Vladimir A. Smirnov. The two-loop vector form factor in the Sudakov limit. *Eur. Phys. J.*, C47:671–695, 2006.

[55] Michael Melles. Mass gap effects and higher order electroweak Sudakov logarithms. *Phys. Lett.*, B495:81–86, 2000.

[56] Michael Melles. Subleading Sudakov logarithms in electroweak high energy processes to all orders. *Phys. Rev.*, D63:034003, 2001.

[57] Michael Melles. Electroweak radiative corrections in high-energy processes. *Phys. Rept.*, 375:219–326, 2003.

[58] Ansgar Denner, B. Jantzen, and S. Pozzorini. Two-loop electroweak next-to-leading logarithmic corrections to massless fermionic processes. *Nucl. Phys.*, B761:1–62, 2007.

[59] Johann H. Kuhn, F. Metzler, and A. A. Penin. Next-to-Next-to-Leading Electroweak Logarithms in W-pair Production at ILC. *Nucl. Phys.*, B795:277–290, 2008.

[60] Ansgar Denner, Bernd Jantzen, and Stefano Pozzorini. Two-loop electroweak next-to-leading logarithms for processes involving heavy quarks. *JHEP*, 11:062, 2008.

[61] **CMS Collaboration** Collaboration, Vardan Khachatryan et al. Measurement of top quark-antiquark pair production in association with a W or Z boson in pp collisions at $\sqrt{s} = 8$ TeV. *Eur.Phys.J.*, C74:3060, 2014.

[62] J. Alwall, R. Frederix, S. Frixione, V. Hirschi, F. Maltoni, O. Mattelaer, H.-S. Shao, T. Stelzer, P. Torrielli, and M. Zaro. The automated computation of tree-level and next-to-leading order differential cross sections, and their matching to parton shower simulations. 2014.

[63] Aneesh V. Manohar and Michael Trott. Electroweak Sudakov Corrections and the Top Quark Forward-Backward Asymmetry. *Phys.Lett.*, B711:313–316, 2012.

[64] Gerard 't Hooft. Symmetry Breaking Through Bell-Jackiw Anomalies. *Phys.Rev.Lett.*, 37:8–11, 1976.

[65] H. Georgi and S.L. Glashow. Unity of All Elementary Particle Forces. *Phys.Rev.Lett.*, 32:438–441, 1974.

[66] Harald Fritzsch and Peter Minkowski. Unified Interactions of Leptons and Hadrons. *Annals Phys.*, 93:193–266, 1975.

[67] Jogesh C. Pati and Abdus Salam. Lepton Number as the Fourth Color. *Phys.Rev.*, D10:275–289, 1974.

[68] **Super-Kamiokande Collaboration** Collaboration, H. Nishino et al. Search for Proton Decay via $p \to e^+ pi^0$ and $p \to mu^+ pi^0$ in a Large Water Cherenkov Detector. *Phys.Rev.Lett.*, 102:141801, 2009.

[69] **Super-Kamiokande Collaboration** Collaboration, H. Nishino et al. Search for Nucleon Decay into Charged Anti-lepton plus Meson in Super-Kamiokande I and II. *Phys.Rev.*, D85:112001, 2012.

[70] W. Buchmuller and D. Wyler. Effective Lagrangian Analysis of New Interactions and Flavor Conservation. *Nucl.Phys.*, B268:621–653, 1986.

[71] B. Grzadkowski, M. Iskrzynski, M. Misiak, and J. Rosiek. Dimension-Six Terms in the Standard Model Lagrangian. *JHEP*, 1010:085, 2010.

[72] Steven Weinberg. Baryon and Lepton Nonconserving Processes. *Phys.Rev.Lett.*, 43:1566–1570, 1979.

[73] Frank Wilczek and A. Zee. Operator Analysis of Nucleon Decay. *Phys.Rev.Lett.*, 43:1571–1573, 1979.

[74] L.F. Abbott and Mark B. Wise. The Effective Hamiltonian for Nucleon Decay. *Phys.Rev.*, D22:2208, 1980.

[75] Elizabeth E. Jenkins, Aneesh V. Manohar, and Michael Trott. Renormalization Group Evolution of the Standard Model Dimension Six Operators I: Formalism and lambda Dependence. *JHEP*, 1310:087, 2013.

[76] Elizabeth E. Jenkins, Aneesh V. Manohar, and Michael Trott. Renormalization Group Evolution of the Standard Model Dimension Six Operators II: Yukawa Dependence. *JHEP*, 1401:035, 2014.

[77] Rodrigo Alonso, Elizabeth E. Jenkins, Aneesh V. Manohar, and Michael Trott. Renormalization Group Evolution of the Standard Model Dimension Six Operators III: Gauge Coupling Dependence and Phenomenology. *JHEP*, 1404:159, 2014.

[78] Christophe Grojean, Elizabeth E. Jenkins, Aneesh V. Manohar, and Michael Trott. Renormalization Group Scaling of Higgs Operators and $\Gamma(h \to \gamma\gamma)$. *JHEP*, 1304:016, 2013.

[79] Peter Minkowski. $\mu \to e\gamma$ att a rate of one out of 1-billion muon decays? *Phys.Lett.*, page 421.

[80] Murray Gell-Mann, Pierre Ramond, and Richard Slansky. Complex Spinors and Unified Theories. *Conf.Proc.*, C790927:315–321, 1979.

[81] Rabindra N. Mohapatra and Goran Senjanovic. Neutrino Mass and Spontaneous Parity Violation. *Phys.Rev.Lett.*, 44:912, 1980.

[82] J. Schechter and J.W.F. Valle. Neutrino Masses in SU(2) x U(1) Theories. *Phys.Rev.*, D22:2227, 1980.

[83] Mattias Blennow and Enrique Fernandez-Martinez. Parametrization of Seesaw Models and Light Sterile Neutrinos. *Phys.Lett.*, B704:223–229, 2011.

[84] R. Sekhar Chivukula and Howard Georgi. Composite-technicolor standard model. *Physics Letters B*, 188:99–104, 1987.

[85] G. D'Ambrosio, G.F. Giudice, G. Isidori, and A. Strumia. Minimal flavor violation: An Effective field theory approach. *Nucl.Phys.*, B645:155–187, 2002.

[86] Vincenzo Cirigliano, Benjamin Grinstein, Gino Isidori, and Mark B. Wise. Minimal flavor violation in the lepton sector. *Nucl.Phys.*, B728:121–134, 2005.

[87] Sacha Davidson and Federica Palorini. Various definitions of Minimal Flavour Violation for Leptons. *Phys.Lett.*, B642:72–80, 2006.

[88] Rodrigo Alonso, Gino Isidori, Luca Merlo, Luis Alfredo Munoz, and Enrico Nardi. Minimal flavour violation extensions of the seesaw. *JHEP*, 1106:037, 2011.

[89] Emanuel Nikolidakis and Christopher Smith. Minimal Flavor Violation, Seesaw, and R-parity. *Phys.Rev.*, D77:015021, 2008.

[90] R. Alonso, M.B. Gavela, L. Merlo, and S. Rigolin. On the scalar potential of minimal flavour violation. *JHEP*, 1107:012, 2011.

[91] Benjamin Grinstein, Vincenzo Cirigliano, Gino Isidori, and Mark B. Wise. Grand Unification and the Principle of Minimal Flavor Violation. *Nucl.Phys.*, B763:35–48, 2007.

[92] N. Sakai and Tsutomu Yanagida. Proton Decay in a Class of Supersymmetric Grand Unified Models. *Nucl.Phys.*, B197:533, 1982.

[93] Savas Dimopoulos, Stuart Raby, and Frank Wilczek. Proton Decay in Supersymmetric Models. *Phys.Lett.*, B112:133, 1982.

[94] Steven Weinberg. Supersymmetry at Ordinary Energies. 1. Masses and Conservation Laws. *Phys.Rev.*, D26:287, 1982.

[95] Jeremy Bernon and Christopher Smith. Baryonic R-parity violation and its running. 2014.

[96] **BaBar Collaboration** Collaboration, P. del Amo Sanchez et al. Searches for the baryon- and lepton-number violating decays $B^0 \to \Lambda_c^+ \ell^-$, $B^- \to \Lambda \ell^-$, and $B^- \to \bar{\Lambda} \ell^-$. *Phys.Rev.*, D83:091101, 2011.

[97] **CMS Collaboration** Collaboration, Serguei Chatrchyan et al. Search for baryon number violation in top-quark decays. *Phys.Lett.*, B731:173, 2014.

[98] D.E. Morrissey, Timothy M.P. Tait, and C.E.M. Wagner. Proton lifetime and baryon number violating signatures at the CERN LHC in gauge extended models. *Phys.Rev.*, D72:095003, 2005.

[99] Wei-Shu Hou, Makiko Nagashima, and Andrea Soddu. Baryon number violation involving higher generations. *Phys.Rev.*, D72:095001, 2005.

[100] Zhe Dong, Gauthier Durieux, Jean-Marc Gerard, Tao Han, and Fabio Maltoni. Baryon number violation at the LHC: the top option. *Phys.Rev.*, D85:016006, 2012.